LAYER-BY-LAYER ASSEMBLY OF RESPONSIVE POLYELECTROLYTE THIN FILMS AND NANOCOMPOSITES

A Dissertation

by

JOSHUA TAYLOR O'NEAL

Submitted to the Office of Graduate and Professional Studies of
Texas A&M University
in partial fulfillment of the requirements for the degree of

DOCTOR OF PHILOSOPHY

Chair of Committee,	Jodie Lutkenhaus
Committee Members,	Svetlana Sukhishvili
	Jaime Grunlan
	Yossef Elabd
Head of Department,	Ibrahim Karaman

May 2018

Major Subject: Materials Science and Engineering

ABSTRACT

This thesis presents three investigations into the responsive physical and thermal properties of polyelectrolyte layer-by-layer assemblies. The first study focuses on hydrogen bonded, layer-by-layer assembled films and nanocomposites Polyelectrolyte multilayers and layer-by-layer assemblies are susceptible to structural changes in response to changes in the post-assembly environment. The study demonstrates the first reported use of spray-assisted layer-by-layer assembly to produce hydrogen-bonding polymer nanocomposites of poly(ethylene oxide) (PEO) and poly(methacrylic acid) (PMAA) containing discrete regions of gold nanoparticles (AuNPs) vertically positioned throughout the film structure with no substantial aggregation. Elevating the environmental pH disrupts the hydrogen bonding network, resulting in release of the AuNPs, and the rate of release is shown to depend on the pH of the environment.

The second study deals with the swelling response of electrostatic layer-by-layer thin films to changes in ionic environment. The effects of a wide range of KBr concentrations (0 to 1.6 M) on the swelling and deswelling of LbL assemblies formed from poly(diallyldimethylammonium) polycation (PDADMA) and poly(styrenesulfonate) polyanion (PSS) in 0.5 M NaCl were investigated using quartz-crystal microbalance with dissipation (QCM-D) monitoring. The swelling behavior is compared with responses to KCl, NaBr, and NaCl at various concentrations. The results demonstrate anion type dominates swelling response, and that Br^- ions have a much greater effect on the structure of as-prepared thin films than Cl^- at ionic strengths above assembly conditions, likely due to the chaotropic nature of Br^-. Four response regimes are identified that delineate swelling due to electrostatic repulsion, slight contraction, swelling due to doping, and film destruction as ionic strength increases.

The third study focuses on the thermal response of electrostatic layer-by-layer assemblies of PDADMA and PSS to changes in hydration level and counterion type. Modulated differential scanning calorimetry (MDSC) is employed to quantify the influence of changing hydration level, ionic strength and type, as well as assembly conditions on the glass transition temperature (T_g) of free-standing PDADMA/PSS LbL films assembled in 0.5 M NaCl. The results indicate that assembly conditions and post-assembly hydration level are the primary factor in determining the T_g of PDADMA/PSS LbL films when hydration is limited to less than 35 wt%. Hydrating with KBr solutions resulted in no apparent effect on the T_g of the LbL films. Conversely, films assembled in NaCl and KBr at identical ionic strengths show a nearly 20°C difference in T_g, indicating a different internal structure of extrinsic and intrinsic ion pairing. Finally, PDADMA/PSS LbL films show remarkably similar T_g behavior to PDADMA/PSS complexes when hydrated to similar levels.

DEDICATION

This dissertation is dedicated to my beautiful wife, Michelle. She has supported me throughout the course of my entire PhD program. Without her I would not understand the meaning of true joy. I also thank my parents, Randy and Janet, as well as my brother, Zach, and my sister, Rachel, for always supporting me and motivating me to give my best effort in every endeavor. Finally, my work would be meaningless if I did not have a purpose in this life. To that end, I dedicate this dissertation to the God whom I serve. He is the God of Abraham, Isaac, and Jacob, the God who created and sustains the universe by the word of His mouth. It is by belief in the sufficiency of the life, death, and resurrection of His Son, Jesus Christ, to cover the debt of my sin that I have received the gift of salvation. To Him be all glory, honor, power, and dominion both now and in the day of eternity, amen.

ACKNOWLEDGEMENTS

I would like to thank my advisor, Dr. Jodie Lutkenhaus, for her steadfast guidance and support in my research endeavors. I also thank Dr. Svetlana Sukhishvili, Dr. Jaime Grunlan, and Dr. Yossef Elabd for serving on my committee and providing valuable direction in completing my project.

Additionally, I would like to thank my lab mates, past and present, for their meaningful input, support, and kindness over the last several years. The legacy of our research group is truly one of excellence because of you.

Finally, I extend my deepest gratitude and appreciation to Texas A&M University. The unparalleled and unwavering commitment to the core values of honor, service, integrity, and leadership will forever be branded on my heart after my time at this institution. My hope and prayer is that, despite the faltering of our fellow men, the past, present, and future graduates from this great university would hold fast to our core values and moral absolutes and continue to be a beacon of hope for the rest of the world.

CONTRIBUTORS AND FUNDING SOURCES

The work presented in this dissertation was supervised by a dissertation committee consisting of Professor Jodie Lutkenhaus (committee chair) or the Department of Materials Science and Engineering, Professor Svetlana Sukhishvili of the Department of Materials Science and Engineering, Professor Jaime Grunlan of the Department of Mechanical Engineering, and Professor Yossef Elabd of the Department of Chemical Engineering.

Portions of the experimental data in Chapter II, III, and IV were collected by various undergraduate research assistants including Matthew Bolen of the Department of Chemical Engineering, Ethan Dai of the Department of Electrical Engineering, Kyle Clark of the Department of Chemical Engineering, Kathryn Wilcox of the Department of Chemical Engineering, Ian George of the Department of Chemical Enineering, Nandha Ramasamy of the Department of Chemical Engineering, and Daisy Enriquez of the Department of Chemical Engineering.

Helpful discussions and collaborative contributions for Chapter II were made by Piotr Batys and Professor Maria Sammalkorpi of the Department of Chemistry and Materials Science, School of Chemical Technology, at Aalto University in Finland.

The work presented in Chapter I was supported by Lockheed Martin Corporation and National Science Foundation Career Award No. 1049706. The work in Chapter II and III was supported financially by the National Science Foundation Career (DMR) Award No. 1049706 and Grant No. 1609696.

TABLE OF CONTENTS

Page

LIST OF FIGURES

FIGURE Page

FIGURE Page

FIGURE Page

FIGURE Page

FIGURE Page

LIST OF TABLES

CHAPTER I

INTRODUCTION

1.1 Introductory Remarks

Layer-by-layer (LbL) assembly is a simple and diverse technique used to form thin films of polyelectrolytes (PEs) by alternately adsorbing complementary species onto a substrate. Control over the thickness and properties of the resulting assemblies can be readily tuned by altering the assembly or post-assembly conditions including PE type and concentration, salt type and concentration, temperature, pH, etc.[1-2] The versatility of the LbL assembly method makes it possible to select materials and substrates for specific applications including sensing, drug delivery, energy storage, and tissue engineering.[3-5] The growing number of prospective applications suitable for polyelectrolyte LbL assemblies has resulted in numerous publications and review articles over the last few decades. Despite intense study and development in the field, a struggle to gain deep understanding of some fundamental behavior of LbL films and nanocomposites remains.

The purpose of this chapter is to lay a foundation of understanding regarding the basic principles of the LbL assembly technique. First, general background on LbL assemblies will be discussed with respect to formation and properties. Second, current studies dealing with responsive properties of LbL films with respect to physical (i.e. swelling) and thermal properties will be explored.

1.2 General Introduction

1.2.1 Layer-by-Layer (LbL) Assembly Technique

Introduced by Iler[6] and Decher[7] over two decades ago, LbL assembly has been a topic of high interest for researchers across many fields. LbL assemblies are constructed by the alternate adsorption of complementary polyelectrolytes (PEs) onto a substrate. Flexible or rigid substrates of various shapes and materials can be used in this technique, and surface modifications can be used to manipulate film growth behavior. Figure 1.1 illustrates the LbL assembly process. In the first step, the charged or functionalized substrate is immersed in a solution bath containing a polyelectrolyte with a complimentary charge or functionalization. Once this step is complete, the substrate is rinsed with water in order to remove any debris and unbound or loosely bound PE chains from the surface.[7] The substrate is then immersed in the second PE solution, followed by another rinse with water. This sequence of steps constitutes a layer pair. The process is repeated until the desired thickness is reached. Besides immersing the substrate in the complimentary PE solutions, other techniques have been employed to construct LbL films including spray-coating and spin-coating. LbL assembly is not limited to PEs alone. It is also possible to incorporate nano-materials such as nanoparticles[8-10] or nanofibers[11-13] into the film structure in order to form more complex nanocomposite structures. Additionally, due to the repetitive nature of LbL film assembly, the process can be automated easily.

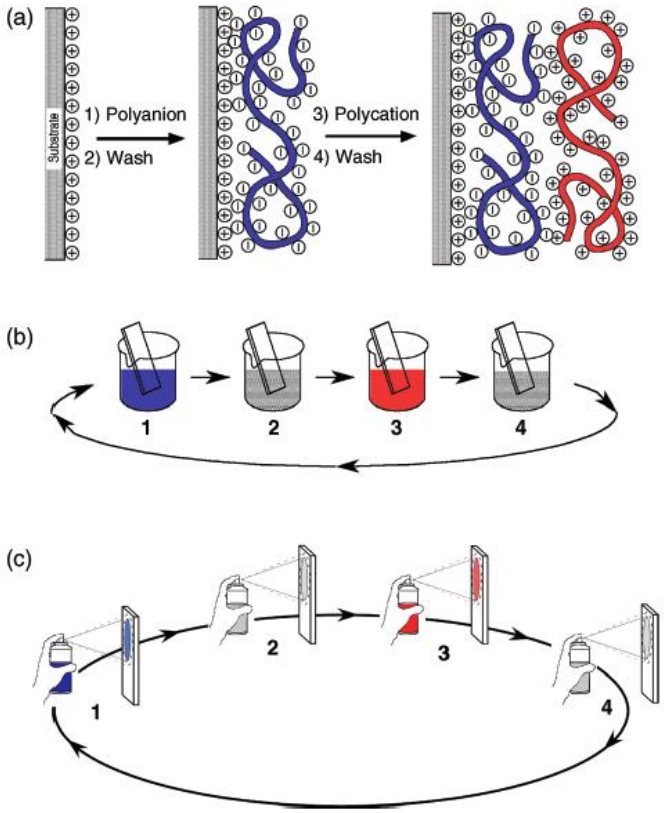

Figure 1.1. Illustration of LbL assembly of polyelectrolyte films using different techniques. Reprinted with permission from ref. 14. Copyright 2012 Wiley-VCH Verlag GmbH & Co. KGaA. Reprinted by permission of John Wiley & Sons, Inc.

The structure and properties of the resulting LbL assemblies can be tuned using material chemistry as well as altering the assembly conditions. For example, charge density is a key parameter controlling the formation of weak polyelectrolyte assemblies.[15] In this case, altering the assembly pH can thus be used to manipulate the LbL film architecture. By setting the assembly pH value below the pKa, the chain conformation of negatively charged PEs is altered from a more extended (rod-like) structure to a more coiled configuration. This is due to reduced ionization

degree. Conversely, above the pKa value, the negatively charged PE chains become extended due to increased electrostatic repulsion caused by stronger ionization at the elevated pH value.

Altering the assembly ionic strength also influences the structure and properties of LbL assemblies, especially for films constructed from strong PEs. In general, thickness of the resulting films increases as the ionic strength increases.[16-19] The reason for this is the additional counterions in solution decrease electrostatic repulsion *via* electrostatic screening, causing the PE chains to take on a more coiled configuration. These coils result in thicker adsorbed layers. Decreasing the ionic strength has the opposite effect on film thickness. Changing salt type can have a large impact on film structure and properties as well.[1, 18, 20] Smaller, less polarizable counterions (kosmotropes) with large, ordered hydration shells result in thinner films with smoother surfaces. On the other hand, larger ions with small, loosely bound hydration shells (chaotropes) result in thicker films with roughened surfaces. The weak hydration shells associated with chaotropic ions allow them to interact more readily with the oppositely charged PE chains. The result is more electrostatic screening from chaotropic ions leading to stronger coiling of associated PE chains. This effect of specific ion types on PDADMA/PSS LbL assemblies has been found to agree with the Hofmeister series, where thickness and roughness of films was shown to increase from $F^- < Cl^- < Br^-$ with respect to anions and from $Li^+ < Na^+ < K^+$ for cations.[18, 20-22]

The complimentary interactions driving LbL assembly are not limited to electrostatic forces. Secondary interactions such as Van der Waals and Hydrogen bonding have also been used.[9, 23-25] LbL films built using hydrogen bonding rely on the proton donor-acceptor relationship between functional groups on the PE chain backbones, allowing the use of neutral polymers in the film buildup process. For example, LbL films of poly(ethylene oxide) (PEO) and poly(methacrylic

acid) (PMAA) rely on the oxygen atoms on the PEO chains as proton acceptors and the carboxylic acid groups on PMAA as proton donors.[9] Hydrogen bonded LbL assemblies were first demonstrated by Stockton and Rubner who explored the buildup of films constructed from polyaniline and various other PEs including PEO.[26] Granick and Sukhishvili have also done extensive work dealing with responsive LbL films and microcapsules built using hydrogen bonding.[27-30] They demonstrated the assembly and subsequent dissociation of LbL assemblies of PEO and polyacids including polyacrylic acid (PAA) and PMAA. By adjusting the pH values above a critical pH, 3.5 for PEO/PAA and 4.6 for PEO/PMAA, the hydrogen bonding between the PEs was disrupted catastrophically, and the films could be disassembled. The destabilized hydrogen bonding network results from increased ionization of the carboxylic acid groups with increasing pH.

1.2.2 LbL Assembly Formation

LbL film formation is driven by an array of various interactions including 1) the interactions between the PE pair, 2) interactions between the PE charge groups and the selected counterions, 3) interactions between the solvent molecules and the PEs, and 4) the interactions between the substrate and the LbL film. LbL assembly can be generally described as a controlled complexation of PEs on a substrate surface, and the stability of the resulting complex depends on the interplay of the interactions mentioned above.[31] Forming a stable complex between two PEs depends on the complexation free energy associated with the PE pair, which consists of both entropic and enthalpic contributions. Coulombic interaction between the PE charge sites dominates the changes in enthalpy while entropic changes are determined by the release of counterions as PE-PE ion pairs (i.e. intrinsic binding sites) are formed.[32]

For many years, it was assumed that Coulombic interactions were the primary driving force for LbL film formation.[33] However, more recent studies have shown the entropy gain associated with counterion release is the dominating force driving LbL film growth, implying that electrostatics play only a minor role with respect to driving construction.[31-32, 34-36] This concept is supported by the several observations. First, LbL films can be assembled at elevated ionic strengths despite elevated electrostatic screening.[36-37] Second, charge reversal and overcompensation requires a large amount of energy, and a purely electrostatic process should halt, in theory, once neutrality is reached. Finally, in a purely electrostatic environment there should be no distinction between how charge sites are compensated, whether by counterions or by incoming PE functional groups.[34]

Entropic contributions may be the primary driving force for LbL assembly, but the enthalpic contribution from the Coulombic interactions can influence LbL assembly properties. Laugel et al. explored the variance of complexation energy in several PE pairs.[31] They reported that highly exothermic complexation reactions, associated with a strong negative enthalpy change, resulted in LbL assemblies that were compact and thin. Conversely, endothermic complexation reactions with positive change in enthalpy yielded thicker, fluffier films. This implies that Coulombic forces do not support complexation, but the entropy gain is still strong enough to drive complexation forward.

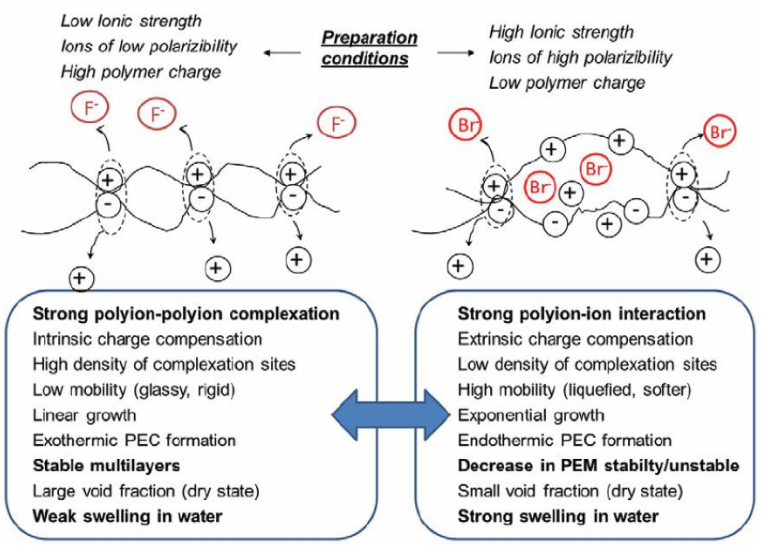

Figure 1.2. Illustration of how various assembly conditions influence the charge compensation, structure, and properties of the resulting LbL films where the structure on the left is dominated by intrinsic binding sites and the structure on the right has a larger number of extrinsic binding sites. Reprinted with permission from ref. 34. Copyright 2014 Elsevier Ltd.

The packing density of the PE chains as well as the stability and mechanical properties of LbL films depend on the type of internal charge compensation. Charge compensation in LbL films is divided into two categories, extrinsic and intrinsic compensation.[38-39] Extrinsic compensation describes a charged functional group on a PE chain that is compensated (neutralized) by a small counterion. Intrinsic charge compensation occurs when the charged group of a PE chain is compensated by directly interacting with the oppositely charged PE. Extrinsic compensation will occur if interacting with the small counterion is more favorable than interacting with the oppositely charged PE. Figure 1.2 illustrates intrinsic and extrinsic charge compensation within an LbL film and the relationship between internal charge compensation and counterion type. Typically, films

with more intrinsic binding sites are smoother and more compact compared to films with internal structures dominated by extrinsic binding sites. The presence of many extrinsic sites gives rise to the film's ability to uptake water because of increases in osmotic pressure.[40-41]

1.2.3 Growth Behavior and Structure of LbL Assemblies

LbL assembly growth patterns are typically classified as linear and non-linear (or exponential). Linear growth describes a trend in which the incremental change in thickness with each additional layer pair is constant. Non-linear growth occurs when the incremental change in thickness increases with increasing number of layer pairs. The internal structure of LbL films influences the growth behavior as well. Assembly conditions directly influence how LbL films assemble, and therefore can be used to manipulate the observed growth in LbL films.

Non-linearly growing LbL films, first reported by Elbert et al.[42], are commonly described using the diffusion model, which assumes if one or both PEs is able to diffuse in and out of the multilayer during assembly the film will grow in a non-linear fashion.[43] If no PE diffusion occurs, the film will grow linearly. In this model, PE chains within the film can diffuse from the bulk to the surface to form complexes while the oppositely charged PE is adsorbed. This additional complex causes an increase in the incremental change in thickness per layer pair because the amount of PE that can diffuse into the bulk of the film depends on the thickness. So the effect becomes more pronounced as film thickness increases.

In some cases early film growth is non-linear, but after several deposited layer pairs the film transitions to linear growth. Such behavior was described by Bieker et al. and Hoda et. al.[15, 44] They proposed that contact time of the substrate with the polyanion solution was the limiting factor determining the amount of complex that could form during a deposition cycle. Diffusion of

the free polycations needed enough time to occur once the film became sufficiently thick, and constant dipping times would not allow enough time for additional free polycations to reach the interface and form extra complexes at the surface. This point, they proposed, constituted the change from exponential to linear growth. However, Porcel et al. showed that internal film restructuring limits polyion diffusion after a certain number of deposited layer pairs. They saw a consistent shift from exponential to linear growth in hyaluronic acid (HA)/poly(L-lysine) (PLL) LbL films around 10-12 layer pairs. This transition point from non-linear to linear proved to be independent of dipping time and PE molecular weight, indicating that diffusion is not the sole contributor to the transition.[45]

To account for the observed growth behavior and expand the diffusion model, the so-called "3-zone model" was proposed. This model separates LbL films into an outer diffusion zone, and inner bulk or restructured zone, and a "forbidden" zone very near to the substrate that is mainly intrinsically compensated. As the diffusion zone continues to grow, the film grows in a non-linear fashion. Once the film reaches a certain thickness, dependent on the PE film constituents, the inner layers begin to restructure giving rise to the restructured zone in which PEs are no longer free to diffuse.[45] The diffusion zone ceases to grow when the inner restructured zone is formed, and the growth pattern transitions from non-linear to linear. Internal restructuring is attributed to the fact that the structure is kinetically stabilized. As more layer pairs are added, PEs deeper in the bulk undergo conformational changes to achieve a more thermodynamically favored state.[46] Schlenoff et al. explored the growth behavior of LbL assemblies of poly(diallyldimethylammonium chloride) (PDADMA) and poly(styrene sulfonate) (PSS). They found that an excess of "free" extrinsically compensated PDADMA accumulated in the film during the growth process. Excess PDADMA diffuses to the surface while PSS is deposited leading to overcompensation by forming additional

complexes. This results in an asymmetric growth pattern in the first 10 layer pairs. During this period, the diffusion zone encompasses nearly the entire film, allowing the PDADMA to diffuse freely in and out during deposition cycles. Beyond this growth period, the film grows linearly as described by the 3-zone model.

The relationship between the type of charge compensation and the growth behavior was explored by Volodkin et al.[34] They described the restructured zone near the substrate as predominantly intrinsically compensated and the outermost diffusion zone as mainly extrinsically compensated. Because intrinsically compensated PEs tend to be more densely packed, the inner regions of LbL films form a "forbidden" zone where PEs are kinetically trapped in place and highly resistant to environmental changes. The extrinsically compensated diffusion zone, however, is more loosely packed and allows for PE diffusion and reconfiguring as the film grows. Decher et al. described the internal structure of LbL assemblies as interdigitated layers rather than a series of well-defined separate PE layers.[7] They proposed a model stating that each deposited layer overlaps with the surrounding five layers. Figure 1.3 shows the model of overlapping layers in an LbL film.

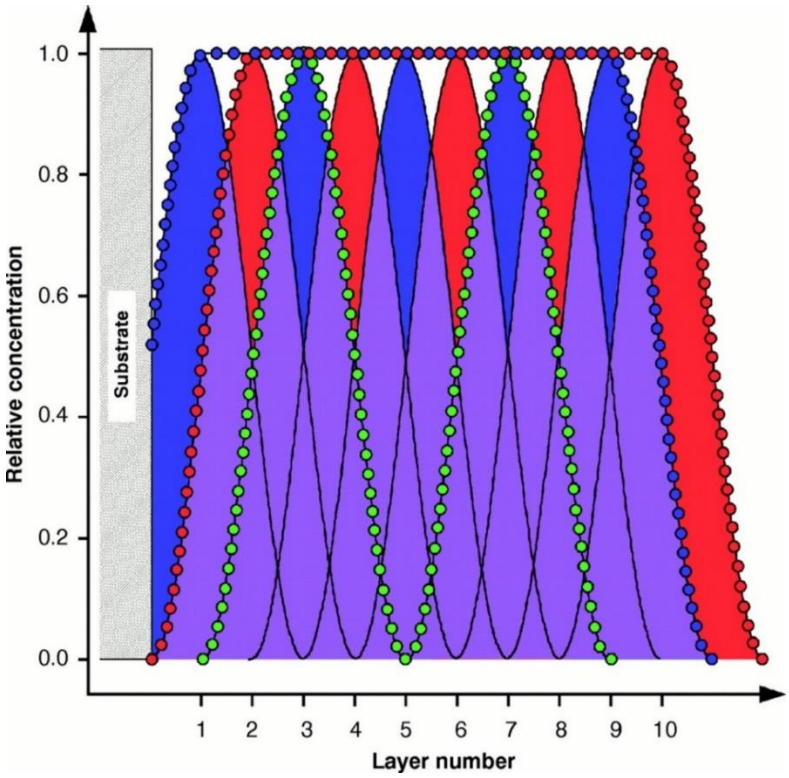

Figure 1.3. Illustration of the interdigitation and charge distribution inside an LbL assembly consisting of ten layer pairs. Reprinted from ref. 7 with permission from AAAS.

The internal structure of LbL films is directly related to the film growth behavior as well as the assembly conditions. Growth behavior and structural properties of films built based on hydrogen bonding interactions, for example, can be tailored by changing the assembly pH. By adjusting the pH above 5.5, LbL films of poly(2-(dimethylamino)ethyl methacrylate) and PMAA change from linear to exponential growth due to a change in charge density of the carboxylic acid functional groups along the PMAA backbone.[47] Using neutron reflectometry, the change to a more interdigitated structure from a layered structure was confirmed. Indeed, thickness of resulting hydrogen bonded LbL films containing polyacids can be manipulated readily. Modulating the

protonation levels of the polyacids changes the effective level of electrostatic repulsion and, therefore, the chain conformation on the film surface. More coiled chains leads to a thicker layer, while a more rod-like configuration leads to thinner layers. With respect to hydrogen bonded LbL assemblies, the strength of the hydrogen bonding between PEs can also influence the resulting structure. For example, weak hydrogen bonded LbL assemblies of PEO/PMAA exhibited layers that were completely interdiffused while PVPON/PMAA films showed a higher internal roughness and a more layered structure.[48]

In electrostatic LbL films, the structure and properties are strongly influenced by the assembly ionic strength. Salomäki et al. studied the effects of various anions along the Hofmeister series on the growth of PDADMA/PSS LbL thin films.[20, 22, 49] They found film properties depended strongly on the anion identity, specifically the anions' position along the series compared to NaCl as a reference point. Ellipsometry showed that films formed in Na^+ and Br^- exhibited the greatest increase in overall thickness compared with films constructed in the same concentration of Na^+ and Cl^- (0.1 M). Atomic force microscopy (AFM) also indicated that films made in the presence of Na^+ and Br^- had surfaces nearly twice the roughness of their counterparts formed in Na^+ and Cl^-. They report that the influence of the specific anion on the film growth behavior is related to the Jones-Dole viscosity coefficient as well as the entropy of hydration, where ions with a more positive hydration entropy give thicker films. The more chaotropic (water structure breaking) anion species show an apparent strong screening effect of polyelectrolyte charges, allowing for a more coiled conformation on the film surface, resulting in a thicker layer with each deposition. On the other hand, the more kosmotropic (water structure forming) anions are less efficient at

screening PE charges. This results in a more planar PE chain configuration on the film surface and, therefore, a thinner layer with each deposition.

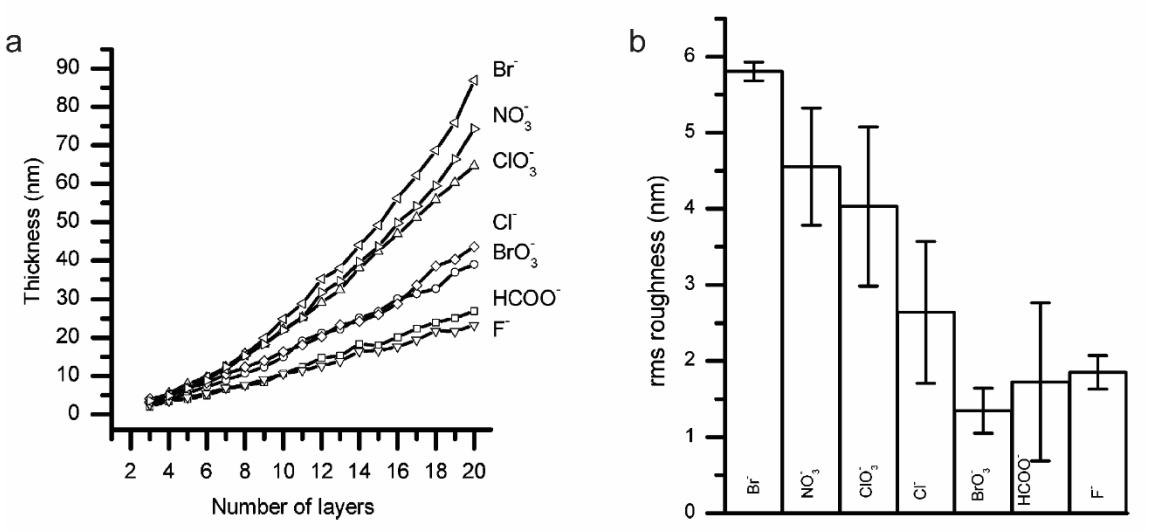

Figure 1.4. Data showing the effects of counterion type during film assembly on (a) thickness and (b) roughness of PDADMA/PSS LbL films determined by ellipsometry and AFM, respectively. Reprinted with permission from ref. 20. Copyright 2004 American Chemical Society.

Liu et al. reported on the dominating influence of the anion species on the growth behavior of hydrated PDADMA/PSS films.[18] Quartz-crystal microbalance with dissipation (QCM-D) demonstrated that film growth behavior strongly depended on the counteranion species, with Br^- having the strongest influence. Films grown in NaBr were more than 200 nm thicker than those grown in NaCl at the same ionic strength (0.5 M) after eight layer pairs.

Overall, thickness of PDADMA/PSS films was reported to increase along the Hofmeister series from $Br^- > Cl^- > HClO_3^- > F^-$ for monovalent anions as well as with increasing ionic strength of the assembly salt. Although clear trends in growth behavior can be linked to the specific counterion type and ionic strength in the assembly conditions, the exact cause of this phenomena is still under investigation.

1.2.4 Structural Response of LbL Assemblies

Factors influencing the structural properties of LbL films and nanocomposites have been the subject of more intense study in recent years.[28, 41, 50-56] Stimuli-responsive LbL assemblies are dynamic materials with a wide range of potential applications including controlled drug delivery, self-healing materials, separation membranes, and sensors.[5, 10, 27, 50, 57-59] Responsive LbL assemblies are macromolecular nanostructures capable of undergoing conformational and mechanical changes when subjected to an applied external stimulus. The response usually involves a change in physical properties that is either reversible, swelling or shrinking of the network, or irreversible, complete dissolution of the assembly. The addition of nanomaterials to LbL the film structure can result in nanocomposites with tunable, switchable properties that depend on the nature of the added nanoscale filler as well as the polyelectrolyte system.[50, 60-62] The two categories of responsive LbL assemblies discussed here are those formed from electrostatic interactions and hydrogen bonding.

1.2.4.1 Responsive Electrostatic LbL Assemblies

LbL films and nanocomposites formed using electrostatic interactions between oppositely charged PEs are among the most heavily studied due to their ease of fabrication. Schönhoff recently explored the humidity controlled conductivity of LbL nanocomposites consisting of

positively charged poly(allylamine hydrocholoride) (PAH) and negatively charged, citrate stabilized gold nanoparticles (AuNPs).[50] They were able to induce swelling and shrinking of the LbL nanocomposites by increasing or decreasing the relative humidity of the environment. The conductivity decreased from 1.8×10^{-1} S cm^{-1} to 0.87×10^{-1} S cm^{-1} as relative humidity was increased from 9-95% due to swelling of the network which disrupted the conductive pathways formed between the AuNPs. This swelling proved to be reversible and repeatable. Additionally, the authors found that by increasing the ionic strength of the assembly solution, the conductivity decreased up to four orders of magnitude across the same relative humidity range. They showed ultimately that by manipulating both the assembly and post assembly conditions, the final properties of the LbL nanocomposites could be finely tuned.

Ionic strength of the post-assembly environment plays a major role in the structural response of electrostatic LbL assemblies. Köhler et al. reported on the swelling and contraction of PDADMA-terminated PDADMA/PSS microcapsules.[63] The capsule diameters could be increased or decreased by changing the solution ionic strength from 1 – 10 mM NaCl which influenced the amount of electrostatic screening. Elevated ionic strength resulted in capsule shrinkage, and decreased ionic strength resulted in capsule expansion due to increased electrostatic repulsion. Dubas et al. reported the structural response of LbL assemblies of PDADMA/PSS by salt annealing.[64] The authors found that restructuring at the film surface takes place when the LbL film is annealed in salt solutions of ionic strength of 1.0 M NaCl for four hours. This restructuring arises from increased mobility of the PE chains during the annealing step and leads to a decrease in surface roughness from about 15 nm to 5 nm over a 400 min period. They also reported LbL films annealed at lower ionic strengths contracted due to osmotic pressure while swelling occurred as ionic strength increased due to increased screening as well as structural plasticization by water.

More recently, Hadi et al. explored the use of cyclic salt annealing and polyelectrolyte uptake as a means to achieve fully intrinsic PDADMA/PSS LbL films.[65] PDADMA/PSS films were subjected to a series of exposures to 2.0 M NaCl for 30 min, 10 mM PSS in 1 M NaCl for 5 min, and a pure water rinse. The series is then repeated cyclically (see **Figure 1.5**). The result is an uptake of additional PSS during each cycle until all of the extrinsically compensated PDADMA is compensated with PSS, leaving a nearly completely intrinsic film with little to no counterions present.

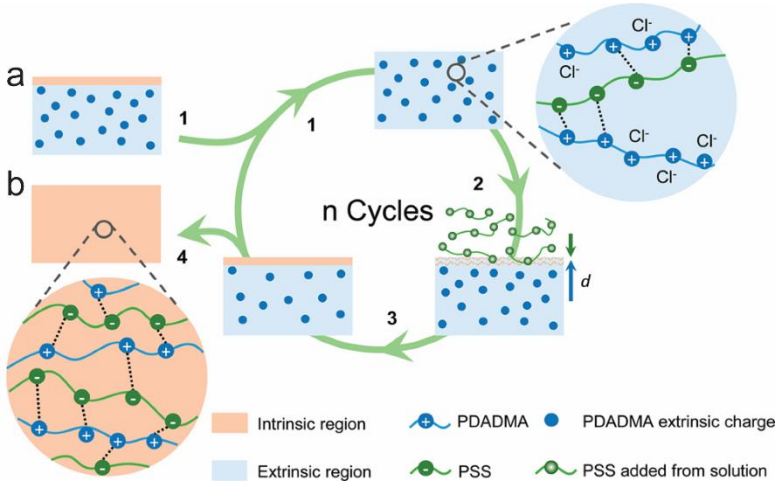

Figure 1.5. Illustration of the mechanism of cyclic salt annealing technique where (a) represents the PDADMA/PSS LbL film after assembly and (b) represents the fully intrinsic film resulting from multiple annealing cycles. Reprinted with permission from ref. 65. Further permissions related to this material excerpt should be directed to the American Chemical Society (http://pubs.acs.org/doi/abs/10.1021/la504910y).

The 2.0 M NaCl is used to promote mobility and dispersion of the extrinsically compensated PDADMA within the multilayer by electrostatic screening that causes swelling accompanied by uptake of counterions and water into the film. Upon immersion into the PSS solution, the highly mobile extrinsic PDADMA can diffuse to the surface and form new complexes with the incoming PSS. This cycle is repeated until the extrinsic PDAMA is exhausted. Similar studies on the effect of ionic strength, counterion type, and PE molecular weight on the uptake of additional PE by LbL films have also been conducted.[54-55]

Han et al. studied the effects of ionic strength of NaCl on the structure of PDADMA-capped PDADMA/PSS LbL thin films using quartz-crystal microbalance (QCM) and quartz-crystal microbalance with dissipation (QCM-D).[51] Films were first assembled to seven layer pairs in 1.0 M NaCl and then subjected to varying concentrations of NaCl with intermittent rinse steps between NaCl exposures.

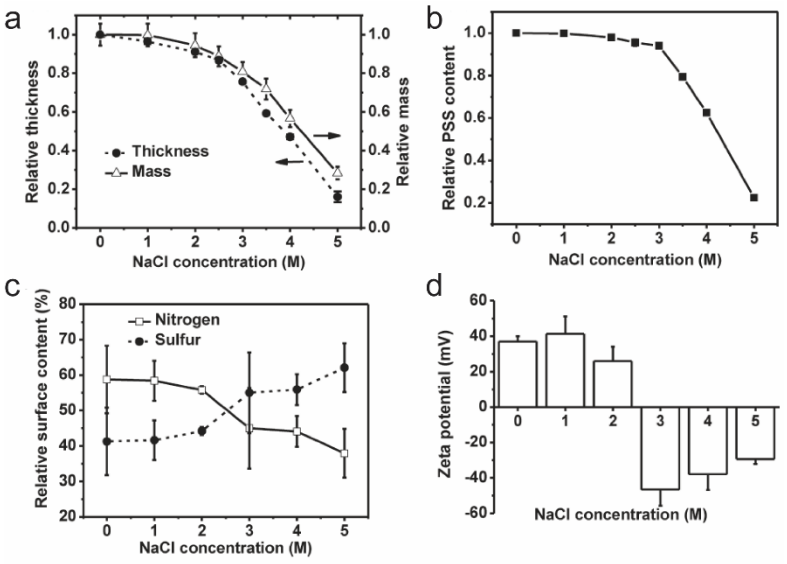

Figure 1.6. Data showing changes in the mass and surface characteristics of $(PDADMA/PSS)_7$ films treated with various NaCl concentrations including (a) QCM-D and ellipsometry data combined to show changes in normalized mass and thickness, (b) UV-Vis data indicating PSS content with increasing NaCl concentration, (c) XPS data showing changes in nitrogen and sulfur content at the film surface, and (d) Changes in zeta potential of the films across the gradient of NaCl concentrations. Reprinted with permission from ref. 51. Copyright 2012 American Chemical Society.

The authors observed films increased in mass with increasing NaCl concentration which they attribute to uptake of water. They also reported that films experienced a net mass loss, up to 75%, during rinse steps that increased with NaCl concentration up to 5 M.

UV-Vis spectroscopy and X-ray photoelectron spectroscopy revealed that the films were releasing PDADMA upon transitioning from the NaCl solution to the rinse solution. The increased mobility of the PDADMA both at the interface as well as within the bulk of the film at elevated ionic

strengths allows for enhanced diffusion. The highly screened PDADMA at the interface is then unable to maintain favorable interactions with the film upon exposure to the rinse solution. Surface charge reversal from positive to negative was observed using zeta potential measurements, indicating loss of the polycation.

The influence of counterions is not limited to their concentration. Changing counterion species and valency can have a dramatic impact on the structure and mechanical properties of LbL films.[22, 41, 51, 66-67] Wei et al. explored the effects of divalent cations on the properties of PDADMA/PSS LbL films capped with PSS and prepared in 0.5 M $NaNO_3$ using QCM-D.[66] Three layer pair films exposed to 0.01 M $Cu(NO_3)_2$ showed irreversible contraction and stiffening, and films exposed to 0.02 M $NaNO_3$ underwent reversible contraction. The behavior was due to ion-induced cross-linking between PE charge sites within the film. The Cu^{2+} ions form bridges between PEs, resulting in a tightening of the network and stiffening of the film.

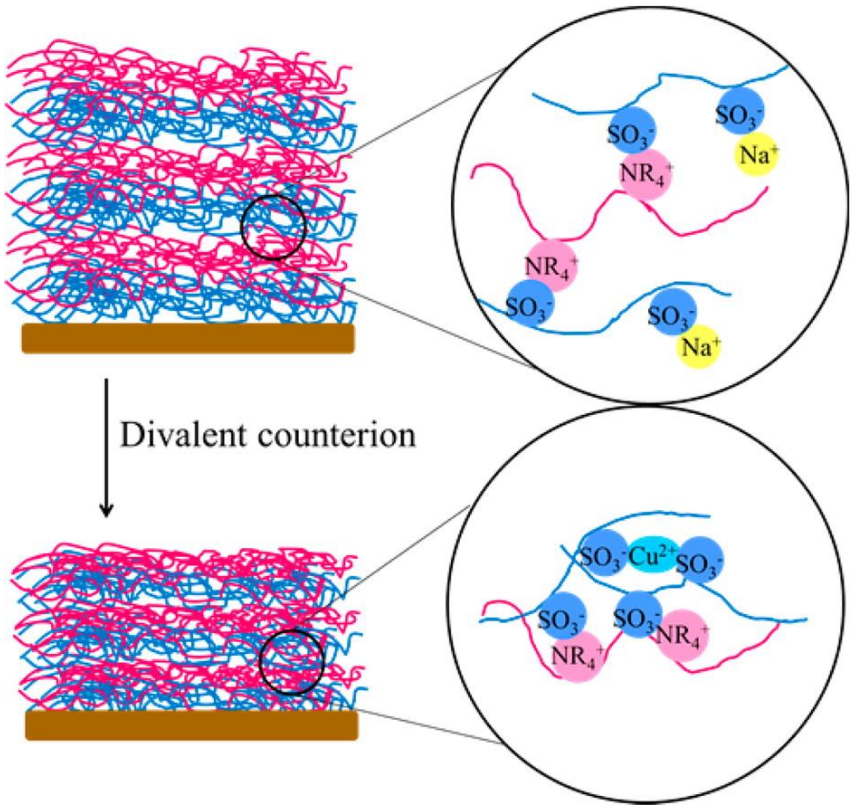

Figure 1.7. Cross-linking within a PDADMA/PSS LbL film induced by the addition of divalent copper cations. Reprinted with permission from ref. 66. Copyright 2013 American Chemical Society.

However, exposure to 0.03 M and 0.1 M $Cu(NO_3)_2$ resulted in irreversible swelling. The authors explain the difference between the two behaviors with respect to elevated external concentration of the exchange salt which causes greater incorporation of water and counterions. The additional incoming counterions convert PE-PE intrinsic ion pairs to extrinsic ion pairs, decreasing cohesive interactions. Reid et al. also studied the effects of divalent counterions on the properties of PDADMA-capped PDADMA/PSS LbL films assembled at 0.5 M NaCl.[41] They found that seven

layer pair films exposed to $MgCl_2$ and $CaCl_2$ exhibited reversible swelling when exposed to various ionic strengths. Below 0.17 M the swelling is dominated by electrostatic repulsion within the multilayer network, and above 0.17 M swelling progresses linearly with increasing ionic strength due to increased doping of the film. Films exposed to Na_2SO_4 exhibited swelling, but the behavior did not show a clear correlation with salt concentration.

1.2.4.2 Responsive Hydrogen Bonded LbL Assemblies

In addition to electrostatic forces, hydrogen bonding as the driving force for LbL films and nanocomposites has gained interest in recent years. This is partly because it is possible to favorably incorporate uncharged species into the hydrogen bonded LbL architecture. Hydrogen bonding is based on the proton donating and proton accepting of the constituent molecules involved in the LbL assembly process to form "bridges" through the shared hydrogen atoms and was first demonstrated by Rubner and co-workers. Films and nanocomposites based on hydrogen bonding typically consist of a poly(acid) like poly(acrylic acid) (PAA) or poly(methacrylic acid) (PMAA) paired with a polybase like poly(ethylene oxide) (PEO) or poly(vinylpyrrolidone) (PVPON). These systems have been studied as models for fundamental studies of hydrogen bonded LbL films and nanocomposite materials to understand the fundamentals of their stimuli responsive properties.

A substantial amount of research has dealt with stimuli responsive hydrogen bonded LbL structures for use in biomedical applications such as coatings and drug delivery carriers.[26-27, 58] Assembly at mild pH values and tunable response to temperature and moderate pH conditions make these types of assemblies good candidates for payload delivery to biological systems.[5, 68] Additionally, single or two-component hydrogels can be formed by varying the degree of

crosslinking within the film matrix.[69-70] Post-assembly crosslinking can add needed stability to the film or nanocomposite while not sacrificing the responsive properties.

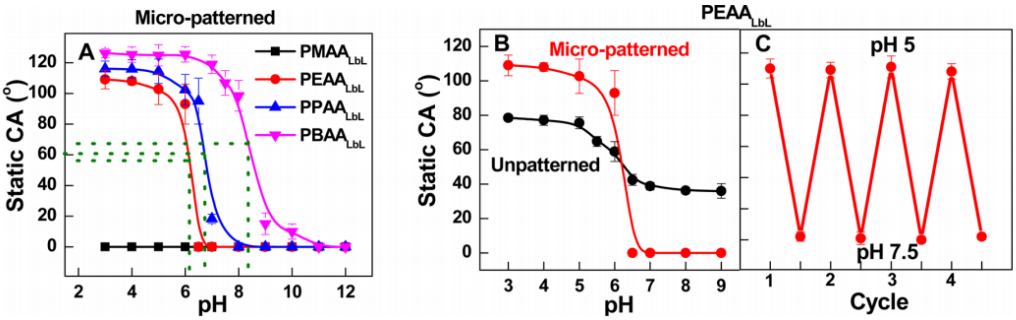

Figure 1.8. (a) Contact angles of PAA derivative-coated micropatterned Si substrate consisting of pillars with a height of 15μm and diameters of 5μm spaced every 5μm, (b) contact angles of PEAA hydrogel coated micropatterned and unpatterned Si substrates, and (c) reversible contact angle changes of the PEAA hydrogel coated micropatterned Si substrates (thickness of coating was ~35nm). Reprinted with permission from ref. 71. Copyright 2013 American Chemical Society.

Lu et al. recently reported on the use of hydrogen bonded LbL assembled thin films to form pH-responsive hydrogels able to control the surface wettability of smooth and patterned silicon substrates.[71] Tunable and reversible wettability of the surface was obtained by utilizing hydrophilic to hydrophobic transitions of various poly(acrylic acid) derivatives with differing degrees of hydrophobicity based on the environmental pH (see **Figure 1.8**). LbL films were deposited on micropatterned silicon substrates by first constructing a base layer consisting of two layer pairs of PMAA/branched poly(ethyleneimene) (BPEI). Films consisted of either 10 layer pairs of

PMAA/PVPON or 15 layer pairs of poly(2-ethylacrylic acid) (PEAA), poly(2-n-propylacrylic acid) (PPAA) or poly(2-n-butylacrylic acid) (PBAA) paired with PVPON. After deposition, the thin films were chemically crosslinked and PVPON, the neutral component, was dissolved from the network leaving a single-component hydrogel. They studied the change in contact angle of water as a result of the protonation or deprotonation of the carboxylic acid groups with changing pH on the PAA polymer chains. Below a critical pH value (pH_{crit}), ionization of the carboxylic acid groups caused the amphiphilic PAA derivatives to transition from a hydrophilic to hydrophobic and precipitated from solution. PMAA, however, remained soluble at all measured pH values. This behavior combined with the increasing length of the alkyl side chain allows for good control of the wettability of the coated surface by modulating the environmental pH.

Zelikin et al. produced pH-sensitive, cross-linked PMAA capsules by first forming LbL assemblies of thiolated PMAA and poly(vinylpyrrolidone) (PVPON) on silica particles. Cross-linking of the PMAA was done by controlled oxidation of the thiol groups to form disulfide linkages.[72] The silica particles were dissolved, and the neutral PVPON was extracted, leaving a cross-linked PMAA capsule, illustrated in Figure 1.9.

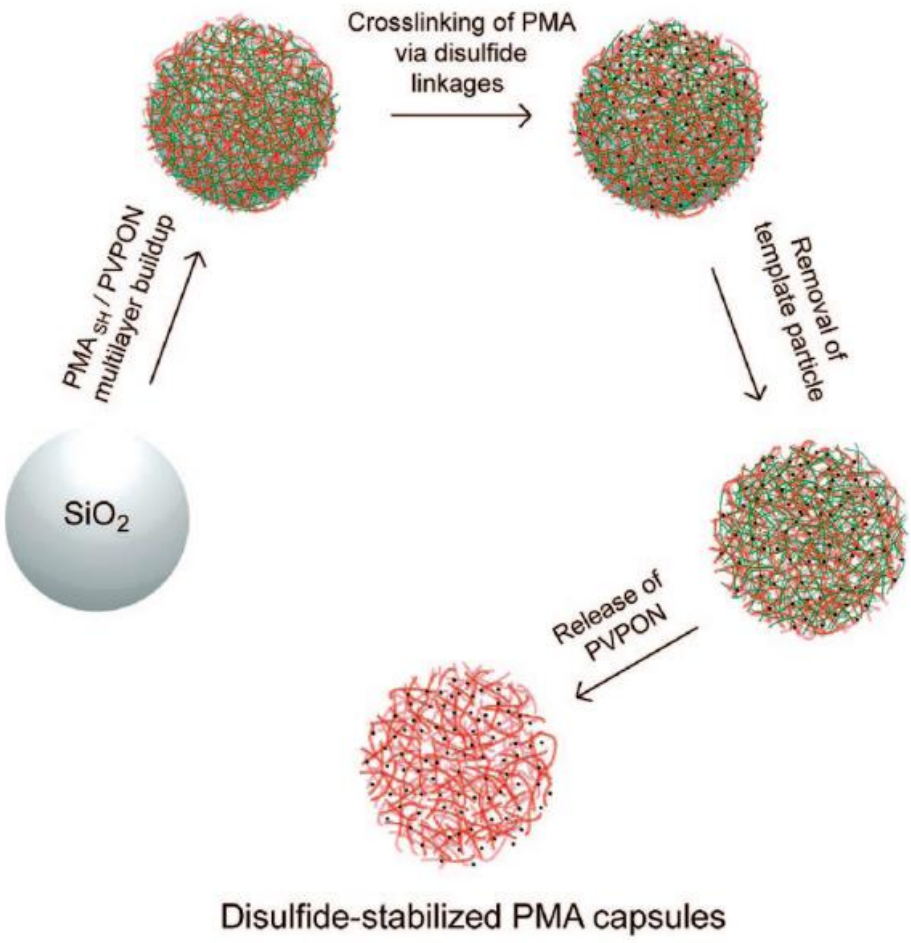

Figure 1.9. Preparation process showing formation of stable cross-linked PMAA capsules using silica particles as a template. Reprinted with permission from ref. 72. Copyright 2008 American Chemical Society.

The controlled degradation of the capsules was tested in an environmental pH of 7.2 in 5 mM solutions of reduced glutathione at 37°C to mimic a biological environment. Capsules were labeled with AF488, and fluorescence was measured over time to observe the rate of degradation. They found that over the course of three hours the capsule radii increased 1.3-fold. Beyond three

hours, the capsules did not maintain spherical shape, and fluorescence became negligible. Similarly, Sukhishvili et al. used the pH sensitivity of the PEO/PMAA and PEO/PAA systems to form erasable hydrogen bonded LbL films.[28-29] The authors report good stability of films when held below the pH_{crit} value. Above this critical value, the films are destabilized by electrostatic repulsion and deconstruct in solution. This dissolution could be hindered by the addition of salt to minimize electrostatic repulsion and keep the multilayer intact. These thin films and capsules make good candidates for biomedical applications like controlled release of therapeutics, and warrant further exploration into their properties and behavior.

Changing temperature is another way to engage the responsive behavior of hydrogen bonded LbL assemblies. Films composed of polymers exhibiting LCST behavior such as poly(N-vinylcaprolactam) (PNIPAM) paired with PMAA undergo microphase separation which can trigger release of water-soluble dye.[24] Swiston et al. demonstrated the temperature-dependent release of living cells from surfaces using hydrogen bonded LbL patches attached to the cell membrane.[73] Swelling and shrinking of the LbL structure with changes in temperature allow for uptake or release of payloads such as drug molecules, and modification of the structure of the hydrogen bonded LbL film or capsule through processes like chemical cross-linking prior to loading of the desired cargo material.

1.3 Thermal Response in LbL Assemblies

Over the past several years, interest in the thermal properties of LbL assemblies has risen considerably, especially with respect to glass transition (T_g) behavior. Understanding the thermal behavior and responsive properties of LbL assemblies in both the dry and hydrated states is key for tailoring such materials for desired applications.

Initial measurements of glass transitions in dry LbL films were conducted by Lutkenhaus et al.[74] Free-standing hydrogen-bonded LbL films of PEO and PAA were analyzed using differential scanning calorimetry (DSC). The authors reported a well-defined T_g, indicative of a fully homogeneous film structure. The T_g was shown to increase with increasing assembly pH. This behavior was attributed to an increase in the PAA content of the films to offset the lack of free carboxylic acid groups available to interact with PEO through hydrogen bonding. Interestingly, the addition of 0.1 M lithium triflate salt made the T_g resistant to change despite increasing assembly pH, likely due to ion-dipole interactions of lithium ions with PEO that facilitate the completion of hydrogen bonding with PAA despite assembly pH alteration. While successful measurement of a T_g of hydrogen-bonded LbL assemblies has been reported, electrostatic LbL assemblies do not exhibit a T_g in the dry state, regardless of adjustments to assembly pH. Rather, they undergo amidation and anhydride formation dependent on film thickness.[75]

The thermal behavior of hydrated electrostatic LbL assemblies has also been explored. Vidyasagar et al. demonstrated the presence of a glass transition in hydrated free-standing PDADMA/PSS LbL films using modulated differential scanning calorimetry (MDSC) and QCM-D.[76] They reported that the presence of salt was necessary to observe the glass transition and that the assembly ionic strength produced no shift in the transition temperature (see Figure 1.10).

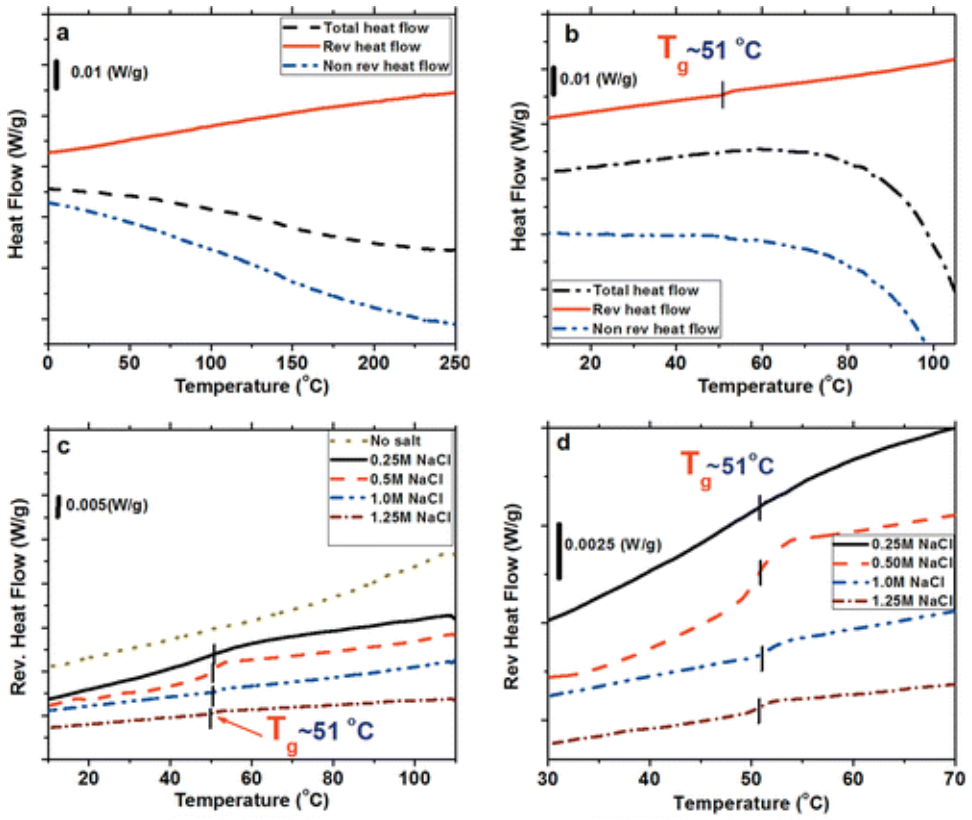

Figure 1.10. MDSC thermograms showing (a) dry PDADMA/PSS LbL films and (b-d) PDADMA/PSS LbL films assembled at various NaCl concentrations in the hydrated state. Reprinted with permission from ref. 76. Copyright 2012 American Chemical Society.

Sung et al. was able to use electrochemical impedance spectroscopy to confirm the presence of glass transition behavior in PDADMA/PSS multilayers.[77] By observing changes in charge transfer resistance data, converted from impedance, with respect to increasing temperature it was found that the glass transition decreased with increasing film thickness and increased with increasing assembly ionic strength from 0.5 M to 1.0 M NaCl.

Molecular simulation work done by the Sammalkorpi group with respect to glass transitions in PDADMA/PSS complexes has indicated that the observed glass transition is linked to the arrangement of water molecules in close proximity to the PSS chains.[78] They report that an increase in temperature leads to a decrease in hydrogen bonding lifetime between water molecules and PSS functional groups, increasing the mobility of the PSS chains. Their simulations show a sharp reduction in hydrogen bonding around 67°C and 72°C, matching closely with reported experimentally obtained T_g values for PDADMA/PSS assemblies. Recently, Zhang et al. reported on the role of salt and water in the mechanical and thermal properties of PDADMA/PSS assemblies.[79] They showed using molecular simulations and MDSC that salt ions facilitate enhanced PE chain mobility through provision of additional free volume as well as weaken intrinsic PDADMA-PSS ion pairing through electrostatic screening. These interactions contribute to plasticization of the network. They also report that binding of salt ions with water in their hydration shells leads to decreased mobility of water molecules within the PDADMA/PSS matrix, reducing plasticization. The effects on the T_g are dependent on the interplay between water and salt present LbL film. This concept is illustrated in Figure 1.11. The glass transition behavior of PDADMA/PSS assemblies and complexes is dependent on this relationship as well. Increased PE mobility when adequate water levels are present leads to earlier onset of long-range molecular motion and, therefore, a lower observed T_g. Conversely, decreased PE mobility at higher ion concentrations when less water is present leads to elevated T_g as the structure is more kinetically locked in place.

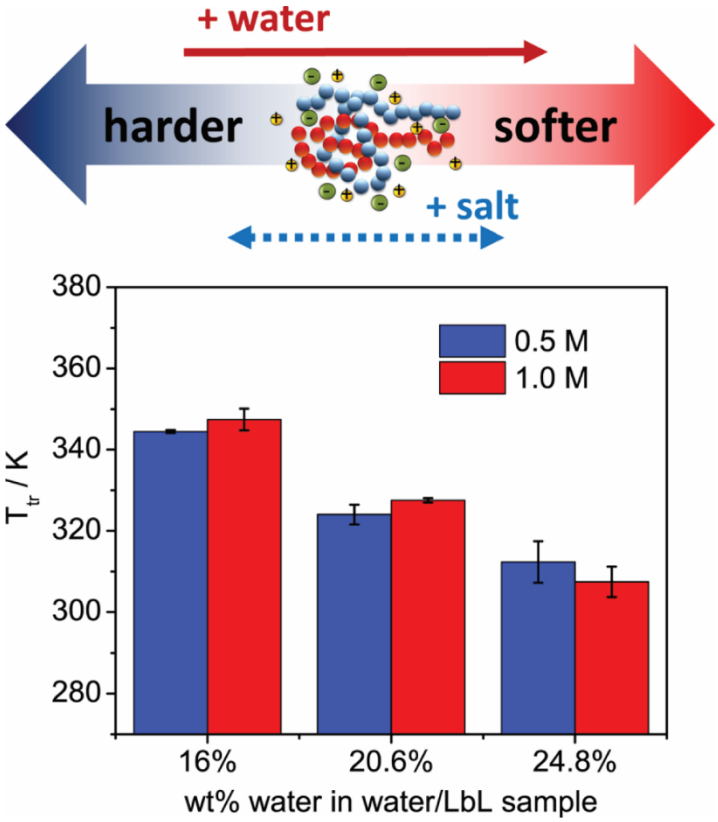

Figure 1.11. Thermal transition (T_{tr}) values for PDADMA/PSS LbL films assembled in NaCl at 0.5 M and 1.0 M ionic strength and hydrated with water of matching salt concentration. Reprinted with permission from ref. 79. Copyright 2017 American Chemical Society.

Reid et al. recently reported on the influence of divalent ions on the thermal transition behavior of PDADMA/PSS LbL assemblies.[41] Free standing films were hydrated to 36 wt % of the dry film mass with aqueous solutions containing $CaCl_2$, $MgCl_2$, and Na_2SO_4 and the thermal transition behavior was analyzed using MDSC (see Figure 1.12). They reported that the T_g of LbL films exposed to Na_2SO_4 showed a more clear dependence on salt concentration, increasing with

increasing salt concentration. The trend was attributed to the stronger interactions of the SO_4^{2-} ions with water than the sulfonate groups of the PSS chains.

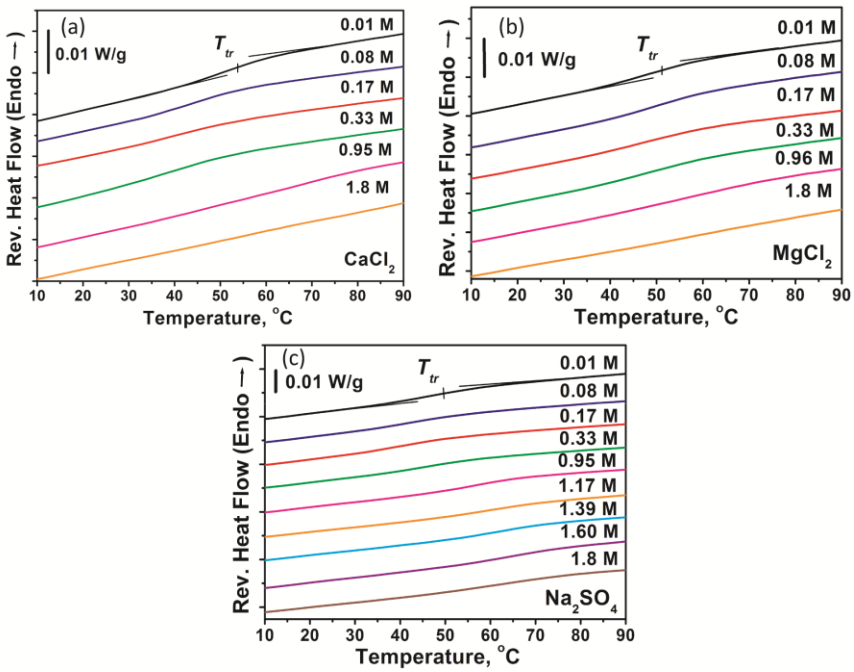

Figure 1.12. MDSC thermograms showing the effect of divalent ions on the thermal transitions of free-standing PDADMA/PSS LbL films hydrated with (a) $CaCl_2$, (b) $MgCl_2$, and (c) Na_2SO_4 at various concentrations. Reprinted with permission from ref. 41. Copyright 2016 American Chemical Society.

These more favorable interactions with water may result in fewer PSS—H_2O interactions, lowering the effectiveness of the water content to plasticize the film structure. Therefore, more energy would be required to initiate a thermal transition. Films hydrated with solutions of $CaCl_2$ and Mgl_2 only exhibited thermal transitions below 0.33 M. They hypothesize that the disappearance of the transition at elevated concentrations is due to more excessive doping of the film and disruption of intrinsic binding sites, driving the transition out of the observed temperature range.

1.4 Thesis Overview

Responsive polymer LbL assemblies have become the subject of a great deal of research in the areas of drug delivery, smart coatings, self-healing materials, separation membranes, and energy storage systems. Much of the work surrounding these materials deals specifically with their assembly and formation under varying conditions, while relatively little work focuses on the post-assembly responsive behavior. The objective of this thesis is to explore the responsive physical and thermal behavior of LbL assemblies with respect to changing post-assembly conditions.

Chapter II presents the physical, optical, and pH-responsive properties of PEO/PMAA LbL films fabricated using spray-assisted LbL assembly. This system has been known to dissociate above a pH_{crit} of 4.5, and has been used to demonstrate the release of a small molecule dye.[28-29] Chapter II discusses the formation of PEO/PMAA LbL films containing discrete layers of AuNPs separated by "empty" regions of polymer film. TEM is employed to study the internal structure of the resulting films, and the optical properties are analyzed using UV-Vis spectroscopy and optical microscopy. The time-dependent release of the AuNPs is reported as a function of pH of the

surrounding environment. The thermal properties of Lbl assemblies made from PEO and PMAA have been reported previously.[80]

Chapter III discusses the swelling response of PDADMA/PSS LbL films assembled in NaCl with respect to changing ionic environment using QCM-D. This technique has been used to study the growth behavior, mechanical properties, and ionic effects of LbL assemblies with high sensitivity and accuracy.[18, 41, 66] Swelling and contraction of PDADMA/PSS LbL films in the presence of a wide concentration range of KBr is explored, and a relationship between concentration and structural changes is elucidated. Swelling behavior of films in the presence of KBr, NaBr, KCl, and NaCl are also compared, and conclusions about the observed differences in response are discussed. Additionally, free-standing PDADMA/PSS LbL films are subjected to ion exchange with various KBr concentrations and the ion content is quantified using NAA.

Chapter IV gives an overview of ongoing research efforts dealing with the influence of ion type, salt concentration, and hydration level on the T_g of free-standing PDADMA/PSS LbL films. Some preliminary data is shown, and a brief discussion of expectations and future work is included.

CHAPTER II

HYDROGEN-BONDED POLYMER NANOCOMPOSITES CONTAINING DISCRETE LAYERS OF GOLD NANOPARTICLES*

2.1 Introduction

Metallic nanoparticles have generated interest because of their unique optical and electrical properties. Specifically, gold nanoparticles (AuNPs) have been utilized for numerous applications including drug-deliv[1]ery, surface-enhanced Raman spectroscopy, optoelectronics, biosensing and imaging, and photothermal therapy in cancer treatment.[81-87] It is often desired to leverage AuNPs by incorporating them into polymer nanocomposites, but aggregation of the nanoparticles is a severe challenge.[88-91] This is often addressed by controlling interactions between the AuNP ligand and the polymer matrix,[92-95] yet this does not wholly address pre-programmed spatial placement of the NP within the polymer matrix.

Layer-by-layer assembly, a technique by which organic and inorganic multicomponent films are built up on various substrates through complementary interactions of the adsorbing species, offers an opportunity for controlling the spatial placement of nanoparticles vertically within a film with nanometer-scale precision.[52, 96-97] Complementary interactions between species can be electrostatic (alternating between positively and negatively charged species) or secondary forces like Van der Waals and hydrogen bonding. The species used to build up the film do not

---

* Reprinted from "Hydrogen-bonded polymer nanocomposites containing discrete layers of gold nanoparticles" by Joshua T. O'Neal, Matthew J. Bolen, Yichen Y. Dai, and Jodie L. Lutkenhaus, *J. Colloid Interface Sci.* **2017,** *485*, 260-268, copyright 2017 American Chemical Society.

have to be explicitly polymers and can include biological molecules and inorganic nanoscale fillers for a range of applications.[5, 27, 80-81, 83, 98-101] For example, AuNPs have been assembled into LbL nanocomposites films to demonstrate tunable conductivity,[50, 102] sensing platforms,[10] drug delivery,[27, 82, 100] and optoelectroics.[103] The vast majority of these studies have dealt with the LbL assembly of AuNPs by electrostatic interactions and by a form of LbL assembly called "dip-assisted" LbL assembly, which relies on total immersion of the substrate.[98-99, 104-106]

Fewer studies have been dealt with hydrogen-bonded LbL systems with AuNPs, which are interesting alternatives to their electrostatic counterparts. The pH sensitivity of hydrogen-bonded multilayer systems renders them stimuli-responsive with tunable, switchable properties for potential use in biomedical applications such as drug delivery systems.[27, 100-101, 107] The ability to add non-charged molecules or particles to the hydrogen-bonded composite structure is also of interest for sensor-type or delivery-type systems that utilize changes in environmental conditions to release pay-loads through controlled dissolution of the LbL structure.[27] In one example, the Tsukruk group reported the reversible controlled distribution of gold nanorods (AuNRs) within hydrogen-bonded poly(*N*-vinylpyrrolidone)(PVPON)/PMAA multilayer films by changing the pH of the environment, which altered the optical properties of the films.[8]

AuNP-containing multilayer films have been prepared by dip-assisted and spin-assisted LbL assembly methods.[8, 10, 50] Dip-assisted LbL assembly is based on the immersion of the substrate, whereas spin-assisted LbL assembly is based on spin-coating. Both dip-assisted and spin-assisted LbL assembly approaches have drawbacks. Dip-assisted LbL assembly requires relatively long adsorption times, on the order of 1-15 minutes per layer. On the other hand, spin-assisted LbL assembly is much more rapid, on the order of seconds per layer; however, this approach is limited to flat substrates. The spray-assisted LbL technique is perhaps more suitable,

where adsorbing species are alternately sprayed onto a substrate. This requires only a few seconds of exposure and is applicable to a wide range of substrate materials with varying geometries.[13, 102, 108-110] Negatively charged AuNPs have been assembled with a polycation by spray-assisted LbL assembly successfully using electrostatic interactions.[111] However, AuNP-containing hydrogen-bonded multilayer films made by spray-assisted LbL assembly have not yet been reported in the literature.

Here, we report hydrogen-bonded multilayers made by dip-assisted and spray-assisted LbL assembly in which AuNP-rich layers are placed at predetermined depths within the film. PEO/PMAA was selected as the model hydrogen-bonded system,[27-29, 80, 108] for which PEO acts as the hydrogen bond acceptor and PMAA acts as the hydrogen bond donor. This system is pH-responsive, having a reported critical pH of 4.5 above which hydrogen bonds become disrupted.[28] AuNPs were selected as the nanoscale filler because of their optoelectronic properties, which allow us to track aggregation and LbL dis-assembly. The layered nanocomposite structure was verified using TEM, and the distance between the AuNP-rich layers was varied by altering the number of PEO/PMAA layer pairs between AuNP exposures. UV-Vis spectroscopy was used to determine AuNP aggregation (or lack thereof) as well as the time-dependent release of AuNPs from a film exposed to an environmental pH above the critical pH. We hypothesized that incorporating AuNPs into pH-sensitive systems like PEO/PMAA at predetermined depths separated by predictable, variable distances should result in tailorable delivery timescales. This investigation lends a fundamental understanding of the resulting structure of LbL nanocomposites upon addition of AuNPs to PEO/PMAA LbL films using dip- and spray-assisted LbL assembly.

2.2 Experimental

2.2.1 Materials

Poly(ethylene oxide) (PEO) (M_w = 4,000,000 g/mol and M_w = 100,000 g/mol, Sigma Aldrich) and poly(methacrylic acid) (PMAA) (M_w = 100,000 g/mol, Polysciences) were used as received. Chlorauric acid (99.999% trace metal basis, Sigma Aldrich) and trisodium citrate dihydrate (Sigma Aldrich) were used to prepare the AuNP colloidal suspension. Linear poly(ethyleneimine) (LPEI) (M_w = 25,000 g/mol, Polysciences) and poly(acrylic acid) (PAA) (M_w = 50,000, Polysciences) were used as received. For the LbL assembly processes, the PEO and PMAA solutions were prepared with a concentration of 20 mM in Milli-Q water based on repeat unit, and the pH was adjusted to 4 using HCl and NaOH stock solutions. Indium tin oxide (ITO) coated glass slides (Delta Industries) were used as substrates for the LbL assembly procedures. Poly(glycidyl methacrylate) (PGMA, M_w = 25,000 g/mol, Polysciences) was used as-purchased for surface treatment of the substrates.

2.2.2 Preparation of AuNP Colloidal Suspension

The AuNP suspension was prepared using the traditional Turkevich Method.[102, 112] In short, chlorauric acid (1 mM in water) was brought to a boil using a hot plate. A 1 wt% solution of trisodium citrate dihydrate in water was added to the boiling chlorauric acid solution and stirred vigorously for 15 min then removed and allowed to cool to ambient temperature. The solution turned from yellow to clear to black to a deep red color, indicating the completion of the AuNP formation process. The AuNP suspension was kept refrigerated away from light until use to prevent aggregation. The resulting AuNPs were examined using transmission electron microscopy (TEM), and the average diameter was determined to be roughly 15-20 nm.

2.2.3 Substrate Preparation for LbL Film Fabrication

ITO-coated glass substrates were cleaned *via* sonication in 0.5 M NaOH for 10 min followed by rinsing with Milli-Q water and blow-drying with nitrogen gas. The substrates were then immersed in a water/NH_4OH/H_2O_2 (5:1:1 by volume) solution at 75°C for 20 min followed by rinsing three times and sonication in Milli-Q water for 5 min three times. After the rinsing step, the substrates were blow-dried and treated with O_2 plasma for 10 min under vacuum. Next, the substrates were immersed in 0.1% PGMA in methyl ethyl ketone (MEK) solution for 3 min followed by annealing in a convection oven at 110°C for 30 min.[108] After annealing, the substrates were rinsed with MEK 3 times at room temperature. Finally, the substrates were immersed in a PMAA (20 mM in water) solution at room temperature for 20 min followed by annealing at 110°C for 30 min and a final rinsing step with Milli-Q water.

2.2.4 Substrate Preparation for pH-modulated Release Study

ITO-coated glass substrates were exposed to O_2 plasma and PGMA surface treatments as previously described. Then, 4 layer pairs of LPEI and PAA were deposited as anchor layers to initiate film growth. The LPEI/PAA initial layers were used to initiate film growth because a substantially thick initial layer of PEO/PMAA was not necessary as it would not influence the absorbance spectrum of the films during dissolution and release of the AuNPs.

2.2.5 Substrate Preparation for Cross-sectional TEM Analysis

For TEM analysis Dupont Tiejin ST505 7-mil PET was used as the substrate material. PET was cleaned by rinsing with methanol and DI water (4x). They were then exposed to O_2-plasma for 10 min prior to LbL assembly, and PGMA treatment was not conducted.

2.2.6 Dip-assisted LbL assembly of Hydrogen-bonded PEO/PMAA Films and PEO/PMAA Nanocomposite Films Containing AuNPs

PEO/PMAA films were fabricated using a programmable slide-stainer (HMS Series, Carl Zeiss, Inc.). Treated ITO-coated glass substrates were immersed in the PEO solution (20 mM in Milli-Q water by repeat unit) for 15 min followed by 3 consecutive rinsing steps in deionized water baths for 2, 1, and 1 min. The substrates were then immersed in the PMAA solution (20 mM in Milli-Q water by repeat unit), for 15 min followed by the same rinsing pattern. The pH was adjusted to 4 for all solutions. This cycle constitutes a layer pair, and was repeated *n* times. Hence, LbL films of PEO/PMAA are denoted $(PEO/PMAA)_n$ where *n* is the number of layer pair cycles.

AuNP-containing nanocomposite films were prepared using similar methods as described for $(PEO/PMAA)_n$ films with some modification to the procedure. Periodically, PEO/AuNP layers were deposited by hand instead of PEO/PMAA layers. To do this, the films were immersed in PEO solution for 15 min followed by rinsing in deionized water for 2, 1, and 1 min. The films were subsequently immersed in AuNP suspension for 14 min followed by the same rinsing steps (following prior literature[102]). The pH was adjusted to 4 for all solutions.

2.2.7 Spray-assisted LbL Assembly

As in the dip-assisted LbL procedure just described, identical solutions of the same concentration (20 mM) as well as pH (4) were used for spray-assisted LbL assembly of the $(PEO/PMAA)_n$ films. Films prepared on ITO-coated glass and Dupont Tiejin ST505 7-mil PET (for TEM imaging) were cleaned and exposed to O_2-plasma as mentioned earlier. The PET substrates were not subjected to PGMA surface treatment because the required annealing

temperature was too high. The films were assembled using an automated spraying system (Svaya Nanotechnologies). All substrates used for spray-assisted LbL assembly were placed roughly 20 cm away from the spray nozzles, and the solutions were sprayed at a pressure of about 40 psi. First, the PEO solution was sprayed on the substrate for 10 s followed by 10 s of draining and 10 s of rinsing with Milli-Q water with a 10 s pause to allow excess solution to drain between layer pair cycles. The PMAA solution was then sprayed following the same pattern. This deposition cycle was repeated until the desired number of layer pairs (n) were deposited on the surface.

Nanocomposite films containing AuNPs were prepared in a similar fashion to the AuNP-free films. The assembly pH was adjusted to 4 for all solutions as well as the AuNP suspension. Initial layers of PEO/PMAA (typically around 50 layer pairs) were deposited as base layers in order to ensure substantial growth behavior of the film. We found that films produced using fewer initial PEO/PMAA layer pairs were much thinner than those produced with a more substantial base layer of PEO/PMAA. Once the base layers were complete, alternating layers of PEO solution and AuNP suspension were deposited using the same timing parameters as mentioned in the previous section until the desired number of PEO/AuNP layer pairs (m) was achieved. Then, a predetermined number of PEO/PMAA layer pairs was deposited in order to separate the previous $(PEO/AuNP)_m$ region from the next one. This spraying sequence was repeated until the desired amount of $(PEO/AuNP)_m$ regions was achieved. The film was then capped with a final layer of $(PEO/PMAA)_s$, where s varied from 10-20 layer pairs.

For the pH-responsive study, nanocomposite films were prepared *via* spray-assisted LbL assembly. In order to facilitate initial growth of the film, anchor layers of $(LPEI/PAA)_4$ were deposited onto the substrate. The $(LPEI/PAA)_4$ anchor layers were used in place of

$(PEO/PMAA)_{50}$ for these films in order to expedite film fabrication time while still achieving a good foundational layer for quality film growth. All layer pairs were sprayed using the same standard parameters listed previously. Subsequently, $(PEO/AuNP)_m$ regions, where *m* denotes the number of layer pairs, and separator $(PEO/PMAA)_n$ regions, where *n* was either 2 or 12 layer pairs, were deposited to build up the nanocomposite containing discrete regions of AuNPs. Once the desired film composition was achieved, the films were capped with $(PEO/PMAA)_{10}$.

2.2.8 TEM Analysis

Cross-sectional TEM imaging was done using a TECNAI F20 Super-Twin transmission electron microscope fitted with a Schottky field emission gun, a 2k × 2k Gatan CCD camera. Distances between AuNP-rich regions of the composite films as well as AuNP sizes were calculated using Digital Micrograph™ software. Dimensions of the films were calculated using scale bars integrated into each image. The nanocomposite LbL films for TEM analysis were prepared in a similar manner to those built upon ITO-coated glass substrates, but Dupont Tiejin ST505 7-mil PET was used as the substrate material instead. The TEM substrates were cleaned by rinsing with methanol and DI water (4x). They were then exposed to O_2-plasma for 10 min prior to LbL assembly. Samples prepared on PET substrates were cut down to 1 mm × 1.5 cm strips and embedded in epoxy using a silicon mold. They were then placed in a vacuum chamber until air pockets were sufficiently removed from the epoxy. The epoxy-embedded substrates were then held at 40°C overnight. Finally, the samples were trimmed to the appropriate size *via* microtoming with care not to damage the LbL film for imaging.

2.2.9 UV-Vis Spectroscopy

UV-Vis spectroscopy was conducted using a Shimadzu SolidSpec-3700 UV-Vis-NIR spectrophotometer. For the AuNP-release study, dry AuNP-containing nanocomposite films on ITO-glass substrates were placed immersed in water and the pH was adjusted in order to induce disruption of the hydrogen bonds. Aliquots of the solution were taken and the absorbance was measured at selected times throughout the experiment in order to monitor the breakdown of the films. After each measurement, the aliquot sample was returned to the film environment to avoid concentration changes that would accompany change in volume. The final pH generally decreased, but remained well above pH 4.5.

2.2.10 Profilometry

Thickness was measured using profilometry (Alphastep D-100, KLA-Tencor). Measurements were taken in at least three different locations across each sample to obtain an average thickness.

2.3 Results and Discussion

2.3.1 Cross-sectional TEM Analysis

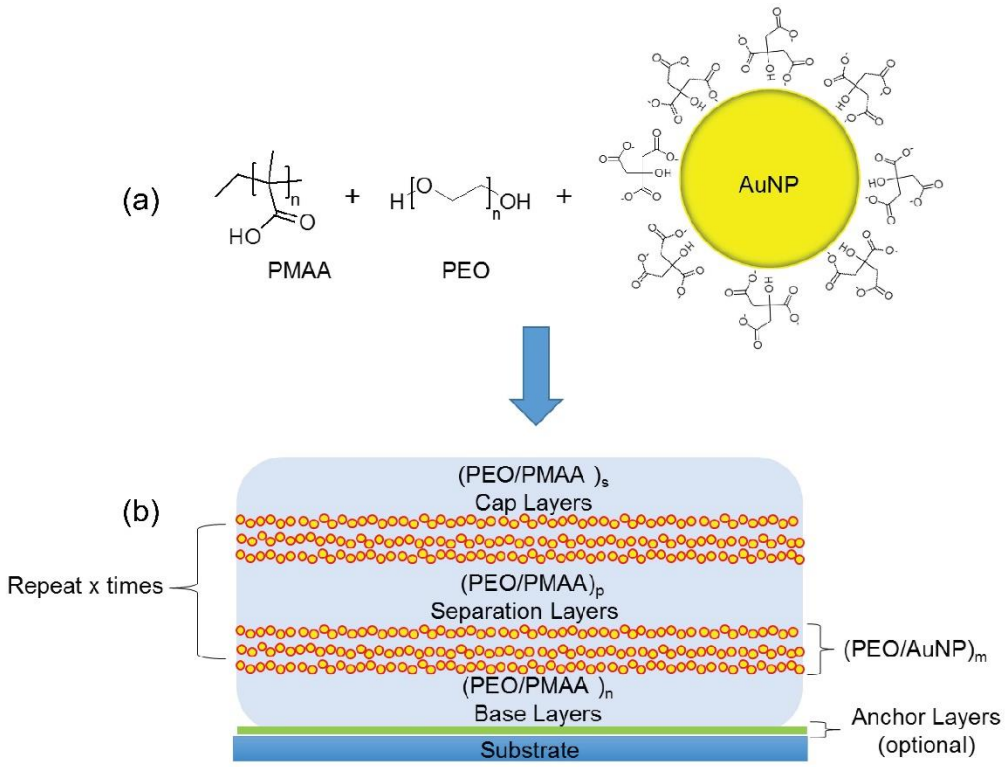

Figure 2.1. (a) Chemical structures of polymers used in the hydrogen-bonded system and illustration of the structure of the citrate-stabilized AuNPs used as nanoscale filler (not drawn to scale) and (b) an illustration of the cross section of an AuNP-containing LbL composite film.

Figure 2.1a shows an illustration of the citrate-stabilized AuNP. For simplicity, only the citrate ligands are shown on the AuNP surface, although it has been shown that some additional oxidation products can form on the surface during the synthetic process.[113-114] In our study, we assume that any effects these impurities may cause are minimal and have no impact on the results

of the study. Figure 2.1b show an LbL assembled nanocomposite films containing discrete regions of AuNPs throughout the film structure. We were able to achieve this type of film architecture using spray-assisted and dip-assisted LbL assembly. The structure of the $(PEO/PMAA)_n/[(PEO/AuNP)_m/(PEO/PMAA)_p]_x/(PEO/PMAA)_s$ nanocomposites film- where *n*, *m*, *p*, *x*, and *s* represent the number of layer pairs making up that region of the film - consisted of base layers to facilitate growth, intermediate layers where there were discrete regions of AuNPs, and cap layers to facilitate TEM imaging and cargo-release studies.

Figure 2.2 (a-b) shows cross-sectional TEM images of dip-assisted nanocomposite films prepared at pH 4 with and without $(PEO/AuNP)_m$ layers for comparison. The pH was adjusted to 4 in order to keep the AuNPs from flocculating and also to stay below the pH_{crit} of the $(PEO/PMAA)_n$ system. In this manner, the entire assembly process proceeded by hydrogen bonding interactions. The regions containing the AuNPs consisted of $(PEO/AuNPs)_1$ separated by $(PEO/PMAA)_2$. It can be seen in the image that the early stages of the film growth show a higher concentration of AuNPs closer to the substrate, with a clear decrease in relative concentration as the number of PEO/AuNPs deposition cycles increased. This was attributed to aggregation of the AuNPs within the reservoir bath used for the dip-assisted LbL process. The aggregation was likely due to loosely bound polymer chains detaching from the substrate into the AuNP suspension during the deposition step (i.e. cross-contamination). Visual verification of the aggregation could be seen in the color change of the AuNP suspension from deep red to a nearly black color throughout the course of the experiment. Cloudy flocculation of the AuNPs could also be seen in the solution after only a few deposition cycles.

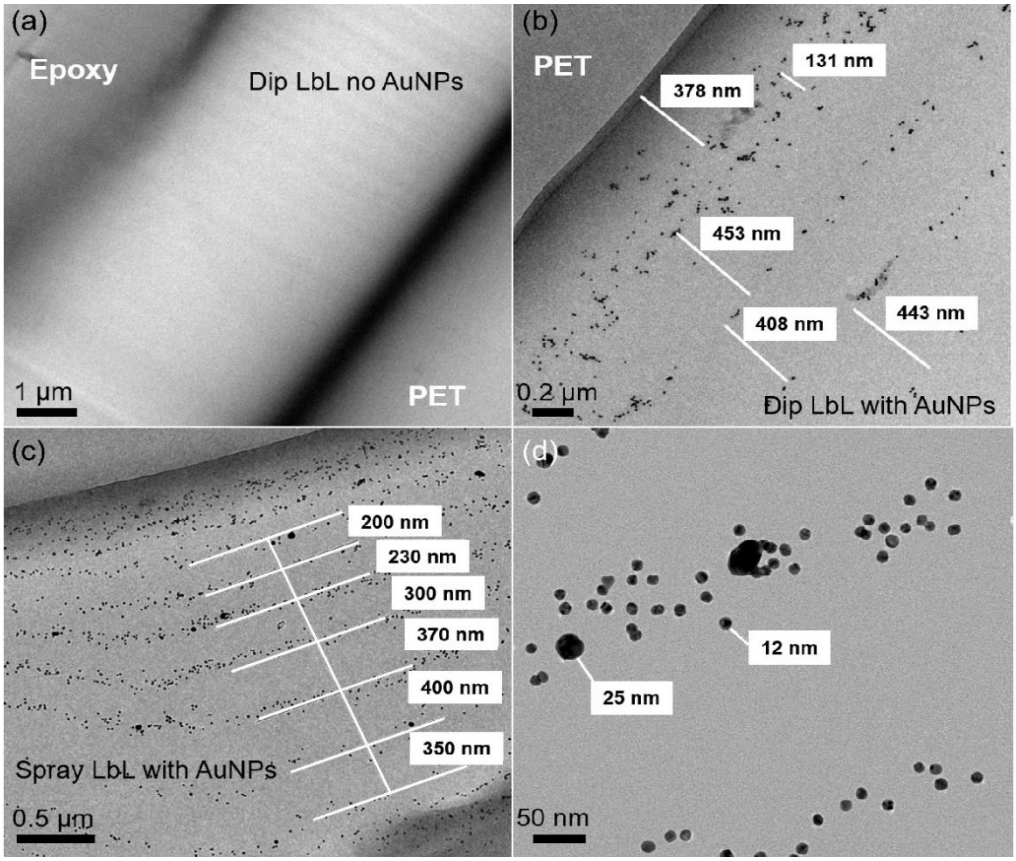

Figure 2.2. TEM images of (a) dip-assisted LbL PEO/PMAA films containing no AuNPs, (b) dip-assisted LbL nanocomposite containing several $(PEO/AuNPs)_1$ regions separated by $(PEO/PMAA)_2$, (c) spray-assisted LbL PEO/PMAA nanocomposite consisting of several $(PEO/AuNPs)_3$ regions separated by $(PEO/PMAA)_{12}$, (d) high-magnification image showing relative sizes AuNPs within the film prepared by spray-assisted LbL assembly. The labels in panels b-c correspond to average distance between Au-rich regions.

In order to eliminate the issue of AuNP aggregation during film buildup, the spray-assisted LbL technique was employed. Using this technique, the possibility of aggregation was minimized because the substrates and polymer chains loosely bound to the film surface no longer directly contacted the AuNP suspension. Figure 2.2 (c) shows a cross-sectional TEM image of one of the nanocomposite films. AuNP-rich regions of the film consisting of $(PEO/AuNPs)_3$ were separated by $(PEO/PMAA)_{12}$. These TEM images show the successful inclusion of distinct, discrete regions of AuNPs separated by "empty" AuNP-free regions. Based on these images, the observed individual layer pair thickness for the PEO/PMAA regions of the spray-assisted LbL film was significantly thinner than that of the dip-assisted regions in which the $(PEO/AuNP)_1$ region was separated by $(PEO/PMAA)_2$. Specifically, the separation between Au-rich regions was 400 nm for $(PEO/PMMA)_2$ by dipping and around 300 nm for $(PEO/PMAA)_{12}$ by spray. This was expected, as previous work demonstrates that spray-assisted LbL generally results in thinner layers.[108] Spray-assisted LbL also affords significantly faster layer-pair deposition times. For films of identical composition, the time scale for sample production can drop from several days to a few hours or minutes, depending on the desired number of layer pairs being deposited.

To examine the effect of the number of PEO/PMAA separation layers (denoted as p in Figure 2.1) in spray-assisted LbL films, two films were prepared at p = 2 and 12 layer pairs. As p increases, the distance between AuNP-rich regions should increase. All other layer pair numbers were fixed as: $(PEO/PMAA)_{15}/[(PEO/AuNPs)_3/(PEO/PMAA)_p]_{50}/(PEO/PMAA)_{10}$. For comparison, an AuNP-free LbL film composition of $(PEO/PMAA)_{520}$ was prepared, which would be analogous to a case where p =12 layer pairs. The films produced with $(PEO/PMAA)_2$ separation layers were significantly thinner than those with separation layers of $(PEO/PMAA)_{12}$ (530 nm vs

4.3 μm, respectively). The thickness of the AuNP-free film was 4.9 μm, slightly higher than the *p* =12 AuNP-containing case. These results indicate indirectly that the separation distance can be tuned by adjusting the number of PEO/PMAA layer pairs *p* between AuNP-rich regions. This demonstrates that a high degree of control over the placement, spacing, and relative concentration per AuNP-rich region can be achieved through changing the number of PEO/PMAA layer pairs separating the AuNP-rich regions or by adjusting the number of PEO/AuNP layer pairs in each of those regions, respectively.

2.3.2 Optical Microscopy

The surface morphology of the PEO/PMAA nanocomposites containing AuNPs was examined using optical microscopy (see Figure 2.3). The films and nanocomposites produced by spray-assisted LbL assembly had smooth surfaces with few defects, similar to previous reports for spray-assisted LbL films consisting of PEO/PMAA.[108] Previous reports on the surface morphology of dip-assisted LbL films consisting of PEO/PMAA attribute roughness on the surface to the hydrophobic interactions between the α-methyl groups on the PMAA backbone.[115] Similar surface roughness behavior was observed by Seo et al. where LbL assemblies of hydrophobically modified PEO and poly(acrylic acid) (PAA) showed large surface grains resulting from PEO micelle formation.[116] In contrast, the smoother morphological nature of spray-assisted LbL films observed here could be due to insufficient time for chain penetration and rearrangement during assembly. Additionally, the shorter contact time afforded by spray-assisted LbL assembly combined with the possibility of chain spreading during the spray process could be responsible for the smooth surface morphology of these films.[117] Figure 2.3 (a) and (b) show some visible features on the surface while (c) shows none. These features are likely caused by phase-separated regions of PEO and

PMAA. The lack of these features on the surface of the LbL nanocomposites with $p = 2$ separation layers could be indicative of the effect of the AuNPs on the interactions between PEO and PMAA. It should also be noted that the LbL nanocomposites with $p = 2$ separation layers were significantly thinner (less than one micron) than the NP-free and the nanocomposites with $p = 12$ separation layers. These thin nanocomposites consist of significantly less polymer while the number of AuNP layers deposited for both $p = 12$ and $p = 2$ nanocomposites were kept the same.

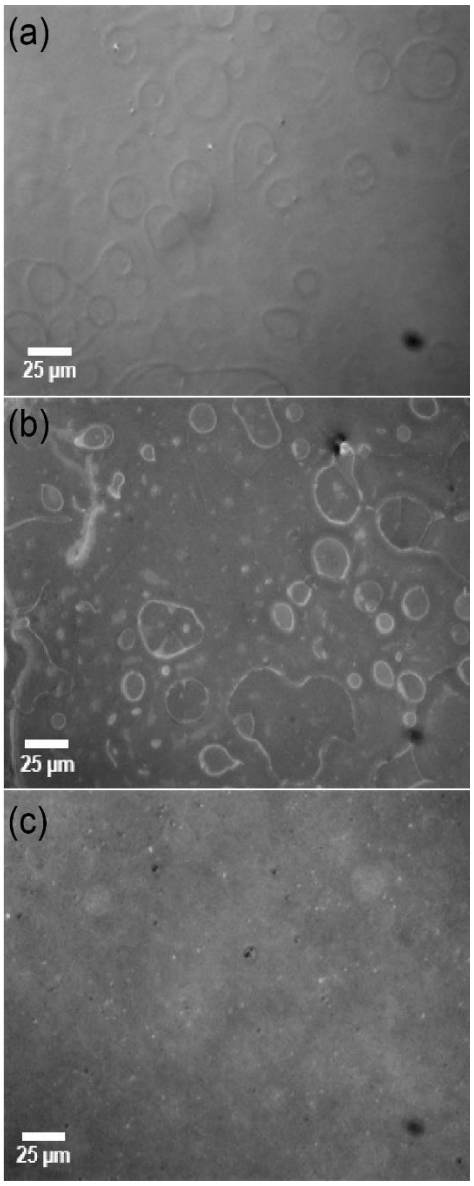

Figure 2.3. Optical microscopy images showing the surface morphology of (a) PEO/PMAA AuNP-free (b) PEO/PMAA nanocomposite with p = 12 and (c) PEO/PMAA nanocomposite with p = 2 LbL films produced by spray-assisted LbL assembly. Images taken at 20x magnification using reflected light. All samples have capping layers of $(PEO/PMAA)_{10}$.

2.3.3 UV-Vis spectroscopy

Spray-assisted PEO/PMAA LbL films with and without AuNPs were analyzed using UV-Vis spectroscopy. Figure 2.4 shows UV-Vis spectra for films of separation layers p = 2 and 12 and of $(PEO/AuNPs)_3$. These films were designed such that the number of AuNP layers are equal for both p = 2 and 12. Notably, the peak absorbance values were similar for both p = 2 and 12, suggesting that these two samples have a similar number of AuNPs. Further, the peak positions are similar at 530 nm, indicating that the AuNPs have similar environments. No significant red-shift in the spectrum was observed, as compared to an AuNP suspension, implying that there was no major aggregation of AuNPs within the film matrix during or after the film deposition process. However, the slight increase in absorption in the 600-900 nm range of the spectra for the nanocomposite films compared to the pure AuNP solution is likely the result of some lateral aggregation within the nanocomposite.[118] This suggests that some small amount aggregation may occur locally within the segregated regions of the film containing AuNPs, causing the slight absorption increase at the higher wavelengths.[119] No significant aggregation of the nanofiller at the surface or within the film implies that spray-assisted LbL provides good control over the dispersion of the AuNPs across the surface of the film during deposition.

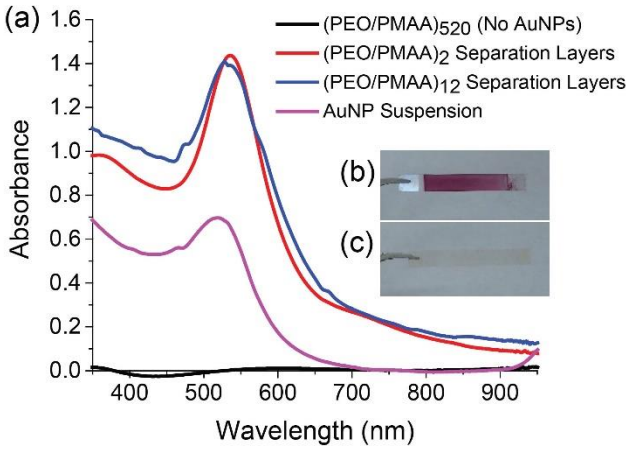

Figure 2.4. (a) UV-Vis spectra showing the absorbance of LbL films fabricated by spray-assisted LbL assembly with and without AuNPs and the as-prepared AuNP suspension. The film compositions presented are $(PEO/PMAA)_{15}/[PEO/AuNPs)_3/(PEO/PMAA)_p]_{50}/(PEO/PMAA)_{10}$ where *p* was 2 (red) or 12 (blue) and $(PEO/PMAA)_{520}$. (b-c) Digital images of a PEO/PMAA film containing discrete regions of AuNPs and pure $(PEO/PMAA)_{520}$ film containing no AuNPs, respectively.

2.3.4 pH-responsive Gold Release Study

The pH-responsive behavior of the nanocomposite films was next explored. This was motivated by the reported pH-responsive properties of the hydrogen-bonding PEO/PMAA system (without AuNPs).[28-29] Previously, the pH-driven deconstruction of PEO/PMAA films was demonstrated by the release of a small molecule dye (Rhodamine 6G) embedded in the film upon exposure to an environmental pH above the pH_{crit} of the polymer film (4.5). At a slightly elevated pH of 5.5, hydrogen bonds were disrupted because of the increase in the ionization of carboxylic acid pendant groups along the PMAA chain. This disruption was followed by electrostatic repulsion among the (COO^-) groups and a change in the physical conformation of the polymer

from a more coiled structure to a more extended structure. The breaking of the hydrogen bonds coupled with the change in chain conformation resulted in the dissolution of the film, and release of the dye contained therein.[23] Here, we demonstrate a pH-responsive, time-dependent release of AuNPs from PEO/PMAA nanocomposites containing AuNPs fabricated using spray-assisted LbL assembly.

Nanocomposite films were prepared *via* spray-assisted LbL assembly with the composition $(LPEI/PAA)_4/[(PEO/AuNP)_3/(PEO/PMAA)_{12}]_{50}/(PEO/PMAA)_{10}$. Dried samples were immersed in 10 mL of water at pH 10 and pH 11 - well above the reported pH_{crit} of the hydrogen bonded system[23] - and stirred vigorously using a small stir bar. As described earlier, the elevated pH induced the breakdown of the LbL nanocomposite structure through disruption of the hydrogen bonds. This breakdown resulted in the release of the AuNPs into the local environment. The release of AuNPs was monitored by retrieving aliquots from the solution and collecting UV-Vis spectra over the course of several hours (see Figure 2.5).

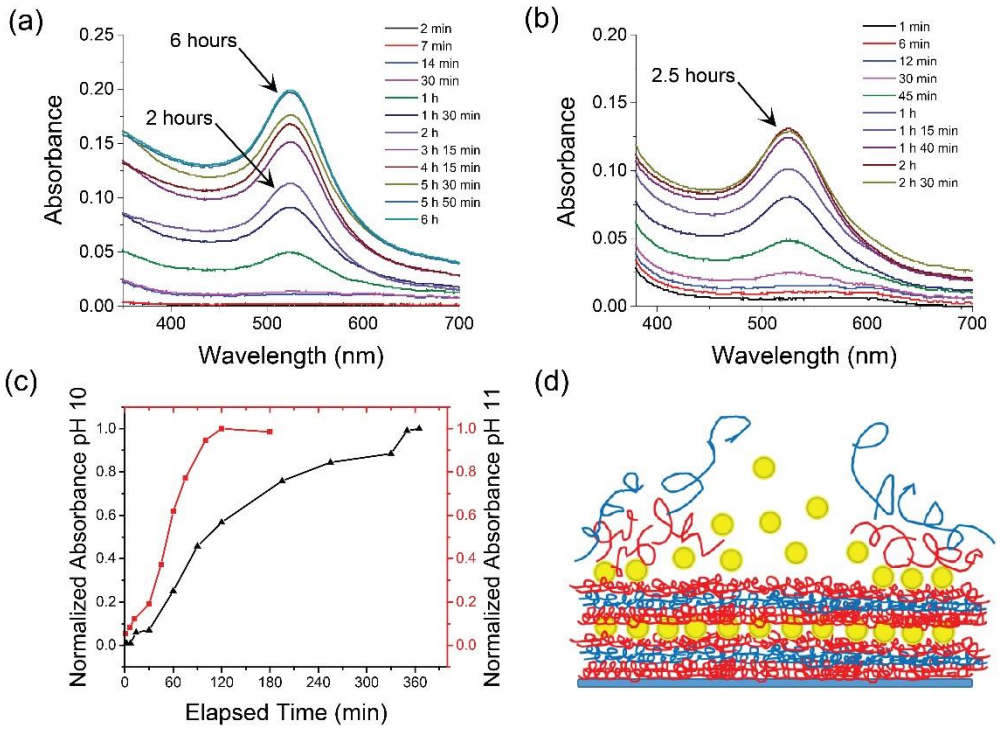

Figure 2.5. (a-b) UV-Vis data collected from a payload release experiment on AuNP-containing nanocomposite films exposed to pH 10 and 11 solutions, respectively, and (c) normalized absorbance with respect to time showing the progression of release of the AuNP payload at both pH levels at a wavelength of 525 nm. (d) An illustration of LbL dis-assembly and release of AuNPs. All films were made by spray-assisted LbL assembly.

As expected, the release of the AuNPs took place faster at pH 11 than at pH 10 because of the greater driving force for film deconstruction. In both cases, the nanocomposites completely dissociated into solution, releasing their entire payload. This is denoted by a steady increase in the peak at 525 nm, attributed to the AuNPs being released into the surrounding solution. Although the data above demonstrates successful erasability of the nanocomposite film and time-dependent

delivery of the AuNP payload, the time scale of the film dissolution was generally longer (on the scale of hours) than expected. It has been shown by the Sukhishvili group that hydrogen bonded films released a dye payload rapidly (on the scale of seconds) upon increasing the pH above the pH_{crit} of the system, but those results were for the release of small molecules, not large nanoparticles, as in our case.[23] Many payload delivery systems reported in the literature deal specifically with single component hydrogels or cross-linked networks that respond to environmental stimuli and rely on swelling and deswelling and diffusion of the payload from the matrix for delivery.[120-123] The differences in the time scale of the release are most likely connected to the large size and mass of the AuNP as compared to that of a small molecule.

We hypothesize that the brief study here shows release of the AuNPs by simple diffusion from the surface of the film as the dissolution takes place. Since no crosslinking was induced by post processing methods, it is likely the film dissolution of the PEO/PMAA layers occurred rapidly as expected. However, the limiting factor involved in the release of the AuNPs could possibly be attributed to favorable interactions (i.e. hydrogen bonding and Van der Waals forces) between the PEO and citrate ligands on the AuNP surfaces. The relatively high surface area of the 15-20 nm diameter particles provides good contact between the AuNPs and the surrounding polymer chains, which could lead to slower diffusion from the surface despite the higher pH of the environment causing disruption of the hydrogen bonds. This may also to possible ligand exchange and chelation with ionized PMAA groups that may also hinder the release. One might have expected a burst-type release from the film, had there been steady surface erosion, but this was not observed. Perhaps this might be attained by increasing the *p*, the number of layer pairs separating the AuNP-

rich regions. In general, the AuNP release from PEO/PMAA LbL assemblies demonstrates the possibility of delivering or controlling payload release using a pH trigger.

2.4 Conclusion

A highly efficient and well-organized method of polymer nanocomposite fabrication was utilized to produce hydrogen-bonded layer-by-layer films containing discrete regions of gold nanoparticles. The hydrogen-bonding polyelectrolytes used in this study were utilized as a vehicle for time-dependent release of the gold nanoparticles when exposed to pH conditions sufficient to disrupt the secondary bonding. These results verified our hypotheses that spray-assisted LbL assembly could be leveraged to controllably place AuNPs through the thickness of the thin film and that the hydrogen-bonding interactions could lead to the programmed dis-assembly of the film and AuNP release.

The high degree of control over the internal structure and placement of the gold nanoparticles provided by the spray-assisted layer-by-layer assembly method offers a vast improvement over alternative nanocomposite fabrication methods such as drop-casting, spin-casting, and dip-coating in terms of fabrication time, uniformity of filler distribution, and minimization of aggregation. These methods often require additional, more extensive surface treatment of the nanoparticles such as ligand exchange or polymer grafting to prevent aggregation within the cast nanocomposite films.[124-126] The scalability of the spray-assisted LbL technique combined with the extensive control over the internal structure and properties of resulting films and nanocomposites is a valuable feature that has the potential to produce novel materials for specialized applications that could otherwise not be achieved.[3] Polymer nanocomposites formed using spray-assisted layer-by-layer assembly could potentially be used as drug delivery systems or incorporated into responsive membranes or materials where external stimuli would activate the

delivery process.[5, 106, 127] To this end, with the approach shown here, the release properties of the films can be altered easily through changing the number of layer pairs separating the nanoparticle regions or by modulating the environmental pH conditions. Our future vision includes translating this approach to other colloidal nanoparticles and polyelectrolyte systems to demonstrate that this approach may be broadly suitable for many other colloidal materials and polymer systems beyond just AuNPs. This would, in turn, show precise vertical placement of a broad range nanomaterials within a well-defined film for numerous applications.[27, 50, 108, 128]

CHAPTER III

QCM-D INVESTIGATION OF SWELLING BEHAVIOR OF LAYER-BY-LAYER THIN FILMS UPON EXPOSURE TO MONOVALENT IONS*

3.1 Introduction

Layer-by-layer (LbL) assembly of complementary polyelectrolytes is a versatile method capable of producing thin films and modified surfaces of tunable properties.[1-2, 7, 25, 30, 76, 129-132] These may be used for applications including sensors, smart coatings, microelectronics, self-healing materials, nanofiltration membranes, and biological applications such as tissue engineering.[57, 62, 133-139] Therefore, it is important to understand how these thin films respond to external stimuli, such as salt, if they are to be deployed in aqueous conditions of varying salt type or concentration.

Thin film polyelectrolyte multilayers (PEMs) prepared using LbL assembly have been described as polyelectrolyte complexes (PECs) that are sequentially deposited on and bound to a substrate in a kinetically trapped state. The structure a[2]nd properties of LbL films formed from strong polyelectrolytes are determined largely by the ionic strength and by the counterion species in the assembly environment. However, LbL film structure and properties are also sensitive to changes in the post-assembly conditions. Generally, it has been shown that increasing salt

---

* Reprinted with permission from "QCM-D Investigation of Swelling Behavior of Layer-by-Layer Thin Films Upon Exposure to Monovalent Ions" by Joshua T. O'Neal, Ethan Y. Dai, Yanpu Zhang, Kyle B. Clark, Kathryn G. Wilcox, Ian M. George, Nandha E. Ramasamy, Daisy Enriquez, Piotr Batys, Maria Sammalkorpi, and Jodie L. Lutkenhaus, *Langmuir* **2017**, *34* (3), 999-1009, copyright 2017 American Chemical Society.

concentration disrupts ion pair crosslinks, even up to the point of disassembling the LbL film.[16-17, 141] To date, there are many studies that discuss the impact of counterion identity and concentration on the assembly growth and structure of LbL films,[19, 21, 40, 130, 142-143] while the post-assembly responsive properties of completed PEMs to changes in ionic environments remains less explored.

For a given LbL assembly, changes in ionic strength and ion type may induce swelling to varying degrees. Salomäki *et al.* explored the effects of monovalent ions on the post-assembly swelling behavior of LbL assemblies formed from poly(diallyldimethylammonium) (PDADMA) and poly(4-styrenesulfonate) (PSS) assembled in the presence of 0.1 M NaF and 0.1 M NaBr.[22] It was reported that the effect of specific anions on the swelling behavior of the films followed a trend in the anion hydration entropies. LbL films assembled in the presence of Br^- exhibited a higher degree of swelling than those assembled in the presence in F^- anions when exposed to various ionic species along the Hofmeister series at equal ionic strengths. This behavior was attributed to the variance in internal film structure (*i.e.* coiled vs. extended chain conformation upon deposition) based on the assembly ionic conditions as well as the relative hydration levels of the various incoming anions after assembly. It was concluded that the post-assembly swelling of the film with regard to anion type mirrored the Hofmeister series. Zan *et al.* reported that the extent of uptake of additional polyelectrolyte by completed PDADMA/PSS thin films exhibited a clear dependence on the polyelectrolyte molecular weight, the counteranions' position along the Hofmeister series, and the ionic strength of the polyelectrolyte bathing solution. They found that the greatest degree of swelling and polyion uptake was associated with Br^- ions, which most effectively disrupted intrinsic binding sites within the LbL film.[54-55] Ghostine *et al.* reported that the PDADMA/PSS system had a higher doping constant for Br^- than for Cl^-.[144] This is odd, however, considering that previous rankings of the halide anions place Cl^- and Br^- close or next to

each other in terms of their net effect on LbL film properties along the Hofmeister series. Typically, Cl^- is regarded as a "null point" in the series. These results point to the strong response of LbL assemblies to Br^-, as compared to other monovalent anions, although the reason for this is not well understood. However, a recent theoretical study on ion condensation[145] showed little difference in the behavior of Cl^- and Br^- ions around isolated PDADMA chains suggesting that the ion specificity could be related to complexation.

Exposure to aqueous solutions of high salt concentration has also been used as a means of salt-annealing LbL thin films. Ghostine *et al.* previously reported on the effects of salt-annealing on the surface roughness of LbL assemblies.[64] PDADMA/PSS multilayers soaked in NaCl solutions at ionic strengths ≥ 1.0 M for 20 h showed significant reduction in surface roughness, which was attributed to the softening and restructuring of the plasticized network. Similarly, Fares *et al.* studied the effects of repeated salt annealing as a means to achieve stoichiometrically balanced LbL assemblies.[65] By repeatedly immersing the films in 2.0 M NaCl solution followed by 10 mMol PSS in 1.0 M NaCl solution, excess PDADMA underwent an extrinsic-intrinsic conversion as PSS was absorbed into the multilayer. This was achieved by swelling of the network and added mobility induced by the 2.0 M NaCl immersion step, allowing for more free diffusion of excess PDADMA to the surface to interact with the incoming PSS in the second step. The result was a nearly complete intrinsic network with a more uniform structure and a smoother surface.

On the other hand, recent studies have utilized various divalent counterions or NaCl at varying ionic strengths to elicit structural responses from LbL assemblies.[56, 63, 146-147] Wei *et al.* reported that PSS-capped PDADMA/PSS multilayers assembled at 0.5 M $NaNO_3$ could be physically cross-linked upon doping with divalent nitrate salts at low concentration (0.01 M).[66] The cross-linking caused the films to contract due to ion bridges formed between polyelectrolyte

charge sites. Similarly, Reid *et al.* explored the reversible swelling behavior and thermal properties of PDADMA/PSS multilayers capped with PDADMA in response to exposure to various divalent ion solutions across a range of ionic strengths.[41] The responsive behavior was divided into two regimes. The first was characterized by swelling induced by electrostatic repulsion at low salt concentrations, and the second was described by swelling resulting from excessive doping at elevated salt concentrations. LbL assemblies exposed to $CaCl_2$ and $MgCl_2$ exhibited linear changes in thickness in high-salt concentration regime with respect to increasing salt concentration, whereas those exposed to $NaSO_4$ showed no clear trend.

Here, we explore the responsive swelling and deswelling behavior and the compositional changes of PDADMA/PSS LbL assemblies upon exposure to monovalent salts (KBr, NaBr, NaCl, and KCl) across a broad range of concentrations to understand the underlying reasons for KBr's influence. The PDADMA/PSS system was selected because it represents a model system of strong polyelectrolytes whose properties have been extensively studied. KBr was selected as the primary focus of this study because previous studies have shown that Br^- ions have a significant effect on the structure and properties of PDADMA/PSS thin films and complexes. NaCl, NaBr, and KCl were selected as a means to compare against other ion combinations, and NaCl was of special interest because of its widespread use in the practice of salt annealing LbL thin films. The primary tool used to explore the response during ion exchange was quartz-crystal microbalance with dissipation (QCM-D) monitoring, which yields changes in the film's hydrated thickness and mass. Free standing LbL films were also analyzed using ^1H NMR and neutron activation analysis (NAA) in order to understand film composition and to quantify changes in ion content. These results are discussed in the broader context of how and why LbL films respond to different ion species and salt concentrations.

3.2 Experimental Section

3.2.1 Materials

Poly(diallyldimethylammonium chloride) (PDADMA, M_w = 200,000−350,000 g/mol, 20 wt % solution), poly(styrenesulfonate sodium salt) (PSS, M_w = 500,000 g/mol), and linear polyethyleneimine (LPEI, M_w = 25,000 g/mol) were purchased from Sigma-Aldrich, Scientific Polymer Products, and Polysciences, Inc., respectively. Sodium chloride (NaCl), sodium bromide (NaBr), potassium chloride (KCl), and potassium bromide (KBr) were all purchased from Sigma-Aldrich. Teflon sheet and quartz crystals were used as substrates and were purchased from McMaster-Carr and Q-Sense, respectively.

3.2.2 Preparation of Free-Standing LbL Films

Free-standing LbL films were fabricated on Teflon substrates using an automated HMS slide stainer (Carl Zeiss, Inc.). PDADMA and PSS were first dissolved in Milli-Q water at 1 mg/mL concentration and ionic strength of 0.5 M NaCl. The Teflon substrates were cleaned prior to use by sonication in ethanol (15 min) followed by rinsing twice thoroughly with Milli-Q water. The assembly sequence for the LbL films was carried out by immersing the substrates in PDADMA solution for 15 min, followed by three rinses for 2, 1, and 1 min in Milli-Q water (0.5 M NaCl). This same sequence was repeated for the deposition of PSS. Films were completed after 140 layer pairs (or cycles), and any excess salt was removed from the surface of the films by a final rinse in pure Milli-Q water (no salt) for 3 s. After rinsing, the films were allowed to dry under ambient conditions in a hood overnight followed by drying under vacuum at 115°C for 3 h. The completed films are denoted as $(PDADMA/PSS)_n$, where n represents the number of layer pairs.

3.2.3 Proton Nuclear Magnetic Resonance Spectroscopy

Proton nuclear magnetic resonance (^{1}H NMR) spectroscopy (500 MHz proton frequency, Varian Inova 500 spectrometer) was used to determine the composition of PDADMA/PSS free-standing films prepared by LbL assembly. Sample preparation was carried out as follows: approximately 10 mg of dried $(PDADMA/PSS)_{140}$ LbL film was dissolved in 0.75 mL of deuterium oxide (D_2O) solution with 2.5 M KBr. The mole percent of the polyelectrolyte components was calculated by comparing the relationship between the aromatic peaks associated with PSS and the aliphatic peaks associated with PDADMA as described in previous reports.[39, 148]

3.2.4 Neutron Activation Analysis of Free-Standing LbL Films

Free-standing LbL films of PDADMA and PSS were assembled as previously described. After completion, an ion exchange was performed by immersing the films into a solution containing the desired concentration of KBr for 1 h followed by a final 3 s rinse in Milli-Q water. The films were then dried under ambient conditions overnight and then under vacuum at 115ºC for 3 h.

Films were then analyzed *via* instrumental NAA using a comparator method, in which the calibrators and the unknown samples were irradiated using a 1 MW TRIGA reactor and the gamma-ray emissions were counted under identical conditions. Due to the strong signal associated with Br^-, two different sets of experimental parameters were employed to obtain data for Br^- and Cl^- (set 1) as well as Na^+ and K^+ (set 2). A more detailed experimental explanation can be found in the Supporting Information. In summary, calibrator solutions were weighed and heat-sealed in acid-washed 2/5-dram polyethylene irradiation vials. The LbL films samples were transferred into pre-weighed irradiation vials inside a dry-nitrogen glove box in order to prevent water uptake prior to the analysis. The closed sample vials were then weighed in ambient conditions and heat sealed

prior to irradiation. Gamma-ray emission spectrometry was performed using a high-purity Ge gamma-ray detector (Ortec). Data analysis was performed using NAA software from Canberra Industries. The values for ion content reported in Table 1 are averages of three separate experimental repeats per data point.

3.2.5 Quartz-Crystal Microbalance with Dissipation Monitoring.

QCM-D data was collected using a Q-Sense E4 instrument. LbL films were assembled on SiO_2 coated AT-cut quartz crystals with a resonant frequency of 4.95 MHz. The quartz crystals were cleaned by plasma treatment using an O_2-plasma etcher for 15 minutes followed by immersion in 2 vol % sodium dodecyl sulfate in water for 10 minutes, rinsing with Milli-Q water, drying with nitrogen, and a final O_2-plasma treatment for 15 minutes. The temperature for all QCM-D experiments was held at 25°C. The flow rate for all solutions was kept constant at about 115 µL/min. A baseline for each measurement was established by flowing Milli-Q water (pH 4.5) over the quartz crystal for approximately 45 min. An anchor layer of LPEI (pH 4.5) was then deposited onto the crystal for 15 min in order to enhance the surface charge and accelerate early growth of the LbL film, followed by a 5 min rinse in Milli-Q water (pH 4.5).[41] The LPEI layer has been shown to skew the LbL stoichiometry towards having excess PDADMA.[149] Deposition of the LbL film was carried out by alternating the flow of 0.1 mg/mL PSS (0.5 M NaCl) and 0.1 mg/mL PDADMA (0.5 M NaCl) for 15 min each. After each polyelectrolyte deposition, the system was rinsed for 5 min with Milli-Q water (0.5 M NaCl). All films in this study were capped or terminated with PDADMA, and the total number of layer pairs was either six or seven, depending on the concentration of the exchange salt. Immediately following the final rinse, the films were exposed to either KBr, KCl, NaCl or NaBr at various concentrations and the system was allowed

to equilibrate for up to 3 hours. Films produced using QCM-D are denoted as LPEI/$(PSS/PDADMA)_m$, where m is the number of layer pairs.

3.2.6 Modeling of QCM-D Data

Changes in frequency and dissipation from each QCM-D experiment were analyzed using QTools modeling software (Biolin Scientific). Specifically, the extended viscoelastic model was used to fit the third, fifth, seventh, and ninth overtones, and the value used for material density (L1) and fluid density was fixed at 1050 kg/m^3, (see Table 3.1). It is acknowledged that the fluid density of various salt solutions differs as concentration increases or decreases. However, altering the value of fluid density in the modeling parameters did not yield significant changes in the reported data trends, and the fixed value proved to be sufficient for the present study (see Figures 3.1 and 3.5). This allowed all results to be collected in a consistent fashion.

Table 3.1. Parameters used to model QCM-D data using the extended viscoelastic model.[a]

Parameters to Fit	**Min**	**Max**	**Iterations**
L1 viscosity (kg/ms)	0.001	0.2	25
L1 shear (Pa)	1000	$X \times 10^{7}$	25
L1 Thickness (nm)	1×10^{-9}	$X \times 10^{-7}$	25
L1 viscfrq (N/A)	-1	1	10
L1 shearfrq (N/A)	0	2	10
Fixed Paramaters			
Fluid density (kg/m^3)	1050		
Fluid viscosity (kg/ms)	0.001		
L1 density (kg/m^3)	1050		

[a] 3rd, 5th, 7th, and 9th overtones were included for all fitting procedures. Max values for thickness and shear modulus were adjusted to optimize fits based on film response.

Additionally, the extended viscoelastic model was chosen due to the lower χ^2 values provided compared to the regular viscoelastic model.[41] Reported values for changes in thickness and dissipation are averages of at least three experiments per data point, and the error bars were produced using the standard deviation.

3.3 Results and Discussion

3.3.1 Composition of PDADMA/PSS Free-Standing LbL Assemblies

It is important to first gain a clear understanding of PDADMA/PSS LbL film composition in order to more accurately comment on the salt exchange behavior discussed later. To do this, ^1H

NMR was employed to determine the PSS:PDADMA molar ratio (by repeat unit) within free-standing $(PDADMA/PSS)_{140}$ LbL films assembled at 0.5 M NaCl and, in turn, the mol % PSS. Previous ^{1}H NMR studies on the PDADMA/PSS system indicate that the PSS:PDADMA ratio can be easily determined *via* a relationship between the aromatic peaks of the PSS chains and the aliphatic peaks associated with both PSS and PDADMA.[148] The mol % PSS was determined to be 35-36 mol % indicating a substantial excess of PDADMA within the PDADMA/PSS LbL films. This result is consistent with previous reports for the PDADMA/PSS polyelectrolyte system.[40, 65, 130,149]

After quantifying the ratio of polyelectrolyte species, the counterion content in the LbL films was explored. Free-standing LbL films were immersed in Milli-Q water for 3 s to remove excess salt from the surface, ion exchanged with KBr at various concentrations, and analyzed using NAA. High activity of the selected ion species within the LbL films allowed for quantification of their content with an average error of 10% or less. Average weight percent values for the species of interest can be found in Table 3.2. Analysis on as-completed films (un-exchanged) revealed that Cl^- comprised nearly 3 wt % of the film, whereas Na comprised less than 0.3 wt %. This is likely due to the excess of PDADMA known to be present in PDADMA/PSS LbL film, which leaves fewer uncompensated PSS charge sites available to pair with small counterions such as Na^+.[51, 65] After exchange with KBr, the observed values for Na^+ and Cl^- were extremely low (<0.01 wt% for Na^+ and <0.1 wt% for Cl^-) compared to values prior to ion exchange (0.28 wt% for Na^+ and 2.9 wt% for Cl^-). . Regardless of the KBr exchange concentration, the amount of Br^- ions present in the film reached an average value of 6-8 wt %. This implies that nearly all available excess PDADMA charge sites are compensated with Br^- ions upon exchange. The NAA data also indicates a successful exchange of K^+ with Na^+ even at the low exchange concentration of 0.01

M KBr, which was well below the assembly concentration (0.5 M NaCl). At KBr concentrations above 0.5 M, there was a slight increase in the amount of K^+ ions within the film. However, countercation species comprised less than 1 wt % of the films before and after the exchange such that the effect was not as dramatic as the Cl^-/Br^- exchange.

Table 3.2. Counter ion wt% within free-standing $(PDADMA/PSS)_{140}$ films after ion exchange with KBr.[a]

[KBr] Exchange	Br (wt %)	Cl (wt %)	K (wt %)	Na (wt %)
Un-Exchanged	ND	2.9	ND	0.28
0.01 M	6.5	0.023	0.0028	ND[b]
0.25 M	6.8	0.065	0.35	0.0097
0.5 M	7.5	0.017	0.18	0.0025
0.75 M	7.8	0.075	0.89	0.0085
1.0 M	7.6	0.039	0.52	0.00058
1.25 M	7.4	0.095	0.92	0.0067

[a] Data was obtained with an average error of 10% or less and reported values are averages of three samples per data point. [b] ND = Not detectable

These results demonstrate that the LbL film prefers to uptake K^+ and release Na^+ and prefers to uptake Br^- and release Cl^-. This may be attributed to the more chaotropic nature of K^+ and Br^- ions,[34, 150] which tend to be larger, more polarizable, and have a higher (more positive) energy of hydration. This could make K^+ and Br^- ions less hindered in their diffusion through the film matrix by water structure networks and more efficient at screening. Combining the NAA results with the

mol % PSS obtained by ^{1}H NMR and by assuming charge neutrality of the overall LbL film, we were able to estimate a K_a value for KBr according to:

$$K_a = \frac{a_{KBr}^2}{(y^+)(y^-)} \quad (1)$$

where $y^+$is the ratio of Br^- to PDADMA, y^- is the ratio of K^+ to PSS within the LbL film, and a_{KBr} is the activity of KBr at a given ionic strength. This represents the tendency of a particular salt to dope the LbL film and disrupt intrinsic ion pairs, with lower values of K_a indicating that doping is more favored. From averaging the results for 0.25 M to 1.25 M in Table 3.2, K_a for KBr was 2.53 ± 0.76. This is similar to the value of 2.42 reported by Schlenoff for PDADMA/PSS polyelectrolyte complexes.[67] The reported K_a value for NaCl is 3.33, which suggests that KBr is more favorable to doping the LbL film in comparison to NaCl.[144] However, it should be noted that our experimental error places our K_a for KBr close to this reported value for NaCl.

The relatively low amount of cation species in the film after exchange with KBr at the low concentration of 0.01 M could be evidence that during the exchange process there is a minor extrinsic-to-intrinsic conversion of some PSS charge sites. At this low exchange KBr concentration, there are fewer K^+ ions available to maintain extrinsic binding sites as compared to the assembly conditions. As PSS chains become intrinsically compensated, the associated Na^+ counterions are released and expelled from the film. Simultaneously, the excess extrinsically compensated PDADMA chains in the film bulk may diffuse throughout the outer, more loosely packed region of the LbL film near the surface-liquid interface.[34, 40, 65] This would result in a greater excess of positive charge at the surface of the film, thereby excluding additional K^+ ions from entering during ion exchange.[59, 151-152]

3.3.2 Swelling Response to KBr Solution

In order to understand the responsive behavior of PDADMA/PSS LbL thin films to changes in the external environment, QCM-D was employed as a tool to monitor real-time changes in film thickness, mass, and viscoelastic properties. LPEI/(PSS/PDADMA)$_{6\text{-}7}$ films were assembled from PDAC and PSS solutions at an ionic strength 0.5M NaCl onto SiO_2-coated quartz crystals as previously reported.[41] The final LbL film thickness was around 140-150 nm for seven layer pair films and around 100-110 nm for six layer pair films (obtained from 10 and 5 experimental trials, respectively). Figure 3.2 shows representative QCM-D data for the LbL assembly and ion exchange of LPEI/(PSS/PDADMA)$_{6\text{-}7}$ films with various KBr concentrations.

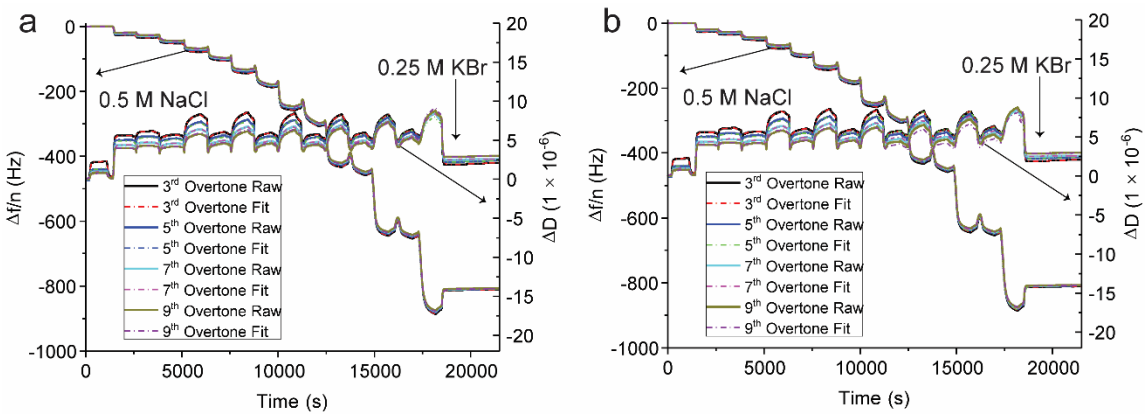

Figure 3.1. Data sets for a LPEI/(PSS/PDADMA)$_7$ film exposed to 0.25 M KBr where the data is modeled using (a) a fixed fluid density of 1.05 g/cm^3 and (b) a fluid density value of 1.001 g/cm^3 for the exchange region. Both plots show $\Delta f_3/n$ -$\Delta f_9/n$ and ΔD_3-ΔD_9 values and corresponding fits.

These reported thickness values represent the hydrated thickness as obtained from viscoelastic modeling of resonant frequency (Δf) and dissipation (ΔD) changes from QCM-D experiments. Figure 3.1 shows a representative example of a fitted QCM-D data set. Additionally, information about the mechanical properties can be gathered by observing changes ΔD. Increases in ΔD correspond to softening of the LbL film while decreases in ΔD imply stiffening.

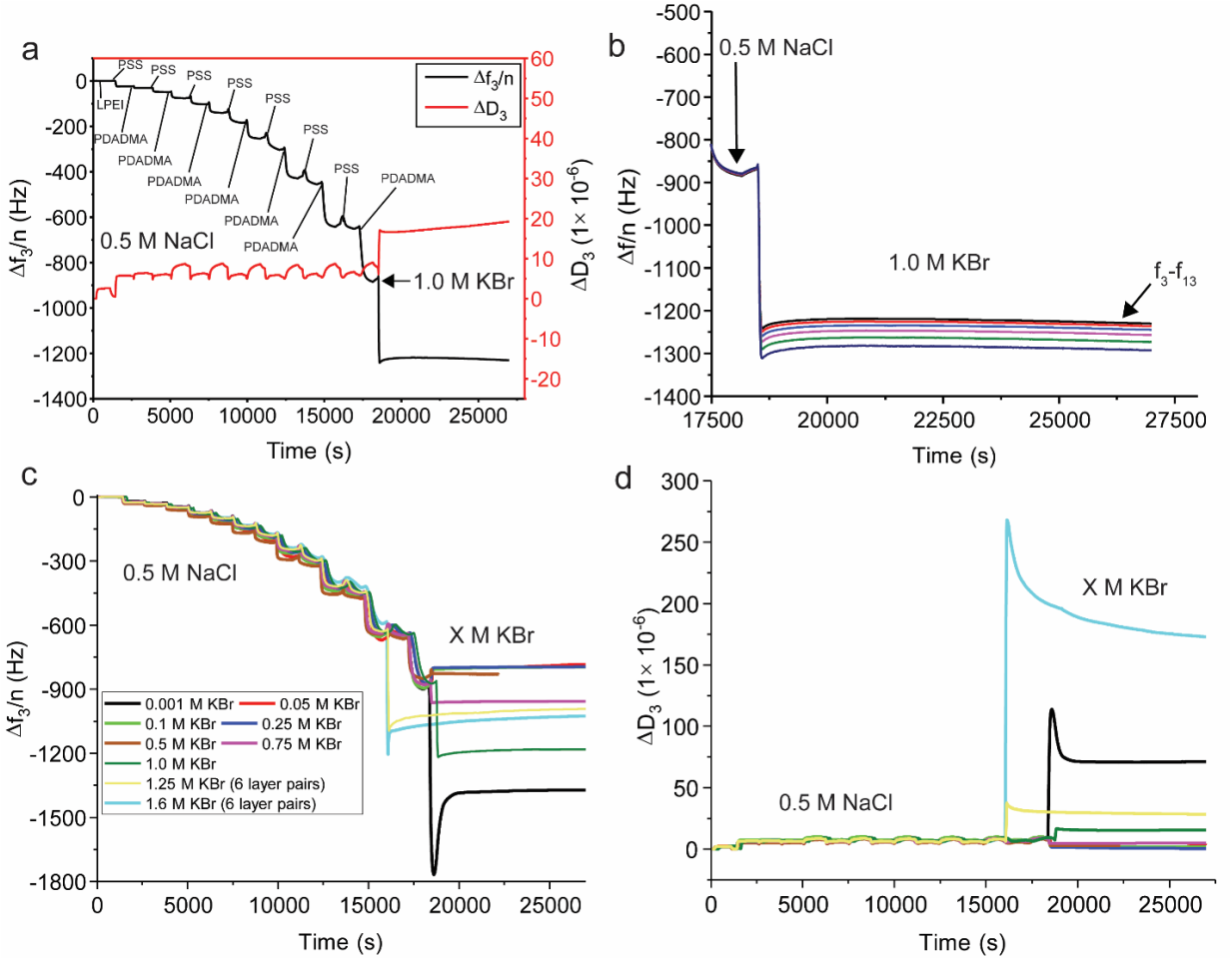

Figure 3.2. QCM-D data showing (a) $\Delta f_3/n$ and ΔD_3 during LPEI/(PSS/PDADMA)$_7$ film assembly and subsequent exposure to 1.0 M KBr and (b) $\Delta f/n$ reflected in the various crystallographic overtones upon exposure of to 1.0 M KBr as well as data overlays of (c) $\Delta f_3/n$ and (b) corresponding ΔD_3 values for LPEI/(PSS/PDADMA)$_{6\text{-}7}$ films assembled at 0.5 M NaCl and subsequently exposed to KBr solutions of varying concentrations. The caption in (c) applies to (d).

Immediately after assembly, the thin films were exposed to various concentrations of KBr under dynamic flow, and the corresponding Δf and ΔD values were monitored throughout the ion exchange and equilibration processes (see Figure 3.2). From this data, the changes in hydrated thickness were estimated. Figure 3.3 shows changes in thickness and dissipation of the LbL films relative to the as-prepared, fully hydrated thickness just prior to exposure to KBr solutions. The behavior in response to altering the KBr exchange concentration can be broken down into four regimes, summarized in Scheme 1. The first regime can be described as the zero-to-near zero concentration regime, from 0 M – 0.001 M KBr. Here, the Debye length (> 10 nm) significantly exceeds the distances between the neighboring charged groups (> 1 nm) and there is an insufficient number of counterions present within the film to provide the electrostatic screening necessary to keep the film in its original compact configuration. The extrinsic charge sites associated primarily with PDADMA are left uncompensated and experience strong electrostatic repulsion from neighboring charge sites, resulting in straightening of the PE chain.[153] causing the film to expand rapidly and dramatically (up to 120%). This expansion is accompanied by the uptake of additional water molecules to occupy the free volume resulting in a large increase in areal mass of the film (up to 119%). As the film rapidly expands, ΔD_3 increases up to 160×10^{-6} units, which indicates a substantial softening of the film associated with the large increase in free volume and influx of water, Figure 3.3b.

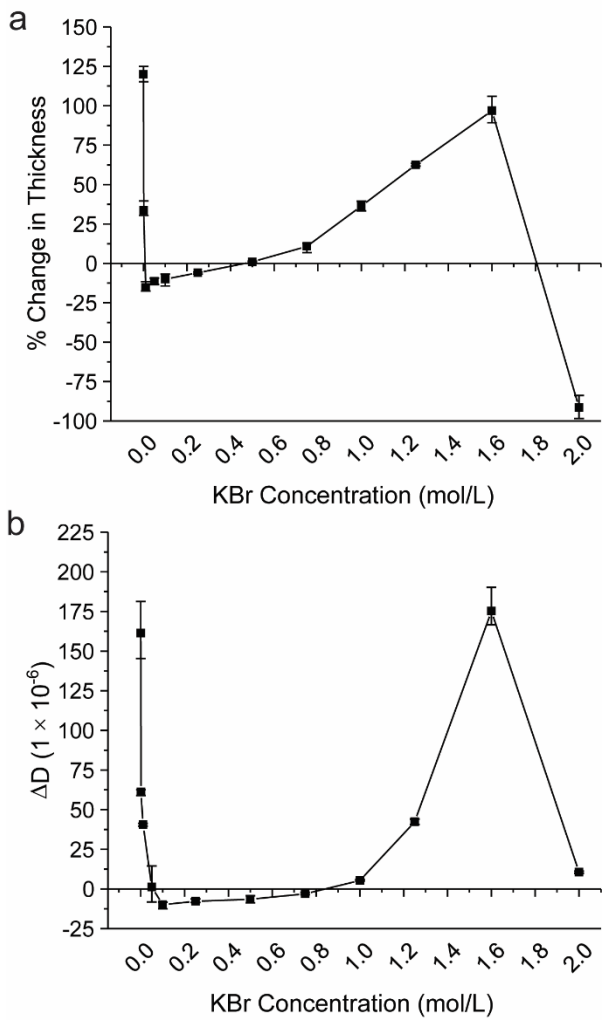

Figure 3.3. Average (a) percent change in thickness and (b) change in dissipation for LPEI/(PSS/PDADMA)$_{6\text{-}7}$ after exchange with various concentrations of KBr. Above 1.25 M KBr, the number of layer pairs was kept to six in order to ensure accurate data collection from the QCM-D due to the large degree of swelling. Reported values are averages of at least three experimental trials, and ΔD values are taken from the third crystallographic overtone. The error bars represent the standard deviation of the trials.

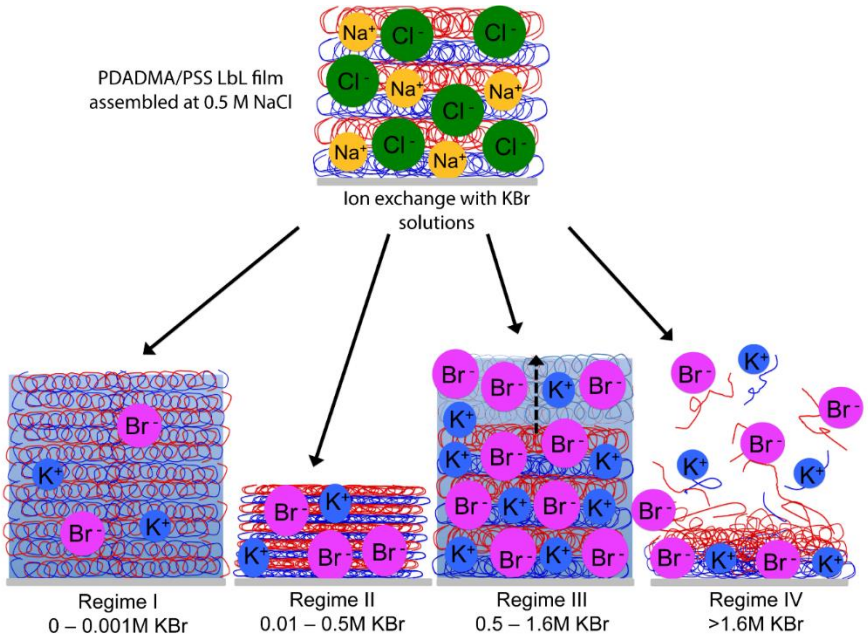

Figure 3.4. Qualitative schematic illustrating the four regimes assigned to the swelling response of PDADMA/PSS LbL films assembled at 0.5 M NaCl and exposed to varying concentrations of KBr.

The second regime, referred to as the low concentration regime, lies in the range of exchange concentrations from 0.01M – 0.5M KBr. In this regime, the film shows slight contraction upon exposure to solutions of ionic strength lower than the assembly ionic strength of 0.5 M NaCl. This behavior may result from an adequate amount of counterions present in the incoming KBr solution that provide enough charge screening of neighboring extrinsic sites to prevent expansion from electrostatic repulsion. Under these conditions, the minor contraction of the film structure possibly gives rise to expulsion of bulk water and free, unassociated counterions. Another explanation for the LbL film contraction is that some conformational change of the polyelectrolyte chains occurs during the counterion exchange process. The slight decrease in ΔD_3 in this low

concentration regime implies that the film takes on a more rigid, compact configuration. The polyelectrolyte network becomes more densely packed as there exists some balance between extrinsic ion compensation and electrostatic repulsion, ultimately causing an increase in film stiffness. The exception to this trend occurs at 0.5 M KBr where only slight changes in frequency and dissipation are observed. Here, the ionic strength of the KBr exchange solution is the same as the NaCl assembly solution, and the overall impact on the internal structure and properties of the LbL film is minimal.

The third regime is referred to as the high concentration regime 0.5 M – 1.6 M KBr. In this regime, the magnitude of the change in hydrated thickness, mass, and dissipation showed clear dependence on the KBr concentration. The reason for the observed swelling in this regime is opposite of that described in the zero-near zero concentration regime. In this case, the increased presence of counterions in the film results in a large degree of electrostatic screening and doping. The effect of the large influx of counterions is two-fold. First, the increased competition of counterions for converting intrinsic sites to extrinsic sites causes disruption of physical ion pair crosslinks. This results in an expansion of the film and an increase in free volume which yields an uptake of bulk water. Second, the influx of K^+ and Br^- ions into the film is accompanied by water in the counterion hydration shell. With this expansion and influx of bulk water and hydrated counterions, the film becomes softer and more gel-like which is reflected in the large increase in dissipation in this regime (ΔD_3 up to 167×10^{-6}).

A closer look at regime III reveals that the percent change in thickness shows a linear dependence on the KBr concentration. Fitting the data from 0.75 M to 1.6 M KBr in this regime gives a line with the equation $\%\Delta t = 103.55C_{KBr} - 66.82$ ($R^2 = 0.99$), where C_{KBr} is the

concentration of the KBr solution. Reid *et al.* reported similar trends with respect to contraction of PDADMA/PSS LbL films exposed to $CaCl_2$ and $MgCl_2$ solutions upon reverting back to assembly conditions (0.5 M NaCl). They reported that the degree of LbL film contraction was linearly dependent on the concentration and identity of the post-assembly divalent salt solutions above 0.17 M. Film swelling in this concentration range was driven by ion doping and electrostatic screening, and film contraction upon returning to assembly conditions was dependent on both ion type and concentration.[41] It is worth noting that the changes in the film thickness in regimes II and III can be correlated with the difference between the salt concentration in the PEM (assembly concentration) and in the bulk solution. This suggests the hydrated ion flux in and out of the multilayer is dominating in the swelling response.

The final regime, referred to as the ultra-high concentration regime, deals with KBr concentrations > 1.6 M. It was observed that at the KBr exchange concentration of 2.0 M, the change in Δf was quite large, indicating an immediate and substantial decrease in film thickness and mass. It was concluded that saturation of the film with counterions resulted in sufficient electrostatic screening and plasticization of the PEM structure, leading to dissolution. The data indicated that the hydrated film mass dropped from 12.4 ± 0.45 μg/cm^2 to 0.53 ± 0.32 μg/cm^2. Visual examination of the quartz crystal substrate after the experiment revealed that only a few small patches of film remained. These results are consistent with other work describing the dissolution of PEMs and PECs at salt concentrations far above their assembly ionic strengths.[17, 53]

A recent study by the Schlenoff group discussed the properties of PDADMA/PSS complexes fabricated using a "backwards" method in the presence of KBr at various concentrations.[53] They found that the PDADMA/PSS complexes underwent distinct property changes as the concentration of the surrounding KBr increased. At low concentrations, the

complexes were stable and glassy. With increasing KBr concentration, the complexes became softer and took on a more expanded configuration until the polyelectrolyte chains became so heavily doped with counterions that they formed elastic liquid coacervates and finally dissociated completely at ~1.8 M KBr, similar to our PDADMA/PSS LbL films. This shows similarities between the salt responses of complexes and multilayers.

Unfortunately, the ion content shown in Table 3.2 cannot be precisely correlated to the data obtained by QCM-D, and therefore to the behavior depicted in Scheme 1 for several reasons. First, the exchange process for free-standing LbL films for NAA measurements took place in a static environment. There was no influx of new solution or removal of solution containing ions exchanged out of the film. The opposite is true of the QCM-D experiments, where the solution was constantly flowing in and out of the sample chamber. This constant addition of new ion-rich solution could be a contributing factor to the responsive behavior observed at elevated concentrations.

3.3.3 Swelling Response to KBr/NaCl Solution Mixtures

To discern the difference between the effects of NaCl and KBr on the swelling behavior, a study was performed in which the overall ionic strength of the post-assembly ion exchange solution was held constant at 1.0 M, but the ratio of NaCl:KBr was altered. All assembly experimental parameters remained the same. In this manner, the effect of ion identity can be probed apart from ionic strength. Figure 4.3 shows the percent changes in thickness of LPEI/(PSS/PDADMA)$_7$ films upon exposure to NaCl/KBr solutions at varying ratios of NaCl:KBr with 1.0 M NaCl and 1.0 M KBr as controls. There is a clear dependence on the presence of KBr despite the fixed ionic strength. Directly comparing pure NaCl and KBr at 1.0 M reveals that $K^+ > Na^+$ and $Br^- > Cl^-$ with respect to impact on swelling thickness. With regard to changes in

dissipation, there is very little effect on ΔD with respect to NaCl/KBr ratio. For this case, it seems that ion type strongly affects swelling thickness, but not viscoelastic properties. This suggests that film is sufficiently rigid at these conditions to prevent energy dissipation.[154]

Previous studies have shown that PDADMA/PSS LbL thin films and complexes are more heavily influenced by the anionic counterion type present during assembly and that the degree of influence follows the Hofmeister series.[19, 21-22, 49, 131] From NAA, it was observed that free standing films immersed in solutions of varying KBr concentration contained >1 wt % of the cationic counterion species while maintaining an elevated amount, 6-7 wt %, of anionic species. This is consistent with reports that Br^- is known to have a greater effect on PEM structure than Cl^-.[22] The increase in film thickness with increasing Br^- concentration is intuitive if Br^- is more capable of disrupting intrinsic ion pairs than Cl^- leading to increased plasticization from hydration water molecules throughout the bulk of the film.[22, 49, 155]

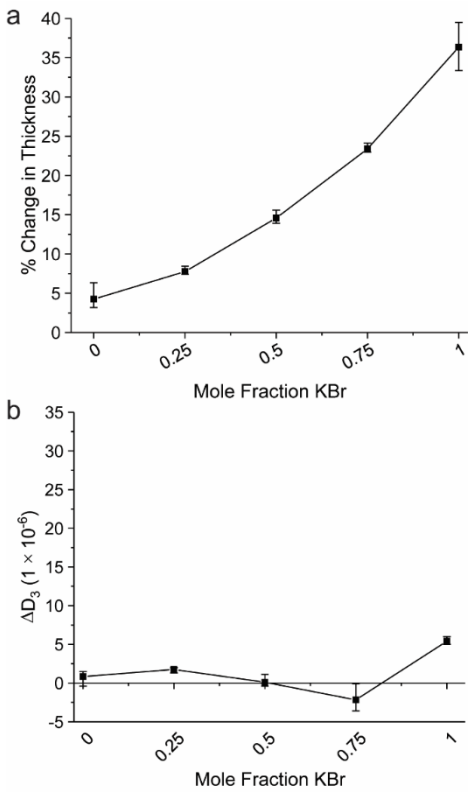

Figure 3.5. (a) Percent change in thickness and (b) absolute changes in dissipation of LPEI/(PSS/PDADMA)$_{6\text{-}7}$ LbL thin films assembled at 0.5 M NaCl and then exposed to NaCl/KBr mixtures where the overall salt concentration was held at 1.0 M and the fraction of KBr was varied. Therefore, a mole fraction of KBr = 0 indicates that the exposure solution was 1 M NaCl. Reported values are averages of at least three experimental repeats, and ΔD values are taken from the third crystallographic overtone. The error bars represent the standard deviation of the trials.

Additionally, the ionic radius of Br^- is slightly larger than Cl^- so the incorporation of many Br^- ions could have a collective steric effect on the film swelling. In sum, the LbL swelling effects arise from the Br^- anion's larger ionic radius, greater polarizability and more loosely bound hydration shell, which$^-$ gives rise to more disruptive interactions within the LbL network.

3.3.4 Reversibility of Swelling Response

The reversibility of the swelling response in the high concentration regime was examined by exposing LPEI/(PSS/PDADMA)$_{6\text{-}7}$ films assembled at 0.5 M NaCl to KBr solutions at 0.75 M, 1.0 M, 1.25 M, and 1.6 M, allowing them to reach equilibrium swelling behavior and then reverting to 0.5 M NaCl. Figure 3.6 shows film thicknesses and dissipation values just after assembly, after equilibration in the selected KBr concentration, and after re-exposure to NaCl. The results indicate that for 0.75 M, 1.0 M, and 1.25 M KBr the films return to a thickness slightly lower than their assembly thickness. This is likely due to a restructuring of the chains when returning from the expanded, swollen state to a more densely packed configuration.[21] This is consistent with the practice of "salt annealing" which is used to smooth and restructure LbL surfaces.[64-65] Representative fits of the raw QCM-D data for reversibility experiments are shown in Figure 3.7.

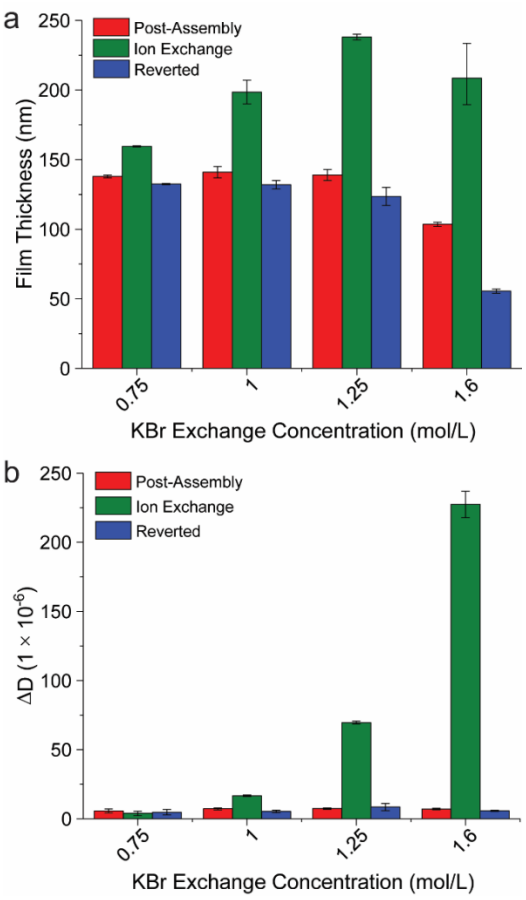

Figure 3.6. Reversible swelling response showing changes in (a) thickness and (b) dissipation after assembly at 0.5 M NaCl (post-assembly in red), exchange with KBr at various concentrations (ion exchange in green), and reverting back to 0.5 M NaCl (reverted in blue). Reported values are averages of at least three experimental repeats, and ΔD values are taken from the third crystallographic overtone. The error bars represent the standard deviation of the trials.

The degree of internal restructuring is directly correlated with the concentration of the KBr exchange solution in the high concentration regime. Previous studies on the effects of assembly with regard to ion type indicate that increasingly chaotropic counterions result in films with more loosely packed internal structures and roughened surfaces.[19] The effect is seen to increase in strength with increasing atomic radii and decreasing hydration shell. This is attributed to the stronger interactions of the ions with the polyelectrolyte charge sites allowing for greater electrostatic screening and coiled conformations during construction and assembly.[19, 21-22] In this case, the post-assembly swelling response of LbL assemblies to increasing KBr concentration follows a similar pattern as to that seen for assembly.[19] The polyelectrolyte chains are entangled in a kinetically trapped network, and the addition of more structurally disruptive ions at ionic strengths above the assembly conditions disrupts intrinsic binding sites allowing the network to loosen. Water enters the LbL assembly and plasticizes the network allowing for further enhanced chain mobility. As the film swells and more ions enter along with bulk water, the effects are exacerbated until a new equilibrium structure is reached. Reversion back to assembly conditions, 0.5 M NaCl in this case, results in a relaxation of the PEM structure to a more compact configuration. The average reductions in thickness for films exposed to 0.75 M, 1.0 M, and 1.25 M KBr upon reverting back to 0.5 M NaCl were 6.5 nm, 16.5 nm, and 26 nm, respectively (or 4%, 7%, and 12% of the initial state). Each of these changes in thickness were accompanied by changes in mass related to the expulsion of bulk water upon collapse of the films.

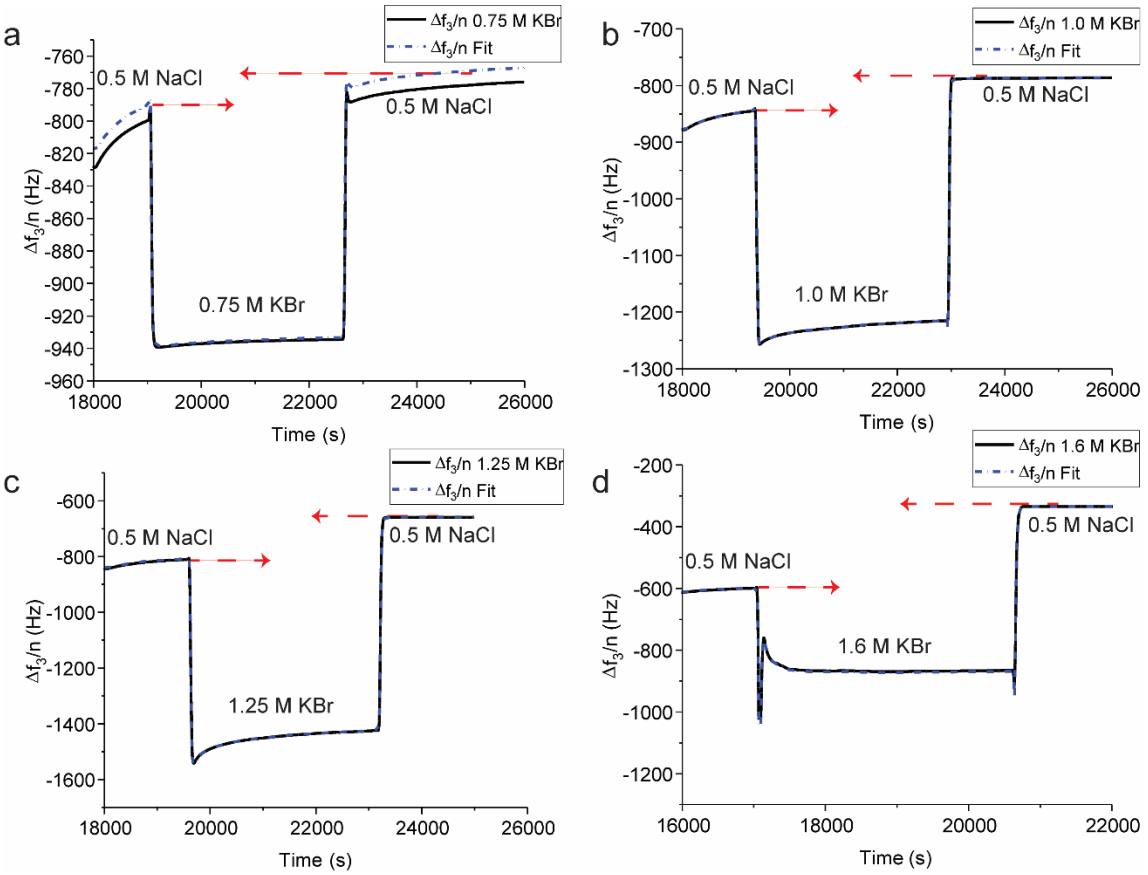

Figure 3.7. Representative fits of the third frequency overtone for each KBr exchange concentration (a) 0.75 M KBr, (b) 1.0 M KBr, (c) 1.25 M KBr, and (d) 1.6 M KBr showing both equilibration in the KBr solution as well as reverted thickness upon changing back to the assembly conditions (0.5 M NaCl). LbL films exposed to 1.6 M KBr were made with six layer pairs to account for large swelling response while all other films were prepared with seven layer pairs.

For films exposed to 1.6 M KBr, the change in thickness upon reverting back to 0.5 NaCl was much larger, averaging around 50% reduction in film thickness. Such a large loss in thickness is likely not only contributed to internal restructuring of the film but also to deconstruction of the film upon reversion. To verify whether or not the films would continue to dissociate upon further switching between 1.6 M KBr and 0.5 M NaCl, this cycle was repeated three consecutive times on the same LPEI/$(PSS/PDADMA)_6$ film. The second, third, and fourth KBr → NaCl exchanges resulted in less than 5 nm change in thickness, which remained near 50% of the post-assembly thickness. This could be attributed to the more intimate interactions between the inner layers of the film and the SiO_2 coated crystal surface, which would yield a more densely packed network associated with the first few deposited layer pairs.[143] This explanation is consistent with the diffusion model and the influence of substrate effects related to PEM growth reported elsewhere.[19, 34, 45] The elevated packing density of the polyelectrolyte chains near the substrate makes them less influenced by changes in the ionic environment.[34, 143]

3.3.5 Swelling Response to NaCl, KCl, and NaBr

To gain a deeper understanding of the differing effects of individual counterion species on the swelling response of LPEI/$(PSS/PDADMA)_m$ LbL thin films, it was necessary to explore different combinations of monovalent ions. To this end, LPEI/$(PSS/PDADMA)_{6-7}$ films assembled at 0.5 M NaCl were exposed to post-assembly solutions of NaCl, KCl, and NaBr at selected concentrations to mirror those performed with KBr. Figure 3.8 shows the comparison of the three counterion combinations. The results indicate that NaBr and KBr had similar effects on the degree of swelling as well as comparable effects on the viscoelastic properties as shown by the magnitude of dissipation changes, which highlights the strong effect of Br^- ions.

In the cases of NaCl and KCl, however, the trend is quite different above and below 0.5 M ionic strength when compared with NaBr and KBr. One substantial difference was reflected in the third concentration regime. At 1.6 M NaCl and KCl, the LbL films swelled by only 19% and 22%, respectively, compared to 93% and 101% in the case of both NaBr and KBr. The ΔD_3 values at this elevated concentration were also considerably smaller for both NaCl, 13×10^{-6}, and KCl, 20×10^{-6}, compared to NaBr and KBr, which showed ΔD_3 values of 124×10^{-6} and 175×10^{-6}, respectively. The implication of this behavior is that there is a relatively small influx of Na^+, K^+, and Cl^- counterions during the exchange process. Since there is already Cl^- present in the film, there is little to no significant competition for binding sites that are already formed between the extrinsic PDADMA/Cl^- sites or pre-formed intrinsic binding sites. Additionally, the films are capped with PDADMA, creating an excess of positive charge at the surface.[40-41, 51, 130] It is possible that the lack of favorable competition for binding sites combined with the excess positive surface substantially shields a large portion of the Na^+ or K^+ counterion species from entering the bulk of the film. Those counterions that do cross the interfacial barrier have only a weak net effect on the film properties as compared to the more disruptive, dominating Br^- anions.

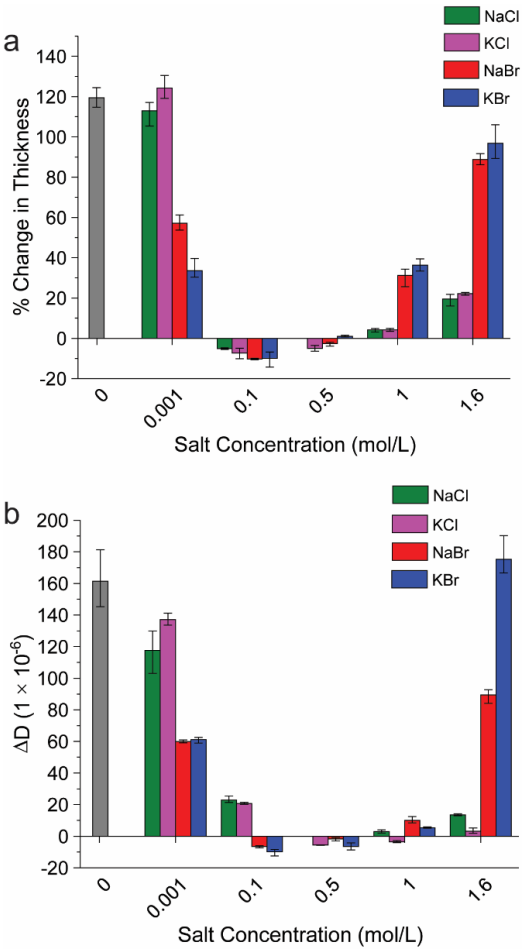

Figure 3.8. Comparison of (a) percent change in thickness and (b) change in dissipation for LPEI/(PSS/PDADMA)$_{6\text{-}7}$ after exchanges with various concentrations of NaCl, KCl, KBr, and NaBr. Reported values are averages of at least three experimental repeats, and ΔD values are taken from the third crystallographic overtone. The error bars represent the standard deviation of the trials.

For the films exchanged with 0.001 M NaCl and KCl, substantial swelling and water uptake were observed as reflected in large decreases in frequency and increases in dissipation. The changes in thickness due to swelling were 115% and 124%, respectively, for NaCl and KCl. These values are comparable to that observed for films exchanged with Milli-Q water (no salt), which swelled by 120%. Electrostatic repulsion among like charge sites causes the film to swell rapidly as the assembly counterions are leached from the film. This theory is supported by the fact that PEMs exposed to 0.001 M of both KBr and NaBr swell by 33% and 57%, respectively. The clear dependence of the anion can be seen by this trend. The ability of Br^- to dope the film at all concentrations more rapidly and efficiently than Cl^- is made clear by the large difference in swelling behavior. Above 0.1 M ionic strength, electrostatic forces are adequately screened, and the films contract slightly by about 5-10% for all salts.

Previous reports on salt mediated self-healing and annealing of polyelectrolyte multilayers and complexes have shown that by adjusting the post-assembly ionic environment, structural defects can be resolved or even totally reversed.[56, 65, 139, 156] The key to self-healing of PEMs is the increased mobility of chains as this allows them to diffuse across damaged regions. As we have just discussed, the type of salt, specifically the anion species, has a significant impact on the polyelectrolyte chain mobility and the structural properties of LbL assemblies. We have shown that exposure of PEMs prepared in NaCl to various KBr and NaBr concentrations above the assembly conditions results in a much larger degree of swelling and increased chain mobility compared to the same elevated concentrations of NaCl and KCl. The ability of Br^- ions to quickly and effectively dope thin films makes them a good candidate for further study in the area of self-healing thin films and coatings.

3.4 Conclusion

The response and salt uptake of PDADMA/PSS LbL thin films assembled in 0.5 M NaCl and exposed to various concentrations of NaCl, KCl, NaBr, and KBr was studied. Salts containing Br^- had substantially greater impact on film swelling than salts containing Cl^-. This likely arose from the Br^- anion's larger ionic radius, greater polarizability and more loosely bound hydration shell, which$^-$ gave rise to more disruptive interactions with intrinsic ion pairs within the LbL network. NAA revealed that countercationic species comprised less than 1 wt% of PDADMA/PSS free-standing films before and after ion exchange with various KBr concentrations. Conversely, counteranion species were present at much higher concentrations before and after exchange, indicating an excess of PDADMA in the PEMs. QCM-D revealed four KBr concentration regimes associated with the swelling response. At 0 M – 0.001 M KBr, swelling was dominated by electrostatic repulsion, and at 0.1 – 0.5 M KBr, slight film contraction and stiffening was observed as the ionic strength approached that of the original assembly conditions. For 0.5 – 1.6 M, swelling in the presence of KBr was reversible and accompanied by a relaxation of the film, consistent with the practice of salt annealing. In this regime, swelling was linear with KBr concentration. Finally, at 1.6 M KBr and higher, partial dissolution of LbL films was observed and was attributed to excessive electrostatic screening and disruption of intrinsic ion pairs. A comparison of post-assembly behavior in the presence of various monovalent salts verified that the anion identity was the dominating factor in the swelling response.

These findings provide insight into the response of LbL thin films in the presence of monovalent ions across a broad range of concentrations and serve to explain the mechanism of salt annealing, self-healing, and KBr's dramatic effects on polyelectrolyte complexes and multilayers.[18-20, 22, 51] Understanding how the structure and properties of LbL assemblies are

affected by both subtle and drastic changes in ionic environment is critical for applications such as sensors, responsive coatings, and separation membranes. Future work could expand to more ion types and concentrations and include various mixtures of counterions to gain further understanding of how these thin films respond to more complex environmental changes.

CHAPTER IV

INFLUENCE OF LIMITED HYDRATION AND COUNTERION TYPE ON THE GLASS TRANSITION TEMPERATURE OF ELECTROSTATIC LAYER-BY-LAYER ASSEMBLIES

4.1 Introduction

The influence of temperature, hydration level, and counterion type have been explored extensively with respect to the impact on physical structure and properties of layer-by-layer (LbL) assemblies of both strong and weak polyelectrolytes.[1, 19, 35, 41, 56, 65, 140, 146, 150] Much less attention has been given to the effects of assembly and post assembly conditions on the thermal properties of LbL assemblies, specifically the glass transition temperature (T_g). Recent reports have discussed the effects of salt and water as plasticizers of the PDADMA/PSS system from both experimental and theoretical approaches.[78-79] However, in most thermal property studies of PE assembles NaCl serves as both the assembly salt and the added salt in hydration solutions.[40, 76, 79, 108, 141] The effects of alternative assembly conditions and post-assembly hydration conditions on the T_g with respect to counterion species are still not well understood. Our group recently reported the effects of various monovalent ions on the swelling and internal structure of PDADMA/PSS LbL films.[140] It was demonstrated that fully hydrated LbL films assembled in NaCl and subsequently exposed to KBr solutions at various ionic strengths exhibited contraction or large degrees of swelling below and above the assembly ionic strength, respectively. This is due to the ability of Br^- ions to disrupt intrinsic binding sites between PDADMA and PSS, implying Br^- is a more efficient doping agent than Cl^-.[49, 144]

With respect to thermal properties, the T_g behavior of polyelectrolyte complexes (PECs) and LbL assemblies has been associated with the presence of excess water and counterions within the

structure.[39, 41, 78-79, 140, 157] The assembly and post-assembly processing conditions such as ionic strength, pH, and hydration level can all play a role in the physical and thermal responsive properties of PECs and multilayers.[21, 35, 49, 143, 158] Water affects the glass transition temperature *via* plasticization of the polyelectrolyte (PE) network, which enhances the mobility of PE chains as hydration increases.[78-79] As the chains become more mobile, the glass transition temperature decreases. Dry PDADMA/PSS LbL assemblies in the glassy state do not exhibit a T_g. However, when hydrated to 40 wt% water, PDADMA/PSS LbL assemblies exhibit a T_g around 25-30°C.[79] The T_g can be further tuned by adjusting the hydration level. It has been reported more recently that, as temperature increases, the hydrogen-bonding lifetime between water and PE functional groups decreases, which facilitates the onset of the glass transtion.[78]

The role of salt in the plasticization of PE assemblies and LbL assemblies has also been widely explored.[76, 144, 158-159] The Schlenoff group developed the concept of salt doping which describes the ability of salt to disrupt intrinsic ion pairs within the hydrated PE assembly network. This disruption decreases the number of ionic cross-links (intrinsic ion pairs) and weakens the integrity of the assembly, allowing the chains to move more readily.[160] Additionally, various ions can affect the network differently. With respect to monovalent ions, the ability for specific species to dope the PE network and disrupt intrinsic ion pairs depends on its position along the Hofmeister series, which is related to its ionic radius and hydration shell dynamics.[18, 20-21, 34, 140]

In this study, we explore the effects on the observed T_g of free-standing PDADMA/PSS LbL assemblies hydrated to various levels with solutions containing KBr. Initially, the films are assembled in 0.5 M NaCl, thoroughly dried, and then hydrated with solutions of different KBr concentrations as well as salt mixtures of KBr and NaCl at fixed ionic strength. Hydration levels are varied from 16 wt% to 33 wt%, and the T_g of the samples is measured using modulated

differential scanning calorimetry (MDSC). Next, free-standing PDADMA/PSS LbL assemblies formed in the presence of 0.5 M KBr are analyzed using neutron activation analysis (NAA) and ^{1}H NMR to determine their composition, including PE and counterion contents. These films are then hydrated to similar levels using solutions of 0.5 M KBr or 0.01 M KBr. The data from the films assembled in NaCl and KBr are compared, and conclusions regarding the structure-property relationships are discussed with respect to the differences in observed T_g values.

4.2 Materials and Methods

4.2.1 Materials

Poly(diallyldimethylammonium chloride) (PDADMA, M_w = 200,000−350,000 g/mol, 20 wt % solution) and poly(styrenesulfonate sodium salt) (PSS, M_w = 500,000 g/mol) were purchased from Sigma-Aldrich and Scientific Polymer Products, respectively. Sodium chloride (NaCl) and potassium bromide (KBr) were purchased from Sigma-Aldrich. Teflon substrates were purchased from McMaster-Carr.

4.2.2 Free-Standing LbL Film Preparation

Free-standing LbL films were fabricated on Teflon substrates using an automated slide stainer (HMS series, Carl Zeiss) as reported previously.[140] The substrates were cleaned prior to use by sonication in ethanol (15 min) followed by rinsing twice thoroughly with Milli-Q water. In short, substrates were alternately immersed in PDADMA and PSS suspensions in Milli-Q water at 1 mg/mL concentration and ionic strength of 0.5 M NaCl for 15 min each. Between each polyelectrolyte adsorption step the substrates were rinsed in milli-Q water (0.5 M NaCl) three times for 2, 1, and 1 min. Films were completed after 140 layer pairs (or cycles), and excess salt was removed from the film surfaces by a final short rinse in pure Milli-Q water (no salt) for three

seconds. After rinsing, the films were dried under ambient conditions in a hood for 24 h followed by drying under vacuum at 115°C for 3 h. The completed films are denoted as $(PDADMA/PSS)_n$, where n represents the number of layer pairs.

4.2.3 Proton Nuclear Magnetic Resonance Spectroscopy

Proton nuclear magnetic resonance (^1H NMR) spectroscopy (500 MHz proton frequency, Varian Inova 500 spectrometer) was employed to ascertain the ratio of PSS:PDADMA within the free-standing films prepared by LbL assembly. Sample preparation was carried out as described in our previous work. In short, 30 mg of dried $(PDADMA/PSS)_{140}$ LbL film was dissolved in deuterium oxide (D_2O) (0.75 mL) at 2.5 M KBr, sufficient to fully dissociate the LbL network. The mole percent of the constituent polyelectrolytes was determined by the relationship between the aromatic and aliphatic peaks associated with PSS and PDADMA, respectively.[39, 148]

4.2.4 Modulated Differential Scanning Calorimetry

After completion, $(PDADMA/PSS)_{140}$ films were quickly rinsed with pure milli-Q and dried as mentioned previously. After drying under vacuum at 115 °C for 3 h, the films were removed from the substrates and separated into samples of 7-10 mg and the hydration level and salt concentration was varied from sample to sample. The films were then sealed in hermetic tzero pans with hermetic lids. Samples were analyzed using a heat—cool—heat—cool cycle model as described in previous work.[39, 140] The heating and cooling rate was fixed at 2 °C min^{-1} over a temperature range of 0-115 °C with an amplitude of 1.272 °C for 60 s.

4.2.5 Neutron Activation Analysis

Free-standing LbL films of PDADMA and PSS were assembled as described earlier. Films were dried overnight under ambient conditions followed by drying under vacuum at 115ºC for 3 h. Once dried thoroughly, films were sealed in sample vials until NAA was performed.

Instrumental NAA was performed using a comparator method as described in previous work.[140] The calibrators and the LbL film samples were irradiated using a 1 MW TRIGA reactor, and gamma-ray emissions were counted under identical conditions. Due to the strong signal associated with Br^-, two different sets of experimental parameters were employed to obtain data for Br^- (set 1) and K^+ (set 2). In short, after being weighted, calibrator samples were heat-sealed in acid-washed 2/5-dram polyethylene irradiation vials. The LbL films samples were transferred into the irradiation vials inside a dry-nitrogen glove box in order to minimize exposure to moisture. The sample vials were then weighed under ambient conditions followed by heat sealing before irradiation. Gamma-ray emission spectrometry was carried out using a high-purity Ge detector (Ortec). NAA software from Canberra Industries was used for final data analysis. Ion content values are reported in Table 1. These values are taken from averages of three separate experimental repeats per data point.

4.3 Results and Discussion

In the current study, free-standing $(PDADMA/PSS)_n$ LbL assemblies, where n denotes the number or layer pairs comprising the film, were assembled in 0.5 M NaCl. The resulting assemblies were extensively dried and then hydrated to various levels between 16 wt% and 33 wt% at 0.01 M, 0.1 M, 0.33 M, 0.5 M, 0.75 M, and 1.0 M KBr. For all LbL assemblies in this study, the number of layer pairs was constant at n = 140. The samples were then analyzed using

MDSC observe changes in T_g with changing hydration conditions, Figure 4.1a. The details of the experimental methods can be found in the supporting information. It is clear that the salt concentration has no significant influence on the T_g while the hydration level produces distinct changes in T_g, ranging from 17°C to 90°C for hydration levels of 33 wt% and 16 wt%, respectively. At the elevated concentrations of 0.75 M and 1.0 M KBr, however, there is a deviation from the trend when the hydration level drops below 20 wt%, and T_g values of 102-103°C are observed. The elevation in T_g values at the lower hydration levels is likely caused by the increasing salt:water ratio.[79] As the relative amount of salt increases, the amount of water utilized in hydration shells of the ions increases. This results in less "free" water that could act to plasticize the LbL network. The network becomes more kinetically rigid and, therefore, the T_g increases.[79]

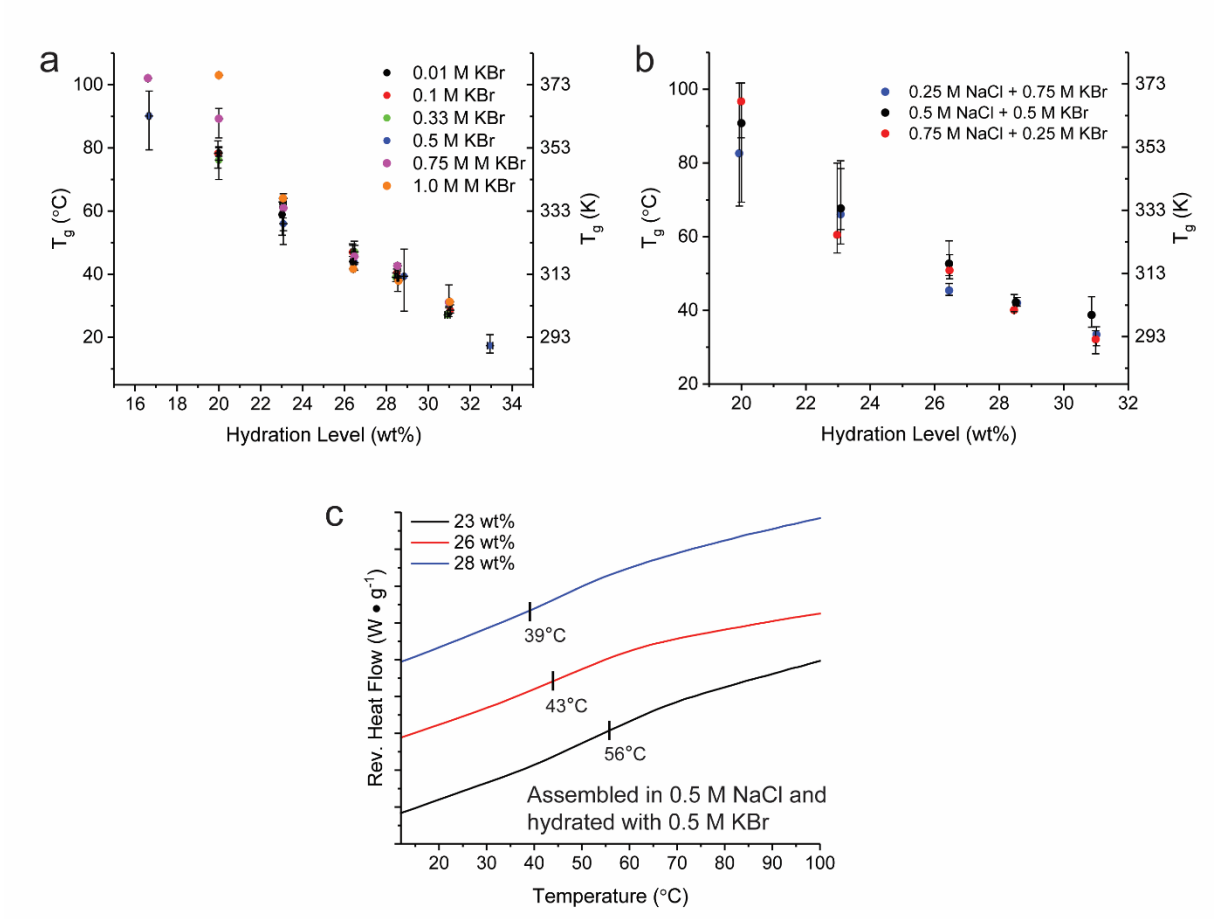

Figure 4.1. Average T_g values of free-standing $(PDADMA/PSS)_{140}$ LbL assemblies constructed in 0.5 M NaCl and hydrated to various levels with (a) KBr solutions of different salt concentrations and (b) salt mixtures of NaCl and KBr with a fixed ionic strength of 1.0 M. (c) Representative reversing heat flow plots for LbL assemblies constructed in 0.5 M NaCl and hydrated with 0.5 M KBr to various wt% values. For the sake of clarity, the curves have been shifted along the y-axis.

This is seemingly different behavior than what was previously observed in PDADMA/PSS thin films using quartz-crystal microbalance with dissipation (QCM-D), where the films swelled and softened readily in the presence of elevated KBr concentrations.[140] However, the films

analyzed by QCM-D were fully submerged and saturated with water for the duration of the experiments. In the present case, the films are only exposed to specific hydration levels. This limited water brings to light the duality of the water/salt relationship and its effects on PDADMA/PSS LbL film properties. Above 20 wt% hydration, the T_g behavior changes predictably with increasing water content, and the KBr concentration has no noticeable effect. An increase in chain mobility associated with increased bulk water, rather than counterions, results in a lower observed T_g. This could imply that the internal structure of the PDADMA/PSS LbL assemblies is relatively fixed upon assembly, and does not change significantly upon addition of counterions when the hydration levels are kept relatively low (below 35%).

To test whether the presence of KBr or NaCl in the hydration solutions would have a greater net effect on the T_g of the PDADMA/PSS films, salt mixtures of NaCl and KBr were prepared with a fixed ionic strength of 1.0 M, and the molar ratio of NaCl:KBr was varied. The films were then hydrated to various levels with solutions of the different salt mixtures and analyzed using MDSC. The resulting T_g values indicate that even with changing ratios of NaCl and KBr, the glass transition behavior is dominated almost entirely by the hydration level (see Figure 4.1b). At 20 wt% hydration, the films showed average T_g's of 96.7°C, 90.8°C, and 82.6°C when hydrated with 0.25 M NaCl + 0.75 KBr, 0.5 M NaCl + 0.5 M KBr, and 0.75 NaCl + 0.25 M KBr, respectively. The large variation in experimental error, however, makes these differences difficult to interpret. This error is likely caused by the elevated salt:water ratio as well as the competition between NaCl and KBr in the doping process. Some sample-to-sample variation is expected at the extreme low end of the hydration level range due to experimental human error as well. Figure 4.1c shows representative reversing heat flow curves for selected experimental runs. It seems that the overall

internal structure of the PDADMA/PSS film remains relatively unchanged by the addition of the salt mixtures when hydration is limited. It is likely that there is not enough water present to facilitate large scale internal restructuring and conversion of intrinsic binding sites to extrinsic binding sites. As the even upper limit of the hydration level was approached, however, the visible trend in T_g is clearly observed. The T_g values in the of 23 wt% to 31 wt% show a strong dependence on hydration level rather than NaCl:KBr ratio.

To determine if internal structure of PDADMA/PSS films is the primary factor influencing T_g at limited hydration levels, LbL assemblies were prepared in 0.5 M KBr, keeping the same ionic strength as the films prepared in NaCl. It was expected that the films assembled in KBr would contain a greater number of extrinsic binding sites due to the ability of Br^- to efficiently dope the PDADMA/PSS system.[140, 144] Upon completion the $(PDADMA/PSS)_{140}$ films were analyzed using ^1H NMR and NAA. The thickness of the films assembled in KBr were significantly higher than films assembled in NaCl, which is attributed to the more coiled chain conformation during deposition of the PE solutions. This difference in thickness of PDADMA/PSS LbL assemblies formed in NaCl and KBr is consistent with previous studies.[18, 20, 34, 49, 161] It has been proposed that larger counterions with small, less ordered hydration shells (chaotropes) have the ability to achieve closer proximity to charge sites on polyelectrolyte chains and, therefore, allow for a more coiled chain conformation.[20, 140, 162] Conversely, counterions with more ordered, larger hydration shells (kosmotropes) are unable to condense as efficiently around charge sites of polyelectrolytes and are less efficient at screening charges locally. The result is more steric hindrance and electrostatic repulsion, giving a more extended conformation of the chains in solution. The deposition of chains in a more coiled configuration results in a more highly interpenetrated structure, greater overall free volume, and elevated bulk water content. Additionally, LbL assembles formed in the presence

of chaotropic counterion species will likely contain a greater number of counterions due to more excessive doping.[40, 144] Figure 4.2 gives an illustration of the difference in resulting internal structures between films assembled in NaCl and films assembled in KBr.

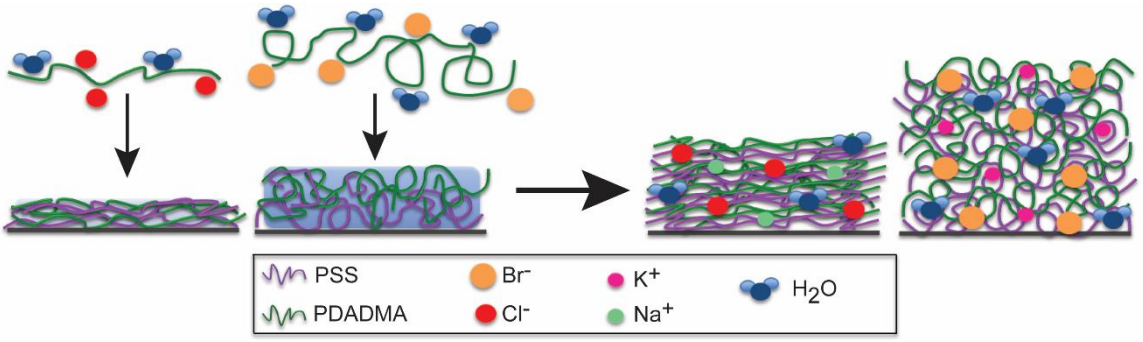

Figure 4.2. Illustrated construction of PDADMA/PSS LbL assemblies in KBr and NaCl showing the internal structure of the films is directly affected by how the counterions dope the PE assembly.

It was found using ^{1}H NMR that the amount of PSS present within the PDADMA/PSS LbL assemblies constructed in 0.5 M KBr was 35-36 mol%. This is the same amount reported for films prepared in 0.5 M NaCl.[140] However, the NAA results displayed in Table 4.1 show that Br^- is present in the films at 12.7 wt%. This is significantly higher than the Cl^- content present in films assembled in 0.5 M NaCl, 2.9 wt%. It is reasonable to conclude, based on this finding, that there are more extrinsic binding sites in PDADMA/PSS LbL assemblies constructed in KBr than those constructed in NaCl at the same ionic strength.

Table 4.1. Counter ion wt% within free-standing $(PDADMA/PSS)_{140}$ films after assembly in NaCl, KBr.[a)]

Assembly Salt	Br^- [wt%]	Cl^- [wt%]	K^+ [wt%]	Na^+ [wt%]
0.5 M NaCl[b)]	ND	2.9	ND	0.28
0.5 M KBr	12.7	ND	0.923	ND
0.5 M NaCl and exchanged with 0.5 M KBr[b)]	7.5	0.017	0.18	0.0025

[a)] Data was obtained with less than 10% error and all values listed are averages of three samples for each data point; [b)] Values taken from reference 140, copyright 2017 American Chemical Society.

The difference in number of extrinsic ion pairs means that the excess PDADMA chains in the bulk of the film are not as kinetically trapped and are more mobile. For films assembled in 0.5 M NaCl and subjected to ion-exchange with 0.5 M KBr, the data indicates a nearly even exchange of all counterions. This implies that the exchange results in minimal disruption of intrinsic ion pairs and supports the notion that the internal film structure is relatively fixed after assembly. This trend was consistent even at ion-exchanges at elevated KBr concentrations.[140]

Figure 4.3a shows the T_g values for $(PDADMA/PSS)_{140}$ LbL assemblies constructed in 0.5 M KBr (or 0.5 M NaCl) and hydrated with 0.5 M KBr solutions. There is a clear difference in T_g values of nearly 20°C between the two data sets with the exception of hydration levels above 30 wt%. Additionally, Figure 4.3b shows the T_g values for $(PDADMA/PSS)_{140}$ films assembled in 0.5 M KBr after being hydrated with 0.1 M KBr or 0.5 M KBr. The data points overlap almost

perfectly across the hydration range. It has been reported that the effects of monovalent counterions on the construction of PDADMA/PSS LbL assemblies are not visible below 0.1 M ionic strength.[21] This is because below this ionic strength, the PE-PE interactions dominate the assembly process. Above 0.1 M, the interactions between PE chains are disrupted by the electrostatic screening caused by the increase in counterions. Here, we see that completed free-standing films hydrated with relatively low ionic strength, 0.1 M KBr, and up to 0.5 M KBr show no significant difference in T_g across the range of hydration levels. This further indicates that the stability of the structure after assembly as well as the fact that water, rather than the added salt, is driving the change in T_g.

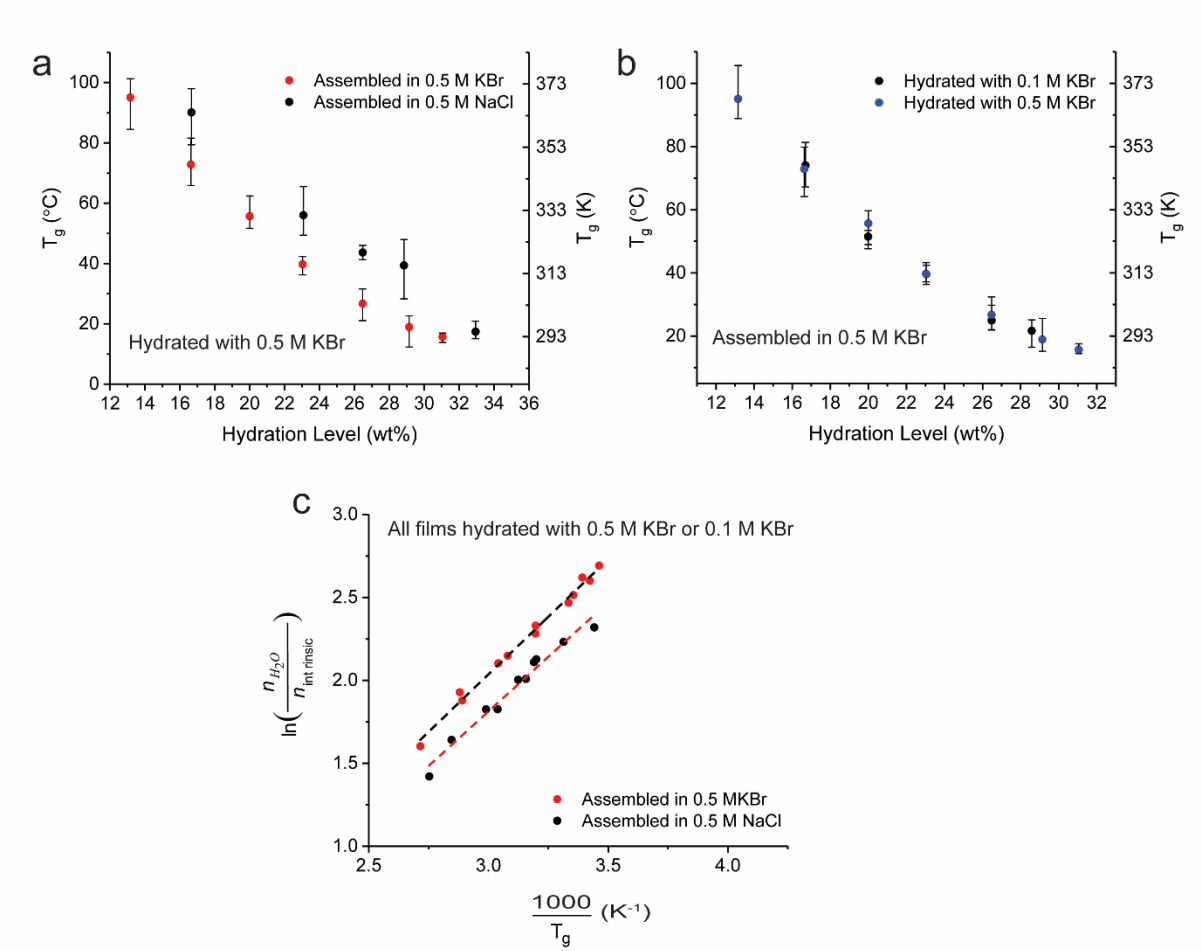

Figure 4.3. (a) Average T_g values of free-standing $(PDADMA/PSS)_{140}$ LbL assemblies constructed in 0.5 M KBr (red circles) or 0.5 M NaCl (black circles), and then hydrated to various levels using solutions containing 0.5 M KBr, (b) Average T_g values for $(PDADMA/PSS)_{140}$ LbL assemblies constructed in 0.5 M KBr and hydrated using solutions containing 0.1 M KBr (black cirlces) and 0.5 M KBr (blue circles), and (c) Overlay of T_g vs water molecules per intrinsic ion pair and linear fits for PDADMA/PSS LbL assemblies formed in 0.5 M NaCl (black circles) and 0.5 M KBr (red circles) and then hydrated with KBr solutions with ionic strengths of 0.1 M or 0.5 M.

Previous reports have revealed the relationship between the T_g of PECs and the number of intrinsic ion pairs as well as the water present within the complex.[39, 78-79] Values plotted in Figure 4.3c were calculated by combining data collected from NAA and ^{1}H NMR. It was assumed that since the PSS mol% was the same for films assembled in NaCl and KBr at the same ionic strength but the wt% or counterions differed, the same only difference between the two LbL films would be the number of intrinsic and extrinsic ion pairs. This allowed for the calculation of the number of water molecules per intrinsic ion pairs through a combination of both data sets. Any inconsistencies or errors can be attributed to breakdown of the assumptions. Fitting analysis of the data in Figure 4.3c gives an activation energy value of E_a = 10.9 ± 1.54 kJ/mol and 11.5 ± 0.59 kJ/mol for films assembled NaCl and KBr, respectively. Their activation energies are similar to the value of disruption of one hydrogen bond, 10.5 ± 2.5 kJ/mol, indicating the potential role of water and the hydrogen bonds between water and the LbL assembly network.[163] The y-intercepts from the two linear fits are slightly different, which could be attributed to the difference in counterion properties such as ionic radii. These findings are consistent with concurrent studies in our group regarding PDADMA/PSS complexes assembled in the presence of NaCl.

The difference in T_g values observed for films assembled in 0.5 M NaCl and 0.5 M KBr is related to the mobility of the chains in the bulk of the LbL assemblies, which is directly influenced by the assembly conditions. In this case, the doping ability of KBr during assembly causes a significant change in the internal structure compared to NaCl. Changes in assembly salt concentration reportedly have a seemingly small influence on the experimentally observed T_g.[79] However, changes in assembly salt *identity* can greatly impact film properties. Even at the same assembly ionic strength, LbL assemblies can exhibit largely different responsive properties, despite maintaining the same polyanion:polycation ratio. It is clear that assembling

PDADMA/PSS LbL assemblies in KBr produces films with highly interpenetrated and more loosely packed structures. Elevated free volume and an increased number of extrinsic binding sites allow the film to be readily plasticized by incoming water, giving a lower T_g value than films assembled in NaCl. The films produced in NaCl have a more tightly packed structure and lower free volume, making plasticization and molecular motion more difficult. To our knowledge, this is the first time the T_g of PDADMA/PSS LbL assemblies has been recorded after assembly in KBr. The results show that the thermal response of these films can be tailored by changing the counterion species used in the assembly process. This finding is key for producing materials for specific applications in which temperature fluctuations are a concern with regards to performance. Adjusting preparation parameters is, in this case, quicker and easier than lengthy post-assembly film modification such as thermal annealing or chemical functionalization.

4.4 Conclusions

Previous studies have reported on the effect of ion type on the growth behavior and resulting properties of LbL assemblies.[18-19, 21, 37, 164] Their results point to the fact that counteranions have a much stronger influence than water alone on the internal structure of the PDADMA/PSS system specifically. A greater degree of internal and surface roughness is associated with increasingly chaotropic anions according to their positions along the Hofmeister series. In particular, salts containing Br^- have the greatest impact on the growth behavior of PDADMA/PSS LbL assemblies, resulting in higher free volume than films assembled in the presence F^- or Cl^-.[21] Our current study reveals a direct connection between the change in internal structure and composition with regard to intrinsic and extrinsic ion pairing associated with changing counterion type and the glass transition. The introduction of additional counterions after assembly has little effect when the overall level of hydration is limited. The salt type employed

during the assembly process directly impacts the resulting internal structure of the PDADMA/PSS LbL assemblies by controlling the number of extrinsic ion pairs. Future work will focus on assembling these films in various salts along the Hofmeister series in order to observe the changes in composition and thermal properties. These findings are important for developing materials for specific applications including filtration membranes, chemical sensors, and implantable biomedical devices in which fluctuating, dynamic environmental conditions of a primary concern.[68, 136, 138]

CHAPTER V

SUMMARY AND FUTURE WORK

5.1 Summary

This thesis investigated the physical and thermal responsive properties of hydrogen-bonded and electrostatic LbL assemblies and nanocomposites. The internal structure and pH sensitivity and release properties of PEO/PMAA LbL films containing segregated regions of AuNPs were studied using TEM and UV-Vis spectroscopy, respectively. The physical swelling and contraction of PDADMA/PSS LbL films in response to changing counterion species was studied in detail using QCM-D, and the complete exchange of counterions was demonstrated using NAA. The glass transition behavior of PDADMA/PSS LbL films was explored using MDSC with respect to changing hydration level, post-assembly addition of salt, as well as assembly ionic conditions.

Hydrogen-bonded LbL films of PEO/PMAA containing discrete layers of AuNPs were successfully fabricated using spray-assisted LbL assembly for the first time. Cross-sectional TEM imaging and UV-Vis spectroscopy revealed that no significant aggregation of the AuNPs occurred during or after assembly. The thickness of the layers containing AuNPs as well as the "empty" PE separation layers proved to be tunable by the addition or subtraction of PE or AuNP depositions. Additionally, the time-dependent release of the AuNPs could be modulated by adjusting the environmental pH. The PEO/PMAA films disassemble at elevated pH values above the pH_{crit} of 4.5, and total disassembly time decreases rapidly from 6 h at pH 10 to 2.5 h at pH 11. Spatial organization of the AuNPs within the PEO/PMAA network proved to be successful and can be adjusted by multiple parameters including, assembly pH, number of layer pairs deposited at different stages of film growth, and post-assembly environmental pH.

Physical swelling and contraction of PDADMA/PSS LbL films in the presence of various monovalent counterions were analyzed using QCM-D. Fully hydrated films assembled in 0.5 M NaCl were exposed to KBr at various concentration and exhibited four behavior regimes associated with different concentration ranges. At ultra-low concentrations, 0.001 M KBr and below, the films swelled up to 120% due to electrostatic repulsion. As KBr concentration increased and approached the assembly ionic strength, 0.5 M, the films contracted due to internal restructuring facilitated by the incoming counterions. Above 0.5 M KBr the LbL films swelled linearly with increasing ionic strength up to 1.6 M, swelling up to 100%, and the films completely disassembled at 2.0 M KBr. The swelling was attributed to excessive doping of the Br^- ions of PDADMA chains and the conversion of intrinsic PE-PE ion pairs to extrinsic PE-counterion pairs. Film dissolution occurs when electrostatic screening becomes too extensive to allow the film to remain intact. A comparison of the swelling behavior of the PDADMA/PSS LbL films in the presence of NaCl, KCl, and NaBr demonstrated that salts containing Br^- have a stronger effect on the swelling than salts containing NaCl. Elemental analysis by NAA showed that films assembled in NaCl could undergo complete ion exchange when immersed in solutions of KBr.

Glass transition behavior of partially hydrated PDADMA/PSS LbL films were analyzed using MDSC. The effects of assembly conditions, limited hydration, and added salt on the observed T_g were compared. The shift in T_g values for films assembled in NaCl and hydrated using KBr salt solutions at various hydration levels points to the fact that water, rather than added salt influences the T_g by plasticizing the network. T_g values decreased as water content increased, but no significant shift was observed with changes in KBr concentration. At elevated salt concentration, 0.75 M and 1.0 M, the T_g values deviated from the trend only at the lowest hydration values, less than 20 wt%. This was caused by the competition for water as a plasticizer in the film

and the formation of counterion hydration shells as the salt:water ratio increases. Upon changing the assembly salt from NaCl to KBr, the observed T_g of the PDADMA/PSS films decreased by around 20°C for hydration levels below 35 wt%. Analysis by NAA and ^{1}H NMR indicate that films formed in the presence of KBr contain a higher concentration of counterions while maintining the same ratio or polyelectrolytes. An elevated number of extrinsic binding sites means the films have a more loosely packed structure than films assembled in NaCl, providing a lower barrier to long-range segmental chain mobility necessary for a T_g. The study connects the assembly conditions, internal structure, and counterion concentration with the thermal properties of PDADMA/PSS LbL films.

5.2 Future Work

Hydrogen-bonded LbL films have the potential to be used in unique applications. The responsive properties as well as the capacity to include uncharged species, biological molecules, and nanoparticles make hydrogen-bonded attractive for extended study. Future work for Chapter II of this could include a study of the effects of varying the ligand groups on the AuNPs in order to increase nanoparticle loading and relative concentration within the AuNP-rich layers. Additionally, changing the thickness of different regions of the films could be further adjusted in order to delay or "burst-release" the payload of AuNPs.

The physical response of electrostatic LbL films to changes in the ionic environment warrants further exploration as well. Studies dealing specifically with the effects of counterions on the internal structure and physical properties of LbL films are rare, and there remains much to understand. Future work in this area could extend to different salt types along the hofmeister series. In addition, molecular modeling and simulation could help yield deeper insight into the dynamics of the interactions between counterions and PE-PE ion pairs within the LbL network.

The quantitative modeling approach would provide a clearer picture of the interatomic interactions, and aid in the understanding of why specific counterions have a much stronger effect on the extrinsiv vs. intrinsic ion pairing behavior within LbL films. Finally, studying additional PE systems and their response to changing ionic environments would begin to widen the field of materials that have potential for use in many applications where environmental adaptability or resistance may be of key importance.

Despite the increasing body of knowledge surrounding the glass transition behavior of polyelectrolyte complexes and multilayers, there is still much to be learned. The factors that influence the T_g of the PDADMA/PSS system alone are still not yet well understood, and no long term studies have been conducted to fully explore them. Future work on this system should include an extensive study of the influence of assembly conditions such as salt type and ionic strength on the T_g. Assembling LbL films in the presence of salts with ionic radii and hydration shell properties would provide clearer insight into the structure and property relationship that seems to significantly influence the thermal properties of resulting LbL films.

REFERENCES

1. Dubas, S. T.; Schlenoff, J. B., Factors controlling the growth of polyelectrolyte multilayers. *Macromolecules* **1999,** *32* (24), 8153-8160.

2. Ariga, K.; Yamauchi, Y.; Rydzek, G.; Ji, Q. M.; Yonamine, Y.; Wu, K. C. W.; Hill, J. P., Layer-by-layer Nanoarchitectonics: Invention, Innovation, and Evolution. *Chem. Lett.* **2014,** *43* (1), 36-68.

3. Richardson, J. J.; Bjornmalm, M.; Caruso, F., Technology-driven layer-by-layer assembly of nanofilms. *Science* **2015,** *348* (6233), 12.

4. Holder, K. M.; Smith, R. J.; Grunlan, J. C., A review of flame retardant nanocoatings prepared using layer-by-layer assembly of polyelectrolytes. *J. Mater. Sci.* **2017,** *52* (22), 12923-12959.

5. Hammond, P. T., Building biomedical materials layer-by-layer. *Materials Today* **2012,** *15* (5), 196-206.

6. Iler, R. K., Multilayers of Colloidal Particles. *J. Colloid Interface Sci.* **1966,** *21* (6), 569.

7. Decher, G., Fuzzy nanoassemblies: Toward layered polymeric multicomposites. *Science* **1997,** *277* (5330), 1232-1237.

8. Kozlovskaya, V.; Kharlampieva, E.; Khanal, B. P.; Manna, P.; Zubarev, E. R.; Tsukruk, V. V., Ultrathin Layer-by-Layer Hydrogels with Incorporated Gold Nanorods as pH-Sensitive Optical Materials. *Chemistry of Materials* **2008,** *20* (24), 7474-7485.

9. O'Neal, J. T.; Bolen, M. J.; Dai, E. Y.; Lutkenhaus, J. L., Hydrogen-bonded polymer nanocomposites containing discrete layers of gold nanoparticles. *J. Colloid Interface Sci.* **2017,** *485*, 260-268.

10. Iqbal, N.; Afzal, A.; Mujahid, A., Layer-by-layer assembly of low-temperature-imprinted poly(methacrylic acid)/gold nanoparticle hybrids for gaseous formaldehyde mass sensing. *Rsc Advances* **2014,** *4* (81), 43121-43130.

11. Wang, X.; Gao, K. Z.; Shao, Z. Q.; Peng, X. Q.; Wu, X.; Wang, F. J., Layer-by-Layer assembled hybrid multilayer thin film electrodes based on transparent cellulose nanofibers paper for flexible Supercapacitors applications. *J. Power Sources* **2014,** *249*, 148-155.

12. Shao, L.; Jeon, J. W.; Lutkenhaus, J. L., Polyaniline nanofiber/vanadium pentoxide sprayed layer-by-layer electrodes for energy storage. *Journal of Materials Chemistry A* **2014,** *2* (35), 14421-14428.

13. Kwon, S. R.; Jeon, J. W.; Lutkenhaus, J. L., Sprayable, paintable layer-by-layer polyaniline nanofiber/graphene electrodes. *Rsc Advances* **2015,** *5* (20), 14994-15001.

14. Decher, G., Layer-by-Layer Assembly (Putting Molecules to Work). In *Multilayer Thin Films*, Wiley-VCH Verlag GmbH & Co. KGaA: 2012; pp 1-21.

15. Bieker, P.; Schonhoff, M., Linear and Exponential Growth Regimes of Multi layers of Weak Polyelectrolytes in Dependence on pH. *Macromolecules* **2010,** *43* (11), 5052-5059.

16. Schoeler, B.; Kumaraswamy, G.; Caruso, F., Investigation of the influence of polyelectrolyte charge density on the growth of multilayer thin films prepared by the layer-by-layer technique. *Macromolecules* **2002,** *35* (3), 889-897.

17. Dubas, S. T.; Schlenoff, J. B., Polyelectrolyte multilayers containing a weak polyacid: Construction and deconstruction. *Macromolecules* **2001,** *34* (11), 3736-3740.

18. Liu, G. M.; Hou, Y.; Xiao, X. A.; Zhang, G. Z., Specific Anion Effects on the Growth of a Polyelectrolyte Multilayer in Single and Mixed Electrolyte Solutions Investigated with Quartz Crystal Microbalance. *J. Phys. Chem. B* **2010,** *114* (31), 9987-9993.

19. Wong, J. E.; Zastrow, H.; Jaeger, W.; von Klitzing, R., Specific Ion versus Electrostatic Effects on the Construction of Polyelectrolyte Multilayers. *Langmuir* **2009,** *25* (24), 14061-14070.

20. Salomaki, M.; Tervasmaki, P.; Areva, S.; Kankare, J., The Hofmeister anion effect and the growth of polyelectrolyte multilayers. *Langmuir* **2004,** *20* (9), 3679-3683.

21. Dodoo, S.; Steitz, R.; Laschewsky, A.; von Klitzing, R., Effect of ionic strength and type of ions on the structure of water swollen polyelectrolyte multilayers. *Phys. Chem. Chem. Phys.* **2011,** *13* (21), 10318-10325.

22. Salomaki, M.; Kankare, J., Specific anion effect in swelling of polyelectrolyte multilayers. *Macromolecules* **2008,** *41* (12), 4423-4428.

23. Kharlampieva, E.; Sukhishvili, S. A., Hydrogen-bonded layer-by-layer polymer films. *Polymer Reviews* **2006,** *46* (4), 377-395.

24. Kharlampieva, E.; Kozlovskaya, V.; Tyutina, J.; Sukhishvili, S. A., Hydrogen-bonded multilayers of thermoresponsive polymers. *Macromolecules* **2005,** *38* (25), 10523-10531.

25. Borges, J.; Mano, J. F., Molecular Interactions Driving the Layer-by-Layer Assembly of Multilayers. *Chem. Rev.* **2014,** *114* (18), 8883-8942.

26. Stockton, W. B.; Rubner, M. F., Molecular-level processing of conjugated polymers .4. Layer-by-layer manipulation of polyaniline via hydrogen-bonding interactions. *Macromolecules* **1997,** *30* (9), 2717-2725.

27. Kharlampieva, E.; Kozlovskaya, V.; Sukhishvili, S. A., Layer-by-Layer Hydrogen-Bonded Polymer Films: From Fundamentals to Applications. *Adv. Mater.* **2009,** *21* (30), 3053-3065.

28. Sukhishvili, S. A.; Granick, S., Layered, erasable polymer multilayers formed by hydrogen-bonded sequential self-assembly. *Macromolecules* **2002,** *35* (1), 301-310.

29. Sukhishvili, S. A.; Granick, S., Layered, erasable, ultrathin polymer films. *J. Am. Chem. Soc.* **2000,** *122* (39), 9550-9551.

30. Kharlampieva, E.; Ankner, J. F.; Rubinstein, M.; Sukhishvili, S. A., pH-induced release of polyanions from multilayer films. *Phys. Rev. Lett.* **2008,** *100* (12), 4.

31. Laugel, N.; Betscha, C.; Winterhalter, M.; Voegel, J. C.; Schaaf, P.; Ball, V., Relationship between the growth regime of polyelectrolyte multilayers and the polyanion/polycation complexation enthalpy. *J. Phys. Chem. B* **2006,** *110* (39), 19443-19449.

32. Bucur, C. B.; Sui, Z.; Schlenoff, J. B., Ideal mixing in polyelectrolyte complexes and multilayers: Entropy driven assembly. *J. Am. Chem. Soc.* **2006,** *128* (42), 13690-13691.

33. Bertrand, P.; Jonas, A.; Laschewsky, A.; Legras, R., Ultrathin polymer coatings by complexation of polyelectrolytes at interfaces: suitable materials, structure and properties. *Macromol. Rapid Commun.* **2000,** *21* (7), 319-348.

34. Volodkin, D.; von Klitzing, R., Competing mechanisms in polyelectrolyte multilayer formation and swelling: Polycation-polyanion pairing vs. polyelectrolyte-ion pairing. *Curr. Opin. Colloid Interface Sci.* **2014,** *19* (1), 25-31.

35. von Klitzing, R., Internal structure of polyelectrolyte multilayer assemblies. *Phys. Chem. Chem. Phys.* **2006,** *8* (43), 5012-5033.

36. Losche, M.; Schmitt, J.; Decher, G.; Bouwman, W. G.; Kjaer, K., Detailed structure of molecularly thin polyelectrolyte multilayer films on solid substrates as revealed by neutron reflectometry. *Macromolecules* **1998,** *31* (25), 8893-8906.

37. Buscher, K.; Graf, K.; Ahrens, H.; Helm, C. A., Influence of adsorption conditions on the structure of polyelectrolyte multilayers. *Langmuir* **2002,** *18* (9), 3585-3591.

38. Schlenoff, J. B.; Ly, H.; Li, M., Charge and mass balance in polyelectrolyte multilayers. *J. Am. Chem. Soc.* **1998,** *120* (30), 7626-7634.

39. Zhang, Y. P.; Li, F.; Valenzuela, L. D.; Sammalkorpi, M.; Lutkenhaus, J. L., Effect of Water on the Thermal Transition Observed in Poly(allylamine hydrochloride)-Poly(acrylic acid) Complexes. *Macromolecules* **2016,** *49* (19), 7563-7570.

40. Ghostine, R. A.; Markarian, M. Z.; Schlenoff, J. B., Asymmetric Growth in Polyelectrolyte Multilayers. *J. Am. Chem. Soc.* **2013,** *135* (20), 7636-7646.

41. Reid, D. K.; Summers, A.; O'Neal, J.; Kavarthapu, A. V.; Lutkenhaus, J. L., Swelling and Thermal Transitions of Polyelectrolyte Multilayers in the Presence of Divalent Ions. *Macromolecules* **2016,** *49* (16), 5921-5930.

42. Elbert, D. L.; Herbert, C. B.; Hubbell, J. A., Thin polymer layers formed by polyelectrolyte multilayer techniques on biological surfaces. *Langmuir* **1999,** *15* (16), 5355-5362.

43. Picart, C.; Mutterer, J.; Richert, L.; Luo, Y.; Prestwich, G. D.; Schaaf, P.; Voegel, J. C.; Lavalle, P., Molecular basis for the explanation of the exponential growth of polyelectrolyte multilayers. *Proc. Natl. Acad. Sci. U. S. A.* **2002,** *99* (20), 12531-12535.

44. Hoda, N.; Larson, R. G., Modeling the Buildup of Exponentially Growing Polyelectrolyte Multilayer Films. *J. Phys. Chem. B* **2009,** *113* (13), 4232-4241.

45. Porcel, C.; Lavalle, P.; Ball, V.; Decher, G.; Senger, B.; Voegel, J. C.; Schaaf, P., From exponential to linear growth in polyelectrolyte multilayers. *Langmuir* **2006,** *22* (9), 4376-4383.

46. Porcel, C.; Lavalle, P.; Decher, G.; Senger, B.; Voegel, J. C.; Schaaf, P., Influence of the polyelectrolyte molecular weight on exponentially growing multilayer films in the linear regime. *Langmuir* **2007,** *23* (4), 1898-1904.

47. Xu, L.; Pristinski, D.; Zhuk, A.; Stoddart, C.; Ankner, J. F.; Sukhishvili, S. A., Linear versus Exponential Growth of Weak Polyelectrolyte Multilayers: Correlation with Polyelectrolyte Complexes. *Macromolecules* **2012,** *45* (9), 3892-3901.

48. Kharlampieva, E.; Kozlovskaya, V.; Ankner, J. F.; Sukhishvili, S. A., Hydrogen-Bonded Polymer Multilayers Probed by Neutron Reflectivity. *Langmuir* **2008,** *24* (20), 11346-11349.

49. Salomaki, M.; Laiho, T.; Kankare, J., Counteranion-controlled properties of polyelectrolyte multilayers. *Macromolecules* **2004,** *37* (25), 9585-9590.

50. Ostendorf, A.; Cramer, C.; Decher, G.; Schonhoff, M., Humidity-Tunable Electronic Conductivity of Polyelectrolyte Multilayers Containing Gold Nanoparticles. *Journal of Physical Chemistry C* **2015,** *119* (17), 9543-9549.

51. Han, L. L.; Mao, Z. W.; Wuliyasu, H.; Wu, J. D.; Gong, X.; Yang, Y. G.; Gao, C. Y., Modulating the Structure and Properties of Poly(sodium 4-styrenesulfonate)/Poly(diallyldimethylammonium chloride) Multilayers with Concentrated Salt Solutions. *Langmuir* **2012,** *28* (1), 193-199.

52. Lee, D.; Omolade, D.; Cohen, R. E.; Rubner, M. F., pH-Dependent structure and properties of TiO2/SiO2 nanoparticle multilayer thin films. *Chemistry of Materials* **2007,** *19* (6), 1427-1433.

53. Wang, Q. F.; Schlenoff, J. B., The Polyelectrolyte Complex/Coacervate Continuum. *Macromolecules* **2014,** *47* (9), 3108-3116.

54. Zan, X. J.; Peng, B.; Hoagland, D. A.; Su, Z. H., Polyelectrolyte uptake by PEMs: Impact of salt concentration. *Polym. Chem.* **2011,** *2* (11), 2581-2589.

55. Zan, X. J.; Hoagland, D. A.; Wang, T.; Peng, B.; Su, Z. H., Polyelectrolyte uptake by PEMs: Impacts of molecular weight and counterion. *Polymer* **2012,** *53* (22), 5109-5115.

56. Dubas, S. T.; Schlenoff, J. B., Swelling and smoothing of polyelectrolyte multilayers by salt. *Langmuir* **2001,** *17* (25), 7725-7727.

57. Song, Y. X.; Meyers, K. P.; Gerringer, J.; Ramakrishnan, R. K.; Humood, M.; Qin, S.; Polycarpou, A. A.; Nazarenko, S.; Grunlan, J. C., Fast Self-Healing of Polyelectrolyte Multilayer Nanocoating and Restoration of Super Oxygen Barrier. *Macromol. Rapid Commun.* **2017,** *38* (10), 7.

58. Zhuk, A.; Pavlukhina, S.; Sukhishvili, S. A., Hydrogen-Bonded Layer-by-Layer Temperature-Triggered Release Films. *Langmuir* **2009,** *25* (24), 14025-14029.

59. Lu, O. Y.; Malaisamy, R.; Bruening, M. L., Multilayer polyelectrolyte films as nanofiltration membranes for separating monovalent and divalent cations. *J. Membr. Sci.* **2008,** *310* (1-2), 76-84.

60. Bogue, R., Nanocomposites: a review of technology and applications. *Assembly Automation* **2011,** *31* (2), 106-112.

61. Tan, H. L.; McMurdo, M. J.; Pan, G. Q.; Van Patten, P. G., Temperature dependence of polyelectrolyte multilayer assembly. *Langmuir* **2003,** *19* (22), 9311-9314.

62. Eckle, M.; Decher, G., Tuning the performance of layer-by-layer assembled organic light emitting diodes by controlling the position of isolating clay barrier sheets. *Nano Lett.* **2001,** *1* (1), 45-49.

63. Kohler, K.; Biesheuvel, P. M.; Weinkamer, R.; Mohwald, H.; Sukhorukov, G. B., Salt-induced swelling-to-shrinking transition in polyelectrolyte multilayer capsules. *Phys. Rev. Lett.* **2006,** *97* (18), 4.

64. Ghostine, R. A.; Jisr, R. M.; Lehaf, A.; Schlenoff, J. B., Roughness and Salt Annealing in a Polyelectrolyte Multilayer. *Langmuir* **2013,** *29* (37), 11742-11750.

65. Fares, H. M.; Ghoussoub, Y. E.; Surmaitis, R. L.; Schlenoff, J. B., Toward Ion-Free Polyelectrolyte Multilayers: Cyclic Salt Annealing. *Langmuir* **2015,** *31* (21), 5787-5795.

66. Wei, J. J.; Hoagland, D. A.; Zhang, G. Y.; Su, Z. H., Effect of Divalent Counterions on Polyelectrolyte Multilayer Properties. *Macromolecules* **2016,** *49* (5), 1790-1797.

67. Fu, J. C.; Fares, H. M.; Schlenoff, J. B., Ion-Pairing Strength in Polyelectrolyte Complexes. *Macromolecules* **2017,** *50* (3), 1066-1074.

68. del Mercato, L. L.; Ferraro, M. M.; Baldassarre, F.; Mancarella, S.; Greco, V.; Rinaldi, R.; Leporatti, S., Biological applications of LbL multilayer capsules: From drug delivery to sensing. *Adv. Colloid Interface Sci.* **2014,** *207*, 139-154.

69. Yang, S. Y.; Rubner, M. F., Micropatterning of polymer thin films with pH-sensitive and cross-linkable hydrogen-bonded polyelectrolyte multilayers. *J. Am. Chem. Soc.* **2002,** *124* (10), 2100-2101.

70. Pavlukhina, S.; Lu, Y. M.; Patimetha, A.; Libera, M.; Sukhishvili, S., Polymer Multilayers with pH-Triggered Release of Antibacterial Agents. *Biomacromolecules* **2010,** *11* (12), 3448-3456.

71. Lu, Y. M.; Sarshar, M. A.; Du, K.; Chou, T. M.; Choi, C. H.; Sukhishvili, S. A., Large-Amplitude, Reversible, pH-Triggered Wetting Transitions Enabled by Layer-by-Layer Films. *ACS Appl. Mater. Interfaces* **2013,** *5* (23), 12617-12623.

72. Zelikin, A. N.; Li, Q.; Caruso, F., Disulfide-stabilized poly(methacrylic acid) capsules: Formation, cross-linking, and degradation behavior. *Chemistry of Materials* **2008,** *20* (8), 2655-2661.

73. Swiston, A. J.; Cheng, C.; Um, S. H.; Irvine, D. J.; Cohen, R. E.; Rubner, M. F., Surface Functionalization of Living Cells with Multilayer Patches. *Nano Lett.* **2008,** *8* (12), 4446-4453.

74. Lutkenhaus, J. L.; Hrabak, K. D.; McEnnis, K.; Hammond, P. T., Elastomeric flexible free-standing hydrogen-bonded nanoscale assemblies. *J. Am. Chem. Soc.* **2005,** *127* (49), 17228-17234.

75. Kohler, K.; Shchukin, D. G.; Mohwald, H.; Sukhorukov, G. B., Thermal behavior of polyelectrolyte multilayer microcapsules. 1. The effect of odd and even layer number. *J. Phys. Chem. B* **2005,** *109* (39), 18250-18259.

76. Vidyasagar, A.; Sung, C.; Gamble, R.; Lutkenhaus, J. L., Thermal Transitions in Dry and Hydrated Layer-by-Layer Assemblies Exhibiting Linear and Exponential Growth. *ACS Nano* **2012,** *6* (7), 6174-6184.

77. Sung, C. H.; Hearn, K. L.; Lutkenhaus, J., Thermal transitions in hydrated layer-by-layer assemblies observed using electrochemical impedance spectroscopy. *Soft Matter* **2014,** *10* (34), 6467-6476.

78. Yildirim, E.; Zhang, Y.; Lutkenhaus, J. L.; Sammalkorpi, M., Thermal Transitions in Polyelectrolyte Assemblies Occur via a Dehydration Mechanism. *ACS Macro Lett.* **2015,** *4* (9), 1017-1021.

79. Zhang, R.; Zhang, Y. P.; Antila, H. S.; Lutkenhaus, J. L.; Sammalkorpi, M., Role of Salt and Water in the Plasticization of PDAC/PSS Polyelectrolyte Assemblies. *J. Phys. Chem. B* **2017,** *121* (1), 322-333.

80. Sung, C.; Vidyasagar, A.; Hearn, K.; Lutkenhaus, J. L., Effect of Thickness on the Thermal Properties of Hydrogen-Bonded LbL Assemblies. *Langmuir* **2012,** *28* (21), 8100-8109.

81. Saha, K.; Agasti, S. S.; Kim, C.; Li, X. N.; Rotello, V. M., Gold Nanoparticles in Chemical and Biological Sensing. *Chem. Rev.* **2012,** *112* (5), 2739-2779.

82. Song, J. B.; Zhou, J. J.; Duan, H. W., Self-Assembled Plasmonic Vesicles of SERS-Encoded Amphiphilic Gold Nanoparticles for Cancer Cell Targeting and Traceable Intracellular Drug Delivery. *J. Am. Chem. Soc.* **2012,** *134* (32), 13458-13469.

83. Jain, P. K.; Huang, X. H.; El-Sayed, I. H.; El-Sayed, M. A., Noble Metals on the Nanoscale: Optical and Photothermal Properties and Some Applications in Imaging, Sensing, Biology, and Medicine. *Accounts of Chemical Research* **2008,** *41* (12), 1578-1586.

84. Jain, P. K.; Huang, X.; El-Sayed, I. H.; El-Sayad, M. A., Review of some interesting surface plasmon resonance-enhanced properties of noble metal nanoparticles and their applications to biosystems. *Plasmonics* **2007,** *2* (3), 107-118.

85. Jain, P. K.; El-Sayed, M. A., Plasmonic coupling in noble metal nanostructures. *Chemical Physics Letters* **2010,** *487* (4-6), 153-164.

86. Hamon, C.; Novikov, S.; Scarabelli, L.; Basabe-Desmonts, L.; Liz-Marzan, L. M., Hierarchical Self-Assembly of Gold Nanoparticles into Patterned Plasmonic Nanostructures. *ACS Nano* **2014,** *8* (10), 10694-10703.

87. De, M.; Ghosh, P. S.; Rotello, V. M., Applications of Nanoparticles in Biology. *Adv. Mater.* **2008,** *20* (22), 4225-4241.

88. Meli, L.; Green, P. F., Aggregation and coarsening of ligand-stabilized gold nanoparticles in poly(methyl methacrylate) thin films. *ACS Nano* **2008,** *2* (6), 1305-1312.

89. Li, D. X.; He, Q.; Cui, Y.; Li, J. B., Fabrication of pH-responsive nanocomposites of gold nanoparticles/poly(4-vinylpyridine). *Chemistry of Materials* **2007,** *19* (3), 412-417.

90. Zhang, H.; Han, J. S.; Yang, B., Structural Fabrication and Functional Modulation of Nanoparticle-Polymer Composites. *Advanced Functional Materials* **2010,** *20* (10), 1533-1550.

91. Green, P. F., The structure of chain end-grafted nanoparticle/homopolymer nanocomposites. *Soft Matter* **2011,** *7* (18), 7914-7926.

92. Kim, B. J.; Fredrickson, G. H.; Kramer, E. J., Effect of polymer ligand molecular weight on polymer-coated nanoparticle location in block copolymers. *Macromolecules* **2008,** *41* (2), 436-447.

93. Corbierre, M. K.; Cameron, N. S.; Sutton, M.; Laaziri, K.; Lennox, R. B., Gold nanoparticle/polymer nanocomposites: Dispersion of nanoparticles as a function of capping agent molecular weight and grafting density. *Langmuir* **2005,** *21* (13), 6063-6072.

94. Kumar, S. K.; Jouault, N.; Benicewicz, B.; Neely, T., Nanocomposites with Polymer Grafted Nanoparticles. *Macromolecules* **2013,** *46* (9), 3199-3214.

95. Rozenberg, B. A.; Tenne, R., Polymer-assisted fabrication of nanoparticles and nanocomposites. *Progress in Polymer Science* **2008,** *33* (1), 40-112.

96. Lee, D.; Gemici, Z.; Rubner, M. F.; Cohen, R. E., Multilayers of oppositely charged SiO2 nanoparticles: Effect of surface charge on multilayer assembly. *Langmuir* **2007,** *23* (17), 8833-8837.

97. Wu, Z.; Lee, D.; Rubner, M. F.; Cohen, R. E., Structural color in porous, superhydrophilic, and self-cleaning SiO2/TiO2 Bragg stacks. *Small* **2007,** *3* (8), 1445-1451.

98. Bassim, N. D.; Dressick, W. J.; Fears, K. P.; Stroud, R. M.; Clark, T. D.; Petrovykh, D. Y., Layer-by-Layer Assembly of Heterogeneous Modular Nanocomposites. *Journal of Physical Chemistry C* **2012,** *116* (2), 1694-1701.

99. Cunningham, A.; Muhlig, S.; Rockstuhl, C.; Burgi, T., Coupling of Plasmon Resonances in Tunable Layered Arrays of Gold Nanoparticles. *Journal of Physical Chemistry C* **2011,** *115* (18), 8955-8960.

100. Johnston, A. P. R.; Cortez, C.; Angelatos, A. S.; Caruso, F., Layer-by-layer engineered capsules and their applications. *Curr. Opin. Colloid Interface Sci.* **2006,** *11* (4), 203-209.

101. Kozlovskaya, V.; Harbaugh, S.; Drachuk, I.; Shchepelina, O.; Kelley-Loughnane, N.; Stone, M.; Tsukruk, V. V., Hydrogen-bonded LbL shells for living cell surface engineering. *Soft Matter* **2011,** *7* (6), 2364-2372.

102. Kim, Y.; Zhu, J.; Yeom, B.; Di Prima, M.; Su, X. L.; Kim, J. G.; Yoo, S. J.; Uher, C.; Kotov, N. A., Stretchable nanoparticle conductors with self-organized conductive pathways. *Nature* **2013,** *500* (7460), 59-U77.

103. Dunklin, J. R.; Forcherio, G. T.; Berry, K. R.; Roper, D. K., Gold Nanoparticle-Polydimethylsiloxane Thin Films Enhance Thermoplasmonic Dissipation by Internal Reflection. *Journal of Physical Chemistry C* **2014,** *118* (14), 7523-7531.

104. Kekicheff, P.; Schneider, G. F.; Decher, G., Size-Controlled Polyelectrolyte Complexes: Direct Measurement of the Balance of Forces Involved in the Triggered Collapse of Layer-by-Layer Assembled Nanocapsules. *Langmuir* **2013,** *29* (34), 10713-10726.

105. Chirea, M.; Pereira, C. M.; Silva, F., Catalytic effect of gold nanoparticles self-assembled in multilayered polyelectrolyte films. *Journal of Physical Chemistry C* **2007,** *111* (26), 9255-9266.

106. Qureshi, S. S.; Zheng, Z. Q.; Sarwar, M. I.; Felix, O.; Decher, G., Nanoprotective Layer-by-Layer Coatings with Epoxy Components for Enhancing Abrasion Resistance: Toward Robust Multimaterial Nanoscale Films. *ACS Nano* **2013,** *7* (10), 9336-9344.

107. Kozlovskaya, V.; Xue, B.; Lei, W. Q.; Padgett, L. E.; Tse, H. M.; Kharlampieva, E., Hydrogen-Bonded Multilayers of Tannic Acid as Mediators of T-Cell Immunity. *Advanced Healthcare Materials* **2015,** *4* (5), 686-694.

108. Sung, C.; Hearn, K.; Reid, D. K.; Vidyasagar, A.; Lutkenhaus, J. L., A Comparison of Thermal Transitions in Dip- and Spray-Assisted Layer-by-Layer Assemblies. *Langmuir* **2013,** *29* (28), 8907-8913.

109. Nogueira, G. M.; Banerjee, D.; Cohen, R. E.; Rubner, M. F., Spray-Layer-by-Layer Assembly Can More Rapidly Produce Optical-Quality Multistack Heterostructures. *Langmuir* **2011,** *27* (12), 7860-7867.

110. Kim, S. Y.; Hong, J.; Kavian, R.; Lee, S. W.; Hyder, M. N.; Shao-Horn, Y.; Hammond, P. T., Rapid fabrication of thick spray-layer-by-layer carbon nanotube electrodes for high power and energy devices. *Energy & Environmental Science* **2013,** *6* (3), 888-897.

111. Lu, C. H.; Donch, I.; Nolte, M.; Fery, A., Au nanoparticle-based multilayer ultrathin films with covalently linked nanostructures: Spraying layer-by-layer assembly and mechanical property characterization. *Chemistry of Materials* **2006,** *18* (26), 6204-6210.

112. Turkevich, J.; Stevenson, P. C.; Hillier, J., A Study of the Nucleation and Growth Processes in the Synthesis of Colloidal Gold. *Discussions of the Faraday Society* **1951,** (11), 55-&.

113. Doyen, M.; Bartik, K.; Bruylants, G., UV-Vis and NMR study of the formation of gold nanoparticles by citrate reduction: Observation of gold-citrate aggregates. *J. Colloid Interface Sci.* **2013,** *399*, 1-5.

114. Wuithschick, M.; Birnbaum, A.; Witte, S.; Sztucki, M.; Vainio, U.; Pinna, N.; Rademann, K.; Emmerling, F.; Kraehnert, R.; Polte, J., Turkevich in New Robes: Key Questions Answered for the Most Common Gold Nanoparticle Synthesis. *ACS Nano* **2015,** *9* (7), 7052-7071.

115. Jiang, M.; Li, M.; Xiang, M. L.; Zhou, H., Interpolymer complexation and miscibility enhancement by hydrogen bonding. In *Polymer Synthesis Polymer-Polymer Complexation*, Abe, A.; Albertsson, A. C.; Cantow, H. J.; Dusek, K.; Edwards, S.; Hocker, H.; Joanny, J. F.; Kausch, H. H.; Kobayashi, T.; Lee, K. S.; McGarth, J. E.; Monnerie, L.; Stupp, S. I.; Suter, U. W.; Thomas, E. L.; Wegner, G.; Young, R. J., Eds. Springer-Verlag Berlin: Berlin, 1999; Vol. 146, pp 121-196.

116. Seo, J.; Lutkenhaus, J. L.; Kim, J.; Hammond, P. T.; Char, K., Development of surface morphology in multilayered films prepared by layer-by-layer deposition using poly(acrylic acid) and hydrophobically modified poly(ethylene oxide). *Macromolecules* **2007,** *40* (11), 4028-4036.

117. Krogman, K. C.; Lyon, K. F.; Hammond, P. T., Metal Ion Reactive Thin Films Using Spray Electrostatic LbL Assembly. *Journal of Physical Chemistry B* **2008,** *112* (46), 14453-14460.

118. Norman, T. J.; Grant, C. D.; Magana, D.; Zhang, J. Z.; Liu, J.; Cao, D. L.; Bridges, F.; Van Buuren, A., Near infrared optical absorption of gold nanoparticle aggregates. *J. Phys. Chem. B* **2002,** *106* (28), 7005-7012.

119. Ghosh, S. K.; Pal, T., Interparticle coupling effect on the surface plasmon resonance of gold nanoparticles: From theory to applications. *Chem. Rev.* **2007,** *107* (11), 4797-4862.

120. Sukhishvili, S. A., Responsive polymer films and capsules via layer-by-layer assembly. *Curr. Opin. Colloid Interface Sci.* **2005,** *10* (1-2), 37-44.

121. Gao, X. Y.; Cao, Y.; Song, X. F.; Zhang, Z.; Zhuang, X. L.; He, C. L.; Chen, X. S., Biodegradable, pH-Responsive Carboxymethyl Cellulose/Poly(Acrylic Acid) Hydrogels for Oral Insulin Delivery. *Macromolecular Bioscience* **2014,** *14* (4), 565-575.

122. Mura, S.; Nicolas, J.; Couvreur, P., Stimuli-responsive nanocarriers for drug delivery. *Nature Materials* **2013,** *12* (11), 991-1003.

123. Kharlampieva, E.; Kozlovskaya, V.; Zavgorodnya, O.; Lilly, G. D.; Kotov, N. A.; Tsukruk, V. V., pH-responsive photoluminescent LbL hydrogels with confined quantum dots. *Soft Matter* **2010,** *6* (4), 800-807.

124. Lim, J.; Yang, H.; Paek, K.; Cho, C. H.; Kim, S.; Bang, J.; Kim, B. J., "Click" Synthesis of Thermally Stable Au Nanoparticles with Highly Grafted Polymer Shell and Control of Their Behavior in Polymer Matrix. *J. Polym. Sci. Pol. Chem.* **2011,** *49* (16), 3464-3474.

125. Kango, S.; Kalia, S.; Celli, A.; Njuguna, J.; Habibi, Y.; Kumar, R., Surface modification of inorganic nanoparticles for development of organic-inorganic nanocomposites-A review. *Progress in Polymer Science* **2013,** *38* (8), 1232-1261.

126. Corbierre, M. K.; Cameron, N. S.; Sutton, M.; Mochrie, S. G. J.; Lurio, L. B.; Ruhm, A.; Lennox, R. B., Polymer-stabilized gold nanoparticles and their incorporation into polymer matrices. *J. Am. Chem. Soc.* **2001,** *123* (42), 10411-10412.

127. Krogman, K. C.; Lowery, J. L.; Zacharia, N. S.; Rutledge, G. C.; Hammond, P. T., Spraying asymmetry into functional membranes layer-by-layer. *Nature Materials* **2009,** *8* (6), 512-518.

128. Kim, Y.; Lee, K. Y.; Hwang, S. K.; Park, C.; Kim, S. W.; Cho, J., Layer-by-Layer Controlled Perovskite Nanocomposite Thin Films for Piezoelectric Nanogenerators. *Advanced Functional Materials* **2014,** *24* (40), 6262-6269.

129. Hou, J.; Li, Q. Y.; Han, X.; Lu, C. H., Swelling/Deswelling-Induced Reversible Surface Wrinkling on Layerby-Layer Multilayers. *J. Phys. Chem. B* **2014,** *118* (49), 14502-14509.

130. Zan, X. J.; Hoagland, D. A.; Wang, T.; Su, Z. H., Ion Dispositions in Polyelectrolyte Multilayer Films. *Macromolecules* **2012,** *45* (21), 8805-8812.

131. Mermut, O.; Barrett, C. J., Effects of charge density and counterions on the assembly of polyelectrolyte multilayers. *J. Phys. Chem. B* **2003,** *107* (11), 2525-2530.

132. Richardson, J. J.; Cui, J. W.; Bjornmalm, M.; Braunger, J. A.; Ejima, H.; Caruso, F., Innovation in Layer-by-Layer Assembly. *Chem. Rev.* **2016,** *116* (23), 14828-14867.

133. Zhou, J.; Romero, G.; Rojas, E.; Ma, L.; Moya, S.; Gao, C. Y., Layer by layer chitosan/alginate coatings on poly(lactide-co-glycolide) nanoparticles for antifouling protection and Folic acid binding to achieve selective cell targeting. *J. Colloid Interface Sci.* **2010,** *345* (2), 241-247.

134. Lichter, J. A.; Rubner, M. F., Polyelectrolyte Multilayers with Intrinsic Antimicrobial Functionality: The Importance of Mobile Polycations. *Langmuir* **2009,** *25* (13), 7686-7694.

135. Lichter, J. A.; Van Vliet, K. J.; Rubner, M. F., Design of Antibacterial Surfaces and Interfaces: Polyelectrolyte Multilayers as a Multifunctional Platform. *Macromolecules* **2009,** *42* (22), 8573-8586.

136. Boudou, T.; Crouzier, T.; Ren, K. F.; Blin, G.; Picart, C., Multiple Functionalities of Polyelectrolyte Multilayer Films: New Biomedical Applications. *Adv. Mater.* **2010,** *22* (4), 441-467.

137. Kim, H.; Doh, J.; Irvine, D. J.; Cohen, R. E.; Hammond, P. T., Large area two-dimensional B cell arrays for sensing and cell-sorting applications. *Biomacromolecules* **2004,** *5* (3), 822-827.

138. de Grooth, J.; Oborny, R.; Potreck, J.; Nijmeijer, K.; de Vos, W. M., The role of ionic strength and odd-even effects on the properties of polyelectrolyte multilayer nanofiltration membranes. *J. Membr. Sci.* **2015,** *475*, 311-319.

139. Reisch, A.; Roger, E.; Phoeung, T.; Antheaume, C.; Orthlieb, C.; Boulmedais, F.; Lavalle, P.; Schlenoff, J. B.; Frisch, B.; Schaaf, P., On the Benefits of Rubbing Salt in the Cut: Self-Healing of Saloplastic PAA/PAH Compact Polyelectrolyte Complexes. *Adv. Mater.* **2014,** *26* (16), 2547-2551.

140. O'Neal, J. T.; Dai, E. Y.; Zhang, Y.; Clark, K. B.; Wilcox, K. G.; George, I. M.; Ramasamy, N. E.; Enriquez, D.; Batys, P.; Sammalkorpi, M.; Lutkenhaus, J. L., QCM-D Investigation of Swelling Behavior of Layer-by-Layer Thin Films upon Exposure to Monovalent Ions. *Langmuir* **2018,** *34* (3), 999-1009.

141. Gui, Z. L.; Du, B. Y.; Qian, J. W.; An, Q. F.; Zhao, Q. A., Construction and deconstruction of multilayer films containing polycarboxybetaine: Effect of pH and ionic strength. *J. Colloid Interface Sci.* **2011,** *353* (1), 98-106.

142. Dressick, W. J.; Wahl, K. J.; Bassim, N. D.; Stroud, R. M.; Petrovykh, D. Y., Divalent-Anion Salt Effects in Polyelectrolyte Multilayer Depositions. *Langmuir* **2012,** *28* (45), 15831-15843.

143. Dodoo, S.; Balzer, B. N.; Hugel, T.; Laschewsky, A.; von Klitzing, R., Effect of Ionic Strength and Layer Number on Swelling of Polyelectrolyte Multilayers in Water Vapour. *Soft Mater.* **2013,** *11* (2), 157-164.

144. Ghostine, R. A.; Shamoun, R. F.; Schlenoff, J. B., Doping and Diffusion in an Extruded Saloplastic Polyelectrolyte Complex. *Macromolecules* **2013,** *46* (10), 4089-4094.

145. Batys, P.; Luukkonen, S.; Sammalkorpi, M., Ability of the Poisson-Boltzmann equation to capture molecular dynamics predicted ion distribution around polyelectrolytes. *Phys. Chem. Chem. Phys.* **2017,** *19* (36), 24583-24593.

146. Ramos, J. J. I.; Llarena, I.; Moya, S. E., Unusual Collapse of Highly Hydrated Polyelectrolyte Multilayers with the Ionic Strength. *J. Polym. Sci. Pol. Chem.* **2011,** *49* (11), 2346-2352.

147. Irigoyen, J.; Han, L.; Llarena, I.; Mao, Z. W.; Gao, C. Y.; Moya, S. E., Responsive Polyelectrolyte Multilayers Assembled at High Ionic Strength with an Unusual Collapse at Low Ionic Strength. *Macromol. Rapid Commun.* **2012,** *33* (22), 1964-1969.

148. McCormick, M.; Smith, R. N.; Graf, R.; Barrett, C. J.; Reven, L.; Spiess, H. W., NMR studies of the effect of adsorbed water on polyelectrolyte multilayer films in the solid state. *Macromolecules* **2003,** *36* (10), 3616-3625.

149. Lyu, X. J.; Peterson, A. M., The Princess and the Pea Effect: Influence of the first layer on polyelectrolyte multilayer assembly and properties. *J. Colloid Interface Sci.* **2017,** *502*, 165-171.

150. Ghimici, L.; Dragan, S., Behaviour of cationic polyelectrolytes upon binding of electrolytes: effects of polycation structure, counterions and nature of the solvent. *Colloid Polym. Sci.* **2002,** *280* (2), 130-134.

151. Krasemann, L.; Tieke, B., Selective ion transport across self-assembled alternating multilayers of cationic and anionic polyelectrolytes. *Langmuir* **2000,** *16* (2), 287-290.

152. Stanton, B. W.; Harris, J. J.; Miller, M. D.; Bruening, M. L., Ultrathin, multilayered polyelectrolyte films as nanofiltration membranes. *Langmuir* **2003,** *19* (17), 7038-7042.

153. Adamczyk, Z.; Jamrozy, K.; Batys, P.; Michna, A., Influence of ionic strength on poly(diallyldimethylammonium chloride) macromolecule conformations in electrolyte solutions. *J. Colloid Interface Sci.* **2014,** *435*, 182-190.

154. Vogt, B. D.; Lin, E. K.; Wu, W. L.; White, C. C., Effect of film thickness on the validity of the Sauerbrey equation for hydrated polyelectrolyte films. *J. Phys. Chem. B* **2004,** *108* (34), 12685-12690.

155. Koehler, R.; Steitz, R.; von Klitzing, R., About different types of water in swollen polyelectrolyte multilayers. *Adv. Colloid Interface Sci.* **2014,** *207*, 325-331.

156. Zhang, H.; Wang, C.; Zhu, G. Y. J.; Zacharia, N. S., Self-Healing of Bulk Polyelectrolyte Complex Material as a Function of pH and Salt. *ACS Appl. Mater. Interfaces* **2016,** *8* (39), 26258-26265.

157. Hodge, R. M.; Bastow, T. J.; Edward, G. H.; Simon, G. P.; Hill, A. J., Free volume and the mechanism of plasticization in water-swollen poly(vinyl alcohol). *Macromolecules* **1996,** *29* (25), 8137-8143.

158. Jaber, J. A.; Schlenoff, J. B., Counterions and water in polyelectrolyte multilayers: A tale of two polycations. *Langmuir* **2007,** *23* (2), 896-901.

159. Shamoun, R. F.; Hariri, H. H.; Ghostine, R. A.; Schlenoff, J. B., Thermal Transformations in Extruded Saloplastic Polyelectrolyte Complexes. *Macromolecules* **2012,** *45* (24), 9759-9767.

160. Schaaf, P.; Schlenoff, J. B., Saloplastics: Processing Compact Polyelectrolyte Complexes. *Adv. Mater.* **2015,** *27* (15), 2420-2432.

161. Liu, G. M.; Zou, S. R.; Fu, L.; Zhang, G. Z., Roles of chain conformation and interpenetration in the growth of a polyelectrolyte multilayer. *J. Phys. Chem. B* **2008,** *112* (14), 4167-4171.

162. Mancinelli, R.; Botti, A.; Bruni, F.; Ricci, M. A.; Soper, A. K., Hydration of sodium, potassium, and chloride ions in solution and the concept of structure maker/breaker. *J. Phys. Chem. B* **2007,** *111* (48), 13570-13577.

163. Walrafen, G. E., Raman Spectral Studies of HDO in H_2O. *J. Chem. Phys.* **1968,** *48* (1), 244.

164. Guzman, E.; Ritacco, H.; Rubio, J. E. F.; Rubio, R. G.; Ortega, F., Salt-induced changes in the growth of polyelectrolyte layers of poly(diallyl-dimethylammonium chloride) and poly(4-styrene sulfonate of sodium). *Soft Matter* **2009,** *5* (10), 2130-2142.

APPENDIX A

QUARTZ-CRYSTAL MICROBALANCE WITH DISSIPATION PROCEDURES

Materials for Solution Preparation

- 0.1 mg/mL PDADMA and PSS solutions prepared at 0.5 M NaCl
- 0.5 M NaCl DI water
- LPEI 1 mg/mL
- pH 4.5 DI water
- Selected salt at selected concentration (varies with experiments)

Experimental Setup

1. Place 2 crystals facing upward in glass dish into oxygen plasma treatment
    a. Make sure to keep track of the crystal order since crystals are numbered in the box

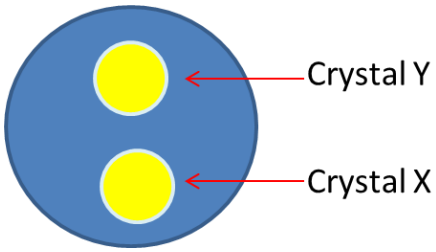

    b. Vacuum for 3 minutes
    c. Treat with pink plasma for 15 minutes
2. Adjust pH of DI water and LPEI for initial layer (pH 4.5)
    a. Calibrate pH meters using buffer solutions on the above shelf (replace the solutions once per month)
    b. Adjust both solutions to pH 4.5 (+/- 0.01) using pH meter (cation)
    c. Start with water then go to LPEI to avoid contaminating the water
    d. This should be done while vacuum/plasma treatment is going on

NOTE: New dilute HCl solution should be made in order to have a clear idea of the solution strength

Experimental Setup

1. Stop the pump if it is still running after an overnight rinse

2. Check the tubing and waste outlet
    a. Look for buildup of polymer residue
    b. Check all connection points to make sure they are secure
    c. Make sure waste outlet is secured via tape to the waste beaker
3. Open module and remove the crystal from previous experiment
    a. Place dirty crystal into special holder in beaker on the desk
    b. Clean out the module with a Kim wipe and make sure no dust or particles are in the module
    c. Examine clean crystal to make sure it has no visible dust particles (blow gently to remove any particles from the surface)
4. Load crystal into the module
    a. Place the crystal reflective side down in the module
    b. Make sure crystal is lined up correctly using markings on crystal and module
    c. Tighten the screws firmly but not too tightly

NOTE: Max of 5 experiments per section of tubing (2 sections per tube) this tubing becomes the rinse tubing until the new tubing reaches the max experiment number and the old tubing is discarded

Computer Initial Setup

1. Click "Acquisition" → "Setup Measurement"
    a. Check the overtones by selecting the overtone in the drop down menu and clicking "find"
        i. 1^{st} overtone should be less than 30
            1. If it is not less than 30 open module and check crystal
            2. If it is 3 times over 30 use the second crystal
        ii. Frequency decreases as overtones increase (trend)
2. Take Picture of Overtones before moving on
3. Make sure the Temperature is set to 25°C (click "apply")
4. Place inlet tubing into the pH 4.5 Rinse Water vial (adjusted in initial setup)
5. Click "Acquisition" → "Start Measurement" to begin data collection
6. Turn on the Pump
    a. Ensure that the liquid is being drawn by the pump
    b. Wait until the data collection begins after solution hits the sensor
    c. Let the data collect for 45 min for a baseline
7. After baseline is collected close the data collection window and do not save the data
8. Click "Acquisition" → "Start Measurement" to begin new collection (still using pH 4.5 rinse water)

a. Looking at only the 3rd overtone let the data collect for 2 min and ensure that there is no change in slope or separation of the collected data points occurs
b. The Image below shows what the data should look for the 2 minute period

9. After 2 minute period is complete
    a. Stop the pump
    b. Place the inlet tube into the LPEI (pH 4.5) vial
    c. Start pump
    d. Click time stamp
    e. Start the timer for 14 min (Actual time of collection until solution switch is 15 min)
    f. Make note of which solution is currently flowing (pH 4.5 LLPEI in this case)

Film Buildup

10. After timer goes off (14 min for LPEI) wait until 15 min exactly (based on previous time stamp and elapsed time indicated) and:
    a. Stop the pump
    b. Switch to pH 4.5 rinse water
    c. Start the pump
    d. Click the time stamp
    e. Start the timer for 4 min (actual rinse time 5 min)

11. After the timer goes off (4 min for pH 4.5 rinse water) wait until exactly 5 min and then:
    a. Stop the pump
    b. Switch solutions to PSS (or whatever first material is for film)
    c. Start the pump
    d. Time stamp
    e. Start the timer for 14 min (15 min actual time)
12. Repeat solution changing procedure to build up the desired amount of layer pairs of polyelectrolytes used:

Baseline Measurement
- pH 4.5 Rinse water (pure Milli-Q) (45 min) (baseline)
- pH 4.5 water (2 min) (checking baseline quality)
- pH 4.5 LPEI (15 min)
- pH 4.5 Rinse water (5 min)

Repeat X times:

- PSS (15 min)
- Regular Rinse water (0.5 M NaCl) (5 min)
- PDADMA (15 min)

Regular Rinse water (0.5 M NaCl)

Selected Salt solution (1-3 h)

Regular Rinse Solution

Selected Salt Solution (1-3 h)

At the end of the experiment make sure to stop data collection and save with appropriate name.

NOTE: When using regularly (consecutive days) it is ok to leave the module rinsing overnight in DI rinse water.

Cleaning Procedures

Vials and Excess Materials

1. Clean polyelectrolyte vials at the end of each week.
    a. Dispose of excess PDADMA and PSS left over in the vials
    b. Wash and rinse thoroughly and dry in oven
2. Clean vial containing LPEI and dispose of excess every 3 weeks
3. Clean and rinse vials containing water and dry in oven

Crystal Cleaning

1. Upon removing crystals from module, place in special containing beaker in correct order and allow to soak in water overnight to loosen up any materials stuck to surface before deep cleaning
2. Remove from container and individually rinse with DI water using spray bottle
3. Dry crystals using nitrogen gas (or place in microscope slide and put in drying oven for 10-15 min)

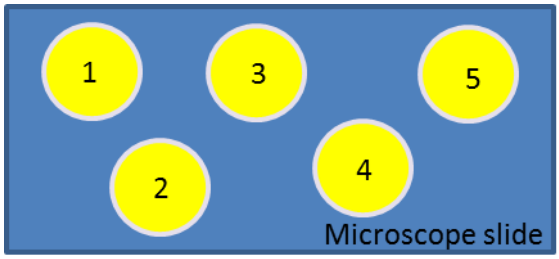

4. Plasma treat (3 min vacuum → 10-15 min pink plasma)
5. Immerse and sonicate crystals in 2.6 M KBr solution for 10 minutes
6. Immerse and sonicate crystals in 2% SDS solution for 5 minutes
7. Rinse with DI water individually
8. Blow Dry with Nitrogen Gas
9. Plasma treat (3 min vacuum → 15 min pink plasma)

NOTE: About 6-10 cleaning cycles can be performed on each crystal before replacement.

Changing the Tubing

1. Max of 4-5 experiments per section of tubing (2 sections per tube)
2. To replace the tubing
    a. Remove the module lid carefully
    b. Remove the inlet and outlet tubing carefully by unscrewing from module
    c. Remove caps from tubing sections (and any excess tubing that may stick to the cap and break from the tubing being removed)
    d. Acquire new tubing section and insert the cap end into the tubing (patiently, it is a tight fit)
    e. Use previous inlet and outlet tubing to measure out new inlet and outlet tubing and cut to proper length
    f. Use new stop cap for new inlet and outlet tubing and move the threaded cap from old to new tubing sections.
    g. Tighten all tubing into place on the module

Cleaning the Sample Module

1. Remove crystal from module (if still present) and put in beaker in special container in correct order under water.
2. Disassemble the module (remove top half and bottom half) by unscrewing the two tension screws on top of the module
3. Set aside the top half
    a. The top half will never be cleaned (send to Biolin Scientific for maintenance if issue arises)

4. Disassemble bottom half of the module
    a. Unscrew the 6 screws holding it together
    b. Remove the gasket
    c. Remove the O-ring
        i. Gasket and O-ring will be completely replaced…
        ii. Make sure to order more replacements when 2 of each are left
5. Immerse in soap solution in beaker
    a. 1 Part SDS + 10 parts water (10mL SDS + 100mL water)
    b. Sonicate for 15-20 min
    c. Remove from sonicator and rinse with DI water with spray bottle (make sure to get all soap out of the holes and crevices thoroughly)
    d. Sonicate in DI water for 20 min
    e. Remove and rinse with DI water
    f. Replace water in beaker and sonicate again for 15 min
    g. Pat dry with paper towel dry in ambient conditions for 1-2 h
    h. Blow dry with Nitrogen gas thoroughly (pat dry with Kim wipe as you go)
    i. Dry in oven overnight
    j. Blow dry with nitrogen one more time

APPENDIX B

MODULATED DIFFERENTIAL SCANNING CALORIMETRY PROCEDURES

Overview of DSC Sample Preparation

1. Construct PDADMA/PSS_{140} LbL assemblies at 0.5 M salt on Teflon substrates over the course of 5 days (See *HMS Slide Stainer Program Procedure*)
2. Dip the completed assemblies in Milli-Q water for 3 seconds. Wait 1 minute and dip the assemblies for another 3 seconds
3. Dry in hood under ambient conditions overnight
4. The day before making DSC samples, dry the assemblies overnight under vacuum at room temperature
5. Put the assemblies into Tzero Aluminum Hermetic DSC Pans with 6-7mg per pan (See *DSC Pan Preparation*).

NOTE: The final weight of the sample will be between 7-8mg so consider how much mass will leave when the sample is vacuum heated and how much mass will be added in rehydration

6. Dry samples in the oven at 115°C under vacuum for 3 hours
7. Remove from oven and **QUICKLY** measure and record the mass of each prepared pan
8. Hydrate to desired hydration level of desired salt solution using the micro syringe
    a. Example calculation for 36%:
    b. Total mass – mass of pan = mass of polymer
    c. Mass polymer * 0.36 = mass of solution needed
9. Put lid on pan and seal using press
10. Let the sample sit overnight in sealed pan
11. Run DSC experiment (See *Running the DSC Experiment*)
12. Analyze the collected data (See *How to Find Glass Transition Temperatures Using Universal Analysis 2000* and *How to Make a Heat Curve DSC Graph in Excel*)

Parameters of the DSC

- 2 heating/cooling cycles ramp the temperature from 0 °C to 115 °C at rate of 2 °C/min at 1.272 °C amplitude for 60s. (Overall temperature change is heat−cool−heat−cool)
- Sample Size: 7-8mg
- Sample Purge Flow: 50ml/min nitrogen

DSC Pan Preparation

1. The day before making DSC samples, dry the assemblies overnight under vacuum at room temperature

2. Weigh the Tzero Aluminum Hermetic Pan and record the pan mass.
3. Pull off the film from the substrate with tweezers and form into a tight, small ball

NOTE: Try to peel off large pieces and fold them into balls

4. Repeat until the desired mass Tzero Aluminum Hermetic Pans in the pan (6-7mg)

NOTE: The final weight of the sample will be between 7-8mg so consider how much mass (about 1mg) will leave when the sample is vacuum heated and how much mass will be added in rehydration (dependent on the hydration level)

5. Record the mass of the polymer and pan
6. Dry samples in the oven at 115°C under vacuum for 3 hours
7. Remove from oven and **QUICKLY** measure and record the mass of each prepared pan
8. Hydrate to desired hydration level of desired salt solution using the micro syringe
9. Put lid on pan and seal using press

Example calculation for 36%

a. Total mass – mass of pan = mass of polymer
b. Mass polymer * 0.36 = mass of solution needed

Running the DSC Experiment

1. Check the nitrogen tank pressure on the tank in the lab hallway.
    a. The left gauge should read about 12psi
    b. The right gauge should be above 500psi (Once at 500psi, it is acceptable to run one DSC experiment and then change the tank)
    c. To change the tank
        i. Use wrench to take off gauges
        ii. Take off "IN SERVICE" tab stub
        iii. Move new tank into place
        iv. Take off lid and put on the old tank
        v. Put on gauges on the new tank using wrench
        vi. Turn on the tank
2. Check the Sample Purge Flow on the DSC computer. It should fluctuate slightly around 50ml/min
3. Use Runs
4. Enter procedure information
5. Under Summary
    a. Use Modulated for mod. Fill in pan type (Tzero Aluminum Hermetic)
    b. Enter the sample size (the polymer and solution total mass)
6. Under Procedure: Go to Editor and select your procedure
7. Under Notes: Do NOT change the nitrogen flow

8. To open the machine lid, go to “Control” on the top menu bar, then “Lid” and then “Open”
9. Place the sample and reference pan in the DSC machine using the DSC tweezers
10. To close the machine lid, go to “Control” on the top menu bar, then “Lid” and then “close”
11. To start the experiment, press the green run button in the top left corner (a green running man should appear nest to your run number)

How to Find Glass Transition Temperatures Using Universal Analysis 2000

1. Click on the Universal Analysis 2000 icon on the Desktop on the DSC computer
2. Go to “File”, then click “Open” and select your desired DSC Run
3. Go to “Edit”, then click “Cycle List”
4. In the text box that appears, unclick cycles 1, 2, and 4
5. To change the axis scales, right click on any of the axis numbers
    a. Usually change the Y2 axis to -0.5 in the first box and 0 in the second box
    b. Change Y1 to capture the upper and lower values of the green line
    c. Change the x-axis to begin at zero
6. Use Glass/Step Transition button (pictured to the left) in the tool bar to determine the glass transition
    a. Move the cross hairs by clicking and holding them
    b. Select a range around the dip in the graph

How to Make a Heat Curve DSC Graph in Excel

1. Open Universal Analysis 2000
2. Open the desired file
3. Go to File → Export Data File → File Signal Only
4. Create a new Excel Spreadsheet
5. In Excel, go to Open File
    a. Go to the bottom drop down menu and change from “All Excel Files to “All Files”
    b. Select the text file that was created in step 3 and open it (a window will appear because it is an Excel file)
    c. Click the finish button
6. Select all the data points (signals) and copy them
7. Paste them on to Sheet 2
8. Insert a row on top of Sheet 2
9. Go back to Sheet 1, copy all the signal names and “paste special” them in the row that was created in Sheet 2 (in the Paste Special window, check the box by transpose)
10. Delete all of the columns EXCEPT for Temperature and Reverse Heat Flow
11. In the first box of Column C (the third column), enter “Reverse Heat Flow (mW/g)”

12. In the second cell (C2) of that column enter "=B2/(mass/-1000))" where 'mass' is the mass of your rehydrated sample

NOTE: The negative sign is to make the graph Exothermal Down

13. Move the cursor over C2 so that a square appears on the bottom right corner as shown below

	A	B	C
1	Temperature (°C)	Rev Heat Flow (mW)	Rev Heat Flow (mW/g)
2	0.4506694	-0.228503	31.64861496

14. Double click the square. This will copy the formula down the entire column
15. Delete all the data point EXCEPT those for Cycle 2
    a. To do this, click the Find and Select button
    b. Check the boxes by "Match case" and "Match entire contents" like the picture below

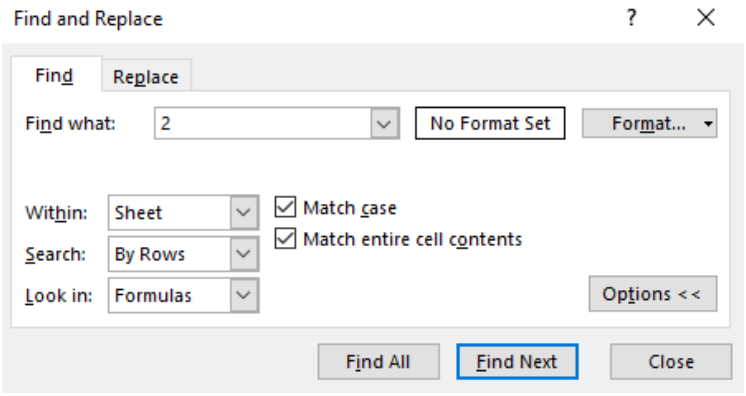

    c. Search for 2 and delete it and all the data points above it for the three columns
    d. Search for 3 and delete it and all the data points below it for the three columns
16. To make the graph, go to the Insert tab and go to Charts. Select the "Scatter w/ smooth lines"
17. For the x axis, select the temperature data (Column A)
18. For the y axis, select the Reverse Heat Flow (mW/g) (Column C)